1973

Studies on crystallization of trans-polybutadiene in stretched networks.

Yoshinori Akana
University of Massachusetts Amherst

STUDIES ON CRYSTALLIZATION OF TRANS-POLYBUTADIENE IN STRETCHED NETWORKS

A Master Thesis Presented

By

Yoshinori Akana

Submitted to the Graduate School of the
University of Massachusetts in
partial fulfillment of the requirements for the degree of

MASTER OF SCIENCE

January 1973

Major Subject: Polymer Science & Engineering

STUDIES ON CRYSTALLIZATION OF TRANS-POLYBUTADIENE IN STRETCHED NETWORKS

A Master Thesis Presented

By

Yoshinori Akana

Approved as to style and content by:

Richard S. Stein
(Chairman of Committee)

(Head of Department)

(Member)

(Member)

Jan 1973
(Month) (Year)

A C K N O W L E D G E M E N T S

The author wishes to express his sincere appreciation to Professor Richard S. Stein, thesis director, for his guidance and suggestions throughout the course of this work and for his personal help during the stay in the U.S.A.

The author extends his gratitude to the thesis committee members, Professor F.P. Price and Professor J.C.W. Chien for their constructive comments and helpful discussion.

Thanks and sincere appreciation are further extended to the faculties and staffs of Polymer Science & Engineering Department and to the staffs of Polymer Research Institute.

The author is much grateful to Mitsui Petrochemical Industries, Ltd. for the financial support for this work.

DEDICATED
TO

MY MOTHER, SUGAKO AKANA
AND
MY FATHER, BENTAROH AKANA

for their love and encouragement in my life.

TABLE OF CONTENTS

1. INTRODUCTION

The distortion of molecular chains in amorphous crosslinked networks from their most probable configuration by stretching gives rise to a decrease in configurational entropy. As a consequence, the tendency toward crystallization is so enhanced that even natural rubber can crystallize upon stretching at room temperature.

Crystallization developed in rubber stretched in simple extension has been directly investigated by X-ray, density and other methods[1-4]. When crystallization takes place in rubber upon stretching, the resulting crystallites prevent slippage of chain molecules past each other because these crystallites act as multifunctional crosslinkages. As a consequence, raw rubber does not show any plastic flow at higher extensions. This was observed by Treloar[5] from an experiment on the recovery of deformed rubber to its original length upon warming.

From the X-ray work of Gehman and Field[6], it was shown that the crystallites which were formed in rubber upon stretching at room temperature were oriented with their c-axis parallel to the stretching direction. The crystal orientation resulting from the crystallization of raw rubber upon stretching was also proposed by Treloar[4] from the observation of the increase in birefringence.

The crystallization accompanying the crystal orien-

tation may lead to substantial deviation from the kinetic theory of rubber elasticity developed by Kuhn and Grun[7,8] and Treloar[9] if crosslinked rubber is used for this study. Treloar[10] showed that the hysteresis of the stress-strain curve and the birefringence-stress curve of the crosslinked natural rubber was a consequence of the oriented crystallization.

Since crystallization of rubber upon stretching results in the growth of oriented crystals, the study on the progress of crystallization may be complicated. It was observed by Treloar[4] that the increase in the birefringence during crystallization at higher elongations is proportional to the crystallinity determined from the density method. Crystallization in stretched natural rubber and synthetic rubber has been studied by many authors by the observation of theassociated relaxation of tensile stress[11-17]. If slightly crosslinked rubber is used for such studies, one can neglect the stress relaxation due to the flow of amorphous chains. Then the stress relaxation after the onset of crystallization may be related to the development of the crystallization as well as to the mode of crystal growth.

A statistical thermodynamic treatment of the crystallization of polymer networks held in simple extension has been developed by Flory[18]. It is assumed in his theory that the chains which traverse the resulting crystallites

are parallel to the stretching direction. He describes the relation between the equilibrium degree of crystallinity and the stress at a given elongation. He also predicts the stress relaxation accompanying the development of crystallization and the increase of the melting temperature of the crystallites.

This prediction of stress relaxation has been verified by many authors[11,16,17]. If the rubber is stretched before any crystallization takes place, subsequent crystallization brings about a reduction in stress. In a certain conditions, the stress exerted to hold the rubber at a constant length falls to zero, and the rubber shows a spontaneous extension of its length[19].

The kinetics of crystallization under stress has been studied by Gent and others[11,12] by observing the corresponding volume contraction. It is observed that the rate of crystallization increases enormously with the applied strain, and that the Avrami index decreases to values close to 1.0 at high elongation, which suggests one-dimensional crystal growth.

The influence of strain on the crystallization is also reflected by the change in the superstructure of the crystallized materials, which causes substantial changes in the physical and mechanical properties in rubber network. This was shown by Andrews[20], using the electron microscope for studies of the morphology of natural rubber

crystallized under stress. He observed that at lower strain, the crystalline filaments (α - filaments) grow perpendicularly to the strain direction and at higher strain, other kind of crystalline filaments (γ -filaments) run in the strain direction. It was proposed that the nuclei of α - filaments are formed spontaneously along the strain direction but can not grow laterally at high elongation because of the existence of nuclei close to each other.

Crystallization may be entropically expected to depend upon the orientation distribution of the amorphous chains brought about by the strain before the onset of crystallization. When the crystallites are formed during stretching, they may act as additional crosslinkages. As a consequence, the average degree of alignment of chain molecules increases drastically with increasing elongation. This is due to the rapid increase in the number of effective crosslinks with elongation. The crystallization is accelerated by the elongation for this reason. Then the Young's modulus of rubber increases drastically with increasing elongation. This is often observed from the pronounced upward curvature in the stress-strain curve[10,21].

The mechanically and physically anisotropic properties of crystalline polymers are affected by the oriented crystallization. The crystal orientation in solid polymer is important for obtaining specific properties appropriate for certain applications of commercial products. The me-

chanical strength and the transparency of films, fibers and bottles are brought about by the industrial processing operations[22-25] which affect the crystalline morphology. The usual industrial procedure for inducing the crystal orientation in the crystalline polymer are extrusion, spinning, blow and injection molding, as well as the cold drawing process. Many of these processes involve the solidification during flow of melt. As a consequence, the initially formed crystallites during solidification may take parts in the network as crosslinking points for the stretched amorphous melt. This causes the further orientation of amorphous chains which accelerates the crystallization in a specific direction, depending upon the strain direction and the temperature gradient in the melt. Then the mechanism of crystal orientation in these processes may depend upon the rate of deformation or shear, and upon the temperature of deformation and solidification.

Many extensive studies have been carried out on the crystal orientation resulting from these processes because of the commercial interest in the development of new properties of solid polymers.

Keller and Machin[26,27] studied the mechanism of the stress-induced crystallization from the melt of polyethylene by observing the superstructure in the crystallized state. They proposed that crystallites grow from the fibril nuclei which are formed from the extensional flow of the

melt, and that at low stress the lamellae grow perpendicularly to the strain direction with the random orientation of the a- and c-axes around the b-axis, to give a texture of spherulitic disks, but that at high stress the lamellae are lie flat in a plane perpendicular to the stretching direction without twisting about the b-axis, to give the c-axis orientation parallel to the strain direction. These are schematically illustrated in Figure 1.

Stein and his coworkers[29,30] observed from the cross-linked polyethylene crystallized at stretched state that there exists a-axis orientation with negative birefringence at low elongation and that the c-axis orientation appears preferentially at high elongation.

From the similar experiment of polyethylene, Krigbaum and Roe[31] observed that the b-axis is always perpendicular to the strain direction in the whole range of elongation and that in addition to this, the preferential c-axis orientation takes place with increasing elongation.

A much more complex system of crystallization under stress is injection molding, because the gradients of temperature and stress in polymer melt after the onset of crystallization are considerably large. Then the morphology of molded material is changed with the depth from the surface to the inside. The extensive studies on the morphology of polyoximethylene molded bar was carried by Clark[32,33]. His observation is schematically illustrated in

Figure 2. Near the surface of the mold wall, the lamellae are oriented perpendicular to both the surface of the wall and the injection direction. These lamellae grow toward the inside of the sample with their growth, and the preferential orientation with respect to the injection direction is lost because the shear stress in melt after the molding decreases with development of the crystallization. The spherulite texture is observed close to the inside of the sample because of the absence of temperature and stress gradients there.

These practical solidification are complex, primarily because they are not the isothermal. It is more simple and straightforward to study the crystallization process under stress under isothermal conditions. If the long chain molecules are crosslinked, it may be possible to specify the amorphous orientation before any crystallization takes place. It may be also possible to apply the kinetic theory of rubber elasticity to the amorphous phase during crystallization[34,35].

Since the birefringence of crystalline polymer depends upon the crystal orientation as well as the crystallinity, the increase in the birefringence during crystallization may give a clue of understanding the crystallization process under stress, just as the stress relaxation does.

Light scattering measurements[36,37] using techniques developed in our laboratory may help further understanding

the mode of crystal growth and the crystal orientation in this crystallization.

In this work, trans 1,4-polybutadiene was chosen because it is readily crosslinked, and because it may be easily extended in the amorphous state and crystallization occurs over a convenient temperature range.

II. THEORETICAL

The X-ray diffraction method is one of the best absolute methods for determining the crystallinity of crystalline polymers[38-41]. It may, however, be impossible to follow the crystallization by observing the change in the X-ray diffraction intensity with time because of the long time required for the measurement of X-ray diffraction intensity. Consequently, it becomes necessary to develop other methods to follow crystallization under stress.

The birefringence of a crystalline polymer may be represented by the equation[42,43]

$$\Delta = \Delta_c X_c + \Delta_a (1 - X_c) + \Delta_F \qquad (1)$$

where Δ_c and Δ_a are the birefringence values per unit volume of crystalline and amorphous materials, respectively, Δ_F is the form birefringence, expressing the contribution of an anisotropic boundary between the crystalline and the amorphous phases[44], and X_c is the volume fraction of crystalline phase. The crystal and amorphous orientation functions, f_c and f_a may be related to the values Δ_c and Δ_a, respectively by the following equations

$$\Delta_c = \Delta_c^o f_c \qquad (2)$$

$$\Delta_a = \Delta_a^o f_a \qquad (3)$$

where Δ_c^o and Δ_a^o are the intrinsic birefringence values for the pure, completely oriented crystalline and amorphous phases, respectively.

By replacing eq.(2) and (3) in eq.(1) and neglecting Δ_F, eq.(1) is transformed to the equation

$$\Delta = \Delta_c^o f_c X_c + \Delta_a^o f_a (1 - X_c) \qquad (4)$$

This equation may describe the relation between the crystallinity and the birefringence during crystallization under stress.

If the Kuhn-Treloar relation[8,9,45] between the birefringence and the stress which occurs in the perfectly amorphous network is still sufficient for describing the amorphous phase during crystallization under stress, the value Δ_a may be related to the tensile stress through the stress-optical coefficient by the equation

$$\Delta_a = C_T \cdot \sigma \qquad (5)$$

where C_T is the stress-optical coefficient of amorphous network at the crystallization temperature and σ is the measured stress. Since the stress-optical coefficient of the amorphous network is given by the equation[8,9,45]

$$C = \Delta_a/\sigma$$

$$= \frac{2\pi}{45kT} \frac{(\overline{n^2} + 2)^2}{\bar{n}} (b_1 - b_2)_s \qquad (6)$$

where $\bar{n}$ is the average refractive index, $(b_1 - b_2)_s$ is the polarizability difference for the amorphous statistical segment, k is Boltzmann constant, then C_T is determined by extrapolating the experimental values of stress-optical coefficient above melting point to the crystallization temperature. The values of C_T for trans 1,4-polybutadiene

are determined as 0.415, 0.425 and 0.435 x 10^{-3} cm^2/Kg for 95, 90 and 85°C of the crystallization temperature, respectively, in this work.

The orientation of crystallites produced during crystallization under stress may not be perfectly parallel to the stretching direction but depend upon the elongation ratio and the crystallization temperature. Then, it is necessary to determine the crystal orientation function f_c by the X-ray method or others in order to estimate the crystallinity from eq.(4). In this work, the value f_c of trans 1,4-polybutadiene was determined from the intensity distribution of the diffracted X-ray of the (100) plane, assuming that the crystal orientation in the final state of crystallization is the same throughout crystallization.

The value of Δ_c^o may be estimated from the theoretical calculation of the polarizability difference of the polymer chain in the crystal $(b_1 - b_2)_c$ using the additivity of bond polarizability values which have been given by Denbigh[46,47]. Δ_c^o may be related to the quantity $(b_1 - b_2)_c$ by the differentiated Lorenz-Lorentz equation

$$\Delta_c^o = \frac{2\pi}{9} \frac{(\overline{n^2} + 2)^2}{\bar{n}} \frac{(b_1 - b_2)_c}{V_c} \qquad (7)$$

where $\bar{n}$ is the average refractive index of crystal, $(b_1 - b_2)_c$ is the polarizability difference of the repeat unit in the unit cell, V_c is the volume per repeat unit in the crystal. Trans 1,4-polybutadiene possesses the al-

ternative zigzag conformation of the planar butadiene unit [48]. Δ_c^o of this polymer is determined as 0.184 cm^3. The procedure for this calculation is given in Appendix I.

The simultaneous measurement of birefringence and stress may give the crystallinity of stretched trans 1,4-polybutadiene during crystallization. For example, the birefringence at 85°C of crystallization temperature is represented by the equation

$$\Delta = 0.184\ f_c\ X_c + 0.435 \times 10^{-3} \cdot \sigma \cdot (1 - X_c) \quad (8)$$

where $f_c = 0.70$, determined by the X-ray method.

By assuming that the crystallites are perfectly oriented parallel to the stretching direction, Flory[18] has developed a theory for the crystallization of rubber which relates the stress for a rubber at elongation α to the crystallinity according to the equation

$$\sigma = N_c\ k\ T\ [(\alpha^2 - 1/\alpha) - \alpha(6n_s/\pi)^{1/2} X_c]\ /(1 - X_c) \quad (9)$$

where σ is the stress per actual area, α is the extension ratio, n_s is the average number of statistical segments between crosslinking points, and N_c is the number of chains per unit volume. The reduction in stress during crystallization is a consequence of the decrease in orientation of the remaining amorphous network chains.

The value n_s may be estimated by dividing the number of segments per cm^3 N_s by the number of chains per cm^3 N_c, or by dividing the molecular weight of a chain between crosslinking points M_c by the molecular weight of a segment

M_s.

$$n_s = M_c / M_s \qquad (10)$$

The value M_c is calculated from the intercept of Mooney-Rivlin plot[49,50], represented by the equation

$$2C_1 = \rho \cdot R\ T\ /\ M_c \qquad (11)$$

where ρ is the density of amorphous phase of trans 1,4-polybutadiene. The value M_c of this polymer which is used for the experiment of crystallization under stress is 16200.

The value M_s may be experimentally estimated from the polarizability difference of the statistical segments $(b_1 - b_2)_s$ which is experimentally determined from eq.(6). If it is assumed that the optical anisotropy of the statistical segment is proportional to its length and is equal to the summed value of monomer units along it, the value M_s may be expressed by the equation

$$M_s = M_o\ (b_1 - b_2)_s\ /\ (b_1 - b_2)_o \qquad (12)$$

where M_o is the molecular weight of monomer unit, and $(b_1 - b_2)_o$ is the anisotropy of monomer unit. The value $(b_1 - b_2)_o$ of trans 1,4-polybutadiene has been calculated by several authors[52-55]. Using Fukuda's value[52] for $(b_1 - b_2)_o$, the value M_s of trans 1,4-polybutadiene is determined as $M_s = 186$. This value corresponds to $n_s = 87$.

If Flory's assumption on the orientation of the subsequent crystallites is sufficient for the crystallization of trans 1,4-polybutadiene in this work, the progress of

crystallization may be simply followed by observing the stress relaxation alone during crystallization, using eq.(9).

III. EXPERIMENTAL

1. Sample preparation

Trans 1,4-polybutadiene was obtained from Phillips Petroleum Company (Bartleville, Oklahoma). This sample was designated Trans-4 and reported to contain 91% trans isomer. This polymer was crosslinked with a conventional curing agent, dicumyl peroxide, after purified by precipitation from benzene solution by methanol. Dicumyl peroxide (25 to 50 mg) was added to the benzene solution of purified polymer at concentration of 5 gr/100 ml and then the films of 5 to 10 mil thick were cast on a glass plate. After evaporation of benzene in vacuum, films were crosslinked at 150°C at 6000 psi for 60 min in a laboratory press in which the films were held between metal plates covered with cellophane films. After curing, the films were cooled in air. Samples of proper size were cut from these films.

The composition of original purified polymer was determined as 85% trans-content from infrared spectra using Morero's method[56]. The melting point of the crosslinked polymer was determined by differential scanning calorimetry.

Purified polymer was used for the film preparation as soon as possible because it was observed that spontaneous crosslinking occured after two weeks of the storage in vacuum.

2. Measurement of stress-optical coefficient of the amorphous network

Stress and birefringence were measured simultaneously by using the table model Instron tensile tester equipped with the optical attachments, a mercury lamp, a polarizer and a Babinet compensator[57]. The sample was held in the chamber, through which a flow of air passing through a heater was circulated. The schematic diagram of this apparatus is shown in Figure 3 .

Samples of dimensions, 0.35 inch x 1.5 mil were for these measurements. After the sample which was clamped in the chamber reached a given temperature above its melting point, the initial length at zero stress was measured. Then the sample was stretched stepwise by 0.02 inch every 10 min. The measurement of the retardation and the stress was carried out 10 min after streching the sample, by reading the equilibrium values of both.

The birefringence was calculated from the retardation using the equation[58]

$$\Delta = (\lambda_o/d)\ R \qquad (13)$$

where λ_o is the wavelength of mercury light in vacuum (5461 Å), d is the thickness of the film and R is the retardation measured in units of number of wavelength. The value R was determined from the equation

$$R = \Delta x/\Delta x_o \qquad (14)$$

where Δx_o is the distance along the wedge in the compensator corresponding to one wavelength of retardation and Δx is the amount of shift in the fringe pattern of retardation.

The stress-optical coefficient was calculated from the slope of the birefringence value versus stress.

3. Measurement of stress and birefringence during crystallization under stress

Crystallization of the stretched sample was carried in the same chamber used for the measurement of stress-optical coefficient. The sample was stretched in the chamber at 110°C (above its melting point) and held in this state for 10 min. Then the sample was cooled down to the crystallization temperature by circulating preheated air at this temperature. Within 2 min after circulation of the air, the temperature in the chamber became constant. At this time, the measurement of the retardation and the stress was started. The measurement was continued until it became impossible to measure the retardation because of the increase in turbidity of the film with time due to its crystallization.

The increase in birefringence and the decrease in stress were observed with the development of crystallinity. Using the value of stress-optical coefficient of the amor-

phous network at crystallization temperature C_T, the birefringence of the amorphous phase during crystallization Δa was calculated from the same equation developed for the completely amorphous network by Kuhn-Grun[8] and by Treloar[9]

$$\Delta a = C_T \cdot \sigma \qquad (15)$$

where σ is the stress during crystallization. This involves the assumption that the stress on the amorphous region is the same as the total stress on the polymer and that the stress-optical coefficient of the amorphous region in the crystalline polymer is the same as that in the completely amorphous polymer.

4. Measurement of the orientation function of crystallites resulting from the crystallization under stress

The diffracted intensities of the sample without strain were measured at various Bragg angles (2θ) by the normal-beam transmission method, using the dynamic X-ray diffractometer[59]. The measurement of intensities was made at every 0.5° of 2θ in the range of 10 to 15°. From 15 to 25°, it was carried at every 0.2°, and from 25 to 30° at every 0.5° again. The measurement of the intensity distribution with Bragg angle scanning was carried at several temperatures from room temperature to above the melting point.

The intensities of diffracted X-rays at various Bragg angles were corrected for polarization, absorption, Compton scattering and the background intensity, according to the equation[60]

$$I_{corr} = K_{pol}\, K_{abs}\, (I_{exp} - I_{bkg}) - I_{compt} \qquad (16)$$

where

I_{corr} = corrected intensity

I_{exp} = experimental intensity

I_{bkg} = background intensity

I_{compt} = Compton scattering (incoherent) intensity

K_{pol} = polarization correction factor

K_{abs} = correction factor for sample absorption and changes in scattering volume

The Compton intensity is given by the equation[60]

$$I_{compt} = K_{compt}\, F_{incoh} \qquad (17)$$

where

$$F_{incoh} = \sum_{i=1}^{b} x_i \left(Z_i - \sum_{j=1}^{Z_i} f_{ij}^{\,2}\right) \qquad (18)$$

where

x_i = mole fraction of atom type i

Z_i = atomic number of atom type i

f_{ij} = scattering factor for the j^{th} electron of the i^{th} atom

K_{compt} = experimentally determined constant, independent of 2θ

In a previous report from this laboratory[61], K_{compt} was evaluated by assuming that at a sufficiently high 2θ

value (50° was used), the entire sample scattering intensity consists of Compton scattering. However, Krimm and Tobolsky[62] did not assume that the coherent intensity vanishes at large angle 2θ. In this work the previous method developed in our laboratory[61] was chosen for its simplicity. Then the value of K_{compt} is given by the equation

$$K_{compt} = I(50^{\circ})/F_{incoh(50^{\circ})} \qquad (19)$$

where

$I(50^{\circ})$ = intensity of diffracted X-ray at $2\theta = 50^{\circ}$

$F_{incoh(50^{\circ})}$ = the value of F_{incoh} at $2\theta = 50^{\circ}$

Then, the Compton scattering intensity at various Bragg angles was calculated using eq.(17). The atomic scattering factors used in eq.(18) are taken from International Tables for X-ray Crystallography[63].

The polarization correction factor was calculated from the equation

$$K_{pol} = 2/(1 + \cos^2 2\theta) \qquad (20)$$

The absorption correction factor was calculated from the equation derived by Gingrich [65,66] for the incident beam normal to the film surface

$$K_{abs} = \frac{\mu d(1 - \sec 2\theta)}{\exp[\mu d(1 - \sec 2\theta)] - 1} \qquad (21)$$

where

μ = linear absorption coefficient

d = thickness of the film

The linear absorption coefficient μ was calculated from the equation

$$\mu = \rho \sum_i w_i \ (\mu_i/\rho_i) \qquad (22)$$

where

ρ = density of the sample

ρ_i = density of the i^{th} element

w_i = weight fraction i^{th} element in the sample

μ_i = linear absorption coefficient of i^{th} element

The ratio $(\mu/\rho)_i$ of i^{th} element is taken as the mass absorption coefficient from the International Tables of X-ray Crystallography[64].

A computer program for calculation of the corrected intensity of diffracted X-ray is shown in Appendix II.

Orientation functions of crystallites resulting from the crystallization under stress were measured by using the same X-ray diffractometer mentioned above. Crystallization of the stretched specimen was carried in the heated chamber provided with the X-ray diffractometer, whose temperature was controled by circulating heated air. After the crystallization proceeded for more than 5 hours, the measurement of the diffracted intensity from the (100) plane of the hexagonal crystal system of trans 1,4-polybutadiene[47] was started at various azimuthal angles. Azimuthal scanning was carried at every 5^o from 0 to 90^o of the azimuthal angle. The geometry of the experimental system is shown in Figure 4.

Assuming that the intensity of the amorphous halo is symmetrical with respect to its maximum position, the intensity of the diffracted X-ray from the amorphous phase at Bragg angle of the (100) reflection was estimated. The intensity at the Bragg angle which is a symmetric position of the (100) diffraction peak with respect to the maximum position of amorphous halo may be identical to the intensity of the amorphous halo at Bragg angle of the (100) reflection, according to the above assumption.

The correction of X-ray intensity was done by the same method described above.

The orientation function of the (100) normal of the hexagonal crystal system (high temperature form) was calculated as follows[42].

The orientation function of the (100) normal is expressed by the equation

$$f_{100} = (3\,\overline{\cos^2 \alpha_{100}} - 1)/2 \qquad (23)$$

If the incident beam is tilted at Θ_{100} and the detector was set at $(180^\circ - \Theta_{100})$ with respect to the normal of the samplefilm, the value $\overline{\cos^2 \alpha_{100}}$ may be represented by the equation[42]

$$\overline{\cos^2 \alpha_{100}} = \overline{\sin^2 \Omega_{100}} \qquad (24)$$

where Ω_{100} is the azimuthal angle. The value $\overline{\sin^2 \Omega_{100}}$ was estimated from the equation

$$\overline{\sin^2\Omega_{100}} = \frac{\int_0^{\pi/2} I(\Omega_{100}) \sin^2\Omega_{100} \cos\Omega_{100}\, d\Omega_{100}}{\int_0^{\pi/2} I(\Omega_{100}) \cos\Omega_{100}\, d\Omega_{100}} \qquad (25)$$

where $I(\Omega_{100})$ is the relative intensity of the diffracted X-ray by the (100) plane at the azimuthal angle Ω_{100}. The coordinate system used here is shown in Figure 5.

The orientation function of the (100) normal was measured at several extensions from $\alpha = 1.0$ to about 2.0 at two crystallization temperature, 85 and 95°C.

A computer program for calculation of the orientation function of the (100) normal by the above procedure is shown in Appendix III.

5. Calculation of the crystallinity

The crystallinity was calculated from the birefringence value and the stress measured simultaneously and the value of orientation function determined by X-ray method, as follows.

The observed birefringence value during crystallization may be expressed by the equation[41]

$$\Delta = \Delta_c X_c + \Delta_a(1 - X_c) + \Delta_F \qquad (26)$$

where Δ_c and Δ_a are the birefringence values per unit volume of crystalline and amorphous materials, X_c is the volume fraction of the crystalline phase, and Δ_F is the form birefringence. The values Δ_c and Δ_a may be evalu-

ated from the following equations

$$\Delta_c = f_c \Delta_c^o \qquad (27)$$

$$\Delta_a = C_T \cdot \sigma \qquad (28)$$

where Δ_c^o is the intrinsic birefringence of the crystal and f_c is the orientation function of the crystal. The value of the stress-optical coefficient of amorphous network at the crystallization temperature C_T was estimated from the plot of the stress-optical coefficient versus temperature above the melting point. The value Δ_c^o was theoretically determined from the crystalline structure and chain conformation of the high temperature form of trans 1,4-polybutadiene, using the principal of the additivity of bond polarizabilities[67]. The method for this calculation is shown in Appendix I.

Combining eq.(27) and (28) with eq.(26) and neglecting Δ_F, the change in crystallinity during crystallization under stress was calculated.

6. Photographic measurement of small angle light scattering

The light scattering pattern was measured by the conventional method developed in our laboratory, using the monochromatic laser as a light source[68]. The experimental system is shown in Figure 6.

The light scattering patterns of the film quenched

at the dry ice-methanol temperature from the molten state with and without strain were measured at room temperature. For the slowly cooled film from the molten state without strain, it was necessary to use very low film thicknesses, less than 2.0 mil because of the great amount of scattering. However, the thinner films did not give the same scattering pattern at different positions, probably because of inhomogeneous strain distribution in the film.

The light scattering patterns during crystallization without strain were measured using the hot stage designed for the study on the phase transition of liquid crystals. It took about 4 min to cool the specimen in the hot stage from 120 to 85°C (crystallization temperature).

For the experiment of the crystallization under strain, the film was stretched first. The stretched film was clamped between small metal frames and then set in the hot stage. In order to obtain the homogeneous elongation upon stretching the film, the stretching was carried at about 50°C.

The stretched sample in the hot stage was heated at 125°C for 10 min and then cooled down to the crystallization temperature. Temperature was controlled using an electric temperature controller (Versa-Therm).

The sample to film distance was set to about 16 cm. Exposure time was varied from 2 to 1/100 sec. to obtain the appropriate intensity on the picture, except when comparing the intensity differences with each other.

The experimental system for light scattering is illustrated in Figure 6.

To avoid surface scattering of the film, both sides of the film were covered with microscope cover glasses using a silicon oil immersion fluid. The refractive index of silicon oil was chosen to approximately match that of the polymer film.

IV. RESULTS AND DISCUSSION

1. The depression of the melting temperature due to the introduction of crosslinkage

The variation of the melting temperature of uncrosslinked trans 1,4-polybutadiene with the trans-content is shown in Figure 7, together with the results by several authors[52,69-73]. The melting temperature decreases with decreasing trans-content as theoretically expected. This is because cis- and vinyl-isomers randomly distributed along trans-isomer chain may be excluded from the crystalline phase because of their structural irregularity. The melting temperature of pure trans 1,4-polybutadiene has been reported to be 148°C[74].

Introduction of chemically and structurally different units into a homopolymer gives rise to some change in the size and perfection of crystals as well as the rate of crystallization[75], since such units can not occur in the crystalline phase. According to Flory's theory[76,77] of the fusion of copolymers, the depression of the melting temperature for random copolymer, consisting of A units which crystallize and B units which do not, may be represented by the equation

$$1/T_m - 1/T_m^o = -(R/\Delta H_u) \ln X_A \qquad (29)$$

where T_m^o is the melting temperature of homopolymer A,

ΔH_u is the heat of fusion of cryatallizing unit A, X_A is the mole fraction of A units in the random copolymer and R is the gas constant. The depression of the melting temperature was calculated, using ΔH_u = 1100 cal/mole[48] and T_m^o = 421°K. This is shown as a solid line in Figure 7. There exists quite a good agreement between the theoretical and experimental values.

When trans 1,4-polybutadiene (T_m = 96°C) was crosslinked with dicumyl peroxide, a further substantial reduction in the melting temperature was observed. The variation of the melting temperature of crosslinked trans 1,4 -polybutadiene with the molecular weight of network chain M_c is shown in Figure 8. M_c was determined from the intercept of Mooney-Rivlin plot which will be discussed later. The melting temperature appears to depend appreciably upon the degree of crosslinking. This is attributable to the steric irregularity of segments around the crosslinking points.

It has been shown by Mandelkern and his coworkers[78] that for natural rubber network, the melting point depression depends only on the fraction of crosslinked units and not appreciably on the nature of the crosslinking process. Kuhn[79,80] and Mandelkern[81] have studied this type of depression of melting temperature for cis-polybutadiene network crosslinked chemically and for polyethylene network crosslinked by irradiation, respectively.

Since in the process of crystallization, the chain units involved in crosslinkage may be excluded from the crystalline region and exist in the amorphous region, an increase in the entropy of fusion ΔS_m will be expected, compared with an uncrosslinked polymer. As a consequence, if the heat of fusion ΔH_m is independent of the introduction of crosslinking, the melting temperature must be depressed as given by the equation

$$T_m = \Delta H_m / \Delta S_m \qquad (30)$$

Flory[77,82] has theoretically predicted that the introduction of crosslinking will cause a depression of the equilibrium melting temperature. According to his theory, a reduction in the melting temperature for the networks may be represented by the equation

$$1/T_m - 1/T_m^o = (R/\Delta H_u)\cdot \rho \qquad (31)$$

where ρ is the fraction of units involved in crosslinkage. Then if the depression of the melting temperature due to crosslinking is measured, one can estimate the number of segments around each crosslinking point excluded from the crystalline region as follows.

Since ρ is the ratio of the number of units N_u involved in crosslinking and excluded from the crystalline region to the total number of units N_u^o included in networks, ρ is given by the equation

$$\rho = N_u / N_u^o \qquad (32)$$

If it is assumed that N_u is proportional to the number

of chains and that they have the same number of units at their crosslinking points, which are excluded from crystalline region, then

$$N_u = K \cdot \nu \qquad (33)$$

where K is a constant. Since ν and N_u^o are given by the equations

$$\nu = (\rho_o/M_c)A \qquad (34)$$

$$N_u^o = (\rho_o/M_o)A \qquad (35)$$

where ρ_o is the density of amorphous network, A is Avogadro's number, M_c and M_o are molecular weights of the chain and the monomer unit, respectively. Then, eq.(32) is transformed to eq.(36)

$$\rho = K(M_o/M_c) \qquad (36)$$

By replacing eq.(36) in eq.(31),

$$(T_m^o - T_m)/T_m T_m^o = (R/\Delta H_u) \cdot K \cdot M_o \cdot (1/M_c) \qquad (37)$$

As a consequence, $(T_m^o - T_m)/T_m$ may be inversely proportional to M_c and the K value will be calculated.

The quantity $(T_m^o - T_m)/T_m$ is plotted against $1/M_c$ in Figure 9 . There exists quite a good proportionality between $(T_m^o - T_m)/T_m$ and $1/M_c$ which gives K = 10. This means that each network chain may have five monomer units around its crosslinking point which can not participate in crystallization. Since the number of monomer units per statistical segment in amorphous network of trans 1, 4-polybutadiene is about 3.5, then 1.4 segments per chain at a crosslinking point may be prohibited to crystalliza-

tion.

From the dimension of unit cell of trans 1,4-polybutadiene the radius of a cylindrical segment is calculated as $r_o = 2.5$ Å. Since the length of the segment is 3.5×4.65 Å $= 15.3$ Å, the volume around each crosslinking point v_o which is sterically prohibited volume to crystallization is calculated as

$$v_o = 1.7 \times 10^{-21} \text{ cm}^3$$

This value is in a good agreement with Gent's value[83] for crosslinked natural rubber $v_o = 5.1 \times 10^{-21}$ cm^3. He estimated his value from the volume contraction accompanied by crystallization.

The reduction in the segment mobility due to crosslinking may give rise to a significant effect on the retardation of the secondary nucleation on the crystal surface and the subsequent crystal growth. Then it might be said that the real number of segments at each crosslinking point which are prohibited from participating in crystallization is larger than $4 \times 1.4 = 5.6$, obtained in this work.

In the basis of thermodynamic consideration of the fusion of polymers, eq.(31) may not be applicable when there are some restictions in the size and perfection of crystallites. In fact, the film of trans 1,4-polybutadiene was observed to become transparent with an increase in the degree of crosslinking. This may be attributed to the

decrease in size of crystallites and the imperfection of the crystallites as well as the decrease in crystallinity and the decrease in size of the crystalline superstructure. Mandelkern[81] has observed from the change of the half width of the (110) diffraction peak of crosslinked polyethylene that crystallization can not be developed in such a way that crystallite is as perfect as that of the non-crosslinked polymer.

2. The stress-optical coefficient and the anisotropy of the statistical segment of the amorphous network

The stress-strain relations for the amorphous network of trans 1,4-polybutadiene in simple extension are shown in Figure 10. The variation of the stress with strain gradually deviates from a linear relationship at higher extensions than $\alpha^2 - 1/\alpha = 0.6$. This non-linearity of the stress against the value $(\alpha^2 - 1/\alpha)$ plots is attributed to the physical interaction between network chains, such as molecular entanglements.

The statistical theory of rubber elasticity may describe the stress-strain behaviour of a crosslinked ideal rubber by the equation[84]

$$\sigma = N_c K T (\alpha^2 - 1/\alpha) \qquad (38)$$

where N_c is the number of chains per unit volume, α is

the extension ratio, and k is Boltzmann's constant. For strains below those which give rise to the non-Gaussian chain distribution[8,45,85-87] due to the finite extensibility of network chains, the stress may be represented by the equation proposed by Mooney and Rivlin[49,50]

$$\sigma/(\alpha^2 - 1/\alpha) = 2C_1 + 2C_2/\alpha \qquad (39)$$

The constant C_1 is dependent upon the degree of crosslinking and is associated with elastic modulus. The constant C_2 represents deviations from the kinetic theory of rubber elasticity. It is independent of the degree of crosslinking.

A Mooney - Rivlin plot for trans 1,4-polybutadiene for various degrees of crosslinking at 110°C is shown in Figure 11. The molecular weights of network chains determined from the equation $2C_1 = \rho RT/M_c$ are indicated in the same figure. The deviation of the stress from the kinetic elasticity theory is reflected by the slope of this plot. It is clear that the slope of each plot is not affected by the degree of crosslinking.

The optical anisotropy of the deformed network arises from the orientation of anisotropic statistical segments, which is induced by elongation. According to the theoretical treatment by Kuhn and Grun[8,84] and by Treloar[9,58], on the optical properties of the Gaussian network subjected to a simple elongation, the refractive indecies of the strained network for light with its electric vector parallel to the extension direction n_1 and with its electric vector

perpendicular to the extension n_2 are given as the equations

$$n_1 = \bar{n} + \frac{(\bar{n}^2 + 2)^2}{\bar{n}} \frac{4\pi}{135} N_c(b_1 - b_2)_s(\alpha^2 - 1/\alpha) \quad (40)$$

$$n_2 = \bar{n} - \frac{(\bar{n}^2 + 2)^2}{\bar{n}} \frac{2\pi}{135} N_c(b_1 - b_2)_s(\alpha^2 - 1/\alpha) \quad (41)$$

where b_1 and b_2 are the principal polarizabilities of the statistical segment parallel and perpendicular respectively, to its axis, and $\bar{n}$ is the average refractive index of the network which is assumed independent of the strain. Then the birefringence of the stretched network is given by the equation

$$\Delta n = n1 - n2 = \frac{(\bar{n}^2 + 2)^2}{\bar{n}} \frac{2\pi}{45} N_c(b_1 - b_2)_s(\alpha^2 - 1/\alpha) \quad (42)$$

If this equation is combined with eq.(38), one can obtain the linear birefringence-stress relation

$$\Delta n = C \cdot \sigma \quad (43)$$

where C is the stress-optical coefficient which is independent of the strain[58,88]

$$C = \frac{(\bar{n}^2 + 2)^2}{\bar{n}} \frac{2\pi}{45kT} (b_1 - b_2)_s \quad (44)$$

Since eq.(44) does not involve N_c, the stress-optical coefficient is independent of the degree of crosslinking of the network and characteristic of the molecular property of the chain.

The variation of the birefringence for trans 1,4-polybutadiene at 110°C with stress is given in Figure 12. There exists quite a good proportional relation between the birefringence and the stress even if the stress was observed to significantly deviate from eq.(38). The slopes for these plots at the same temperature of measurement are not appreciably changed with the degree of cross-linking.

The stress-optical coefficient given as the slope of the birefringence-stress relation in Figure 12 is shown as a function of temperature in Figure 13. The strain - optical coefficient increases on the same curve with decreasing temperature, irrespective of the difference in the degree of crosslinking. This variation may come from changes in the temperature of measurement, refractive index, and the optical anisotropy of the statistical segment. At the temperatures in this work, the effect of the refractive index change on the value $(\bar{n}^2 + 2)^2/\bar{n}$ was negligibly small. Then the stress - optical coefficient may be a measure of the optical anisotropy of the statistical segment at various temperatures.

The optical anisotropy $(b_1 - b_2)_s$ calculated from eq.(44) is given as a function of temperature in Figure 14. A value of $(b_1 - b_2)_s = 12.3$ $\mathring{A}^3$ for the 85% trans-content sample at 110°C was observed in this work. Values of 10.2 $\mathring{A}^3$ at 100°C by Fukuda[52] and 8.56 $\mathring{A}^3$ at 95°C by

Nagai[89] for 91% trans-content have been reported. These values are slightly different from each other. Figure 14 shows that the values $(b_1 - b_2)_s$ decrease with increasing temperature. This decreases by about 15% as the temperature is increased from 100 to 140°C. It has been reported by Volungis and Stein[90] and by Gent and Vikroy[91] that the value $(b_1 - b_2)_s$ for crosslinked polyethylene decreases by 10 to 30% with increasing temperature from 120 to 170 °C. If one assumes that $(b_1 - b_2)_s$ is proportional to the length of the statistical segment, this may show that the segment becomes shorter and less stiff, or more flexible as temperature is increased.

As has been mentioned before, it is observed that there exists an accurately proportional relation between the birefringence and the stress. Since the stress-strain relation is observed to fit the Mooney-Rivlin equation, the birefringence-strain relation may also be represented by a Mooney-Rivlin type equation[89,92]

$$\Delta n/(\alpha^2 - 1/\alpha) = B_1 + B_2/\alpha \qquad (45)$$

The above observations have been reported for natural rubber and gutta-percha by Saunders[93] and by Smith and Brett[94], and for cis-butadiene and cis-isoprene rubbers by Nagai[92].

In the similar manner as before, the stress-optical coefficient may be given as

$$C = \frac{B_1 + B_2/\alpha}{2(C_1 + C_2/\alpha)} \qquad (46)$$

Since $C_1/C_2 \neq B_1/B_2$ was observed by Nagai[92], C may be strain - dependent. But the fact that the stress-birefringence has an accurately linear relation in this work may show that $C_1/C_2 \simeq B_1/B_2$ within some experimental errors which may mostly come from the difficulty in the precise measurement of homogeneously elongated length. In order to estimate the variation of the birefringence from the change in stress, it may be quite useful to eliminate the extension terms ($\alpha^2 - 1/\alpha$) and ($B_1 + B_2/\alpha$) by taking the ratio of the birefringence to the stress. The amorphous contribution to the total birefringence during crystallization under stress is evaluated from the change in the stress. This will be discussed later.

The deviation of the stress from the kinetic elasticity theory which is represented by C_2 shows that $(b_1 - b_2)_s$ obtained for unswollen state is not a true optical anisotropy characteristic of the statistical segment itself. Many authors[95,96] have noticed that C_2 decreases for the swollen state with swelling ratio and approaches zero. The network chain may become isolated due to the loss of physical molecular interactions caused by swelling. This may reduce the internal field effect of dipoles on the birefringence.

Recently it was reported by Gent[97] and by Nagai[92]

that the stress-optical coefficient of amorphous networks of 1,4-polyisoprene and 1,4-polybutadiene are appreciably affected through the orientation of the solvent molecule with respect to polymer chains by the nature of swelling solvent, such as its size and the optical anisotropy. Thus, it may be said that the exact meaning of C_2-term of eq.(39) is still uncertain.

3. The variation of stress and birefringence during crystallization under stress

The progress of crystallization in the stretched polymer film at constant length could be followed by observing the corresponding changes in tensile stress and birefringence. The sample was stretched in its molten state at 110°C and then rapidly cooled down and held at the required crystallization temperature. Simultaneous measurements of the stress and the birefringence were performed.

The variation of the stress during crystallization at various extension ratios is shown in Figure 15 - 17.

Extension could not exceed 200% because of breaking of the films. The tensile stress decreases gradually as crystallization proceeds. The rate of stress relaxation is quite dependent upon the extension ratio and the crystallization temperature. The stress relaxation in this work is attributed to the formation of oriented crystallites

which result from the progressive alignment of chain segments in the crystallites.

The result of the simultaneous measurement of birefringence and stress is given in Figure 18 - 23. The substantial increase in birefringence with time arises from the resulting crystallites which are oriented at some preferential angle with respect to the stretching direction.

The stress relaxation due to the crystallization is significantly different from the normal stress relaxation phenomena due to plastic flow, which results from the breakdown of the cohesive links due to van der Waal's forces, or due to cohesive mechanical entanglements[5,98]. The stress relaxation phenomena of amorphous polymer due to the flow is always accompanied by a decrease in birefringence, keeping the stress-optical coefficient constant [99-102]. As a consequence, the increase in birefringence in this work indicates that crystallization takes place with molecular orientation with respect to the stretching direction.

In oriented crystallization of polymer network, two significant contribution to entropy change are considered as follows: a segment, when participating in the crystallization, sacrifices all its configurational freedom and accordingly the entropy decreases. The displacement length of a chain in the amorphous portion is altered when crystallization takes place. Since the crystal grows parallel

to the stretching direction (Z-axis) in Flory's theory[18], the Z-component of the displacement vector is decreased. This gives rise to the additional entropy change according to the elasticity theory of a molecular network.

Combining the entropy change above with the enthalpy change due to crystallization, the free energy difference between the semi-crystalline stretched polymer network and the totally crystalline polymer ΔF is calculated. By differentiating the free energy difference ΔF with respect to the extension ratio, one can derive the tensile force of the stretched rubber f subjected to the crystallization.[18]

$$f = (\partial \Delta F/\partial \alpha)$$

$$= (\partial \Delta F/\partial \alpha)_{X_c} + (\partial \Delta F/\partial X_c)_{\alpha}(\partial X_c/\partial \alpha) \qquad (47)$$

where f is the force per unit initial cross-sectional area, X_c is the crystallinity, and α is the extension ratio. Since $(\partial \Delta F/\partial X_c)_{\alpha} = 0$ at equilibrium with respect to crystallinity, the tensile force is given by the equation

$$f = (\partial \Delta F/\partial \alpha)_{X_c} \qquad (48)$$

From this equation, Flory[18] obtained eq.(49) for tensile stress.

$$f = N_c RT\left[(\alpha - 1/\alpha^2) - (6n_s/\pi)^{\frac{1}{2}}X_c\right]/(1 - X_c) \qquad (49)$$

If $\alpha = 1$, eq.(49) reduces to the equation for an amorphous Gaussian chain network[7].

$$f = N_c RT(\alpha - 1/\alpha^2) \qquad (50)$$

or

$$\sigma = N_c RT(\alpha^2 - 1/\alpha) \qquad (51)$$

where σ is the stress per unit actual area.

From eq.(49), it is expected that the crystallization due to elongation decreases the tensile stress. Gent[11,12,103] applied the Flory's theory of equiliblium state for considering progressive crystallization. He considered that the tensile stress at a given degree of crystallinity might be expressed by eq.(49). From eq.(49), the degree of crystallinity is given by the equation

$$X_c = \frac{(\sigma_o - \sigma)(\alpha - 1/\alpha^2)}{\sigma_o(6n_s/\pi)^{1/2} - \sigma(\alpha - 1/\alpha^2)} \qquad (52)$$

If $\sigma_o(6n_s/\pi)^{1/2} \gg \sigma(\alpha - 1/\alpha^2)$, then

$$X_c = \frac{\sigma_o - \sigma}{\sigma_o}(\alpha - 1/\alpha^2)\left(\frac{\pi}{6n_s}\right)^{1/2} \qquad (53)$$

where σ_o is the stress before crystallization takes place. Thus, the amount of stress relaxed $(\sigma_o - \sigma)$ is proportional to the corresponding amount of crystallinity X_c throughout crystallization process. Gent[11] studied this relation by determing the crystallinity from the volume contraction. A good proportionality between both quantities was obtained at high elongations. It should be noted that eq.(53) is only applicable to highly elongated networks since the crystallites have been assumed to be oriented to the stretching direction.

In our experiment, extension was less than about 200%. The measurements of X-ray diffraction and small angle light scattering showed that the orientation of chain axis in crystallities was not parallel to the streching direc-

tion. These will be discussed later.

As has been mentioned in the section II, the statistical theory of rubber elasticity may be applied for the amorphous phase during crystallization as shown in the following equation

$$\Delta_a = \Delta_a^0 \cdot f_a = C_T \cdot \sigma \qquad (54)$$

where Δ_a is the birefringence value per unit volume of amorphous portion. Combining eq.(54) with eq.(4) the amorphous contribution to the total birefringence was calculated. The results are shown in Figure 18-23. As the crystallization progresses, the amorphous contribution decreases. The increase in total birefringence is much larger than the decrease in the amorphous contribution. The decrease in the amorphous contribution is a consequence of a decrease in the amount of amorphous phase as well as decrease in amorphous orientation.

The stress in a highly elongated rubber which crystallizes during stretching is substantially larger than when no crystallization occurs[10,21]. It is involved in non-equilibrium crystallization and is quite different from that described in this work. The change of elastic modulus is attributed to the crystallites formed during isothermal stretching, which may act as additional cross-linking points or as reinforcing fillers. Mechanical properties of very low crystalline polymers (less than 10 to 20%) have been studied by assuming the crystallites to act

as the fillers[104,105].

If crystallites grown during crystallization under stress act as a filler, the tensile stress at a given crystallization time may not arise only from the strain of the amorphous portion. In order to estimate the true stress due to the strained amorphous portion, the theory of filler effect developed by Guth[106] and Smallwood[107] was used.

$$F(\phi) = 1 + 2.5\phi + 14.1\phi^2 \qquad (55)$$

where ϕ is the volume fraction of fillers in the amorphous matrix. Thus, the actual stress σ may be expressed by the equation

$$\sigma = F(\phi) \cdot \sigma_a \qquad (56)$$

where σ_a is the stress due to the strained amorphous portion. As a consequence, eq.(57) may be used for describing the value Δ_a, rather than eq.(54).

$$\Delta_a = C_T \cdot \sigma_a$$

$$= C_T \cdot \sigma / F(\phi) \qquad (57)$$

As a first approximation, Δ_a was calculated from eq.(57), by using the value ϕ which was determined from eq.(4) and (54). The effect of crystallites as the fillers on the amorphous contribution of birefringence is shown as broken lines in Figure 18-23. The amorphous contribution calculated when considering the filler effect decreases more rapidly with time than the value previously calculated from the combination of eq.(4) and (54).

4. The orientation of erystallites resulting from crystallization under stress

The plot of the eorrected intensities of X-ray diffraction from crosslinked trans 1,4-polybutadiene (M_c = 16200) erystallized in the unstreched state versus Bragg angles at various temperatures is shown in Figure 24. At temperatures below the melting point of crystallites (T_m = 91°C), two diffraction peaks were observed for each intensity distribution curve. One is a very intense peak due to (100) refleetion of the hexagonal crystal lattiee indexed by Natta[48], the other is an amorphous halo whieh appears as its shoulder.

The (100) diffraction peak at $2\theta = 22.1^\circ$ at 30°C due to the pseudo-hexagonal erystal system ehanged its position of Bragg angle to the valuc $2\theta = 20.6^\circ$ at about 50°C, due to the hexagonal erystal system (high temperature form). This abrupt change of Bragg angle eomes from the crystal-crystal transition which has been studied by several authors[74,114-116]. With further increase in measurement temperature, the intensity of the (100) diffraction peak deereased and at about 100°C this peak disappeared beeause of the melting of erystallites. On the other hand, the amorphous halo inereased its intensity with inereasing temperature. Thc Bragg angle at whieh the intensity maximum of the (100) diffraetion of the high temperature form

occurs was unchanged with increasing temperature. However, the corresponding Bragg angle of the amorphous halo decreased with increasing temperature.

The length of the a-axis of both hexagonal unit cells were calculated from the (100) spacings which were determined using Bragg's law.

$$d_{100} = \lambda/2\sin\theta_{100} \qquad (58)$$

The calculated values of the length of the a-axis are shown in Table 1, together with Natta's[48] and Takayanagi's[117] values. These values are consistent with each others.

The X-ray diffraction measurement of the orientation of crystallites was made on the sample subjected to crystallization in the stretched state at various elongation at two crystallization temperature, 85 and 95°C. Crystallization was carried out in the heated chamber provided with the X-ray diffractometer. The measurement was started after the crystallization proceeded for more than 5 hours.

The X-ray diffraction patterns which were obtained are shown in Figure 25. The (100) reflection has an intensity distribution in which the maximum intensity is on the equator showing that the (100) planes of the crystal become aligned parallel to the stretching direction. Since the orientation of the c-axis of this crystal form f_c is uniquely defined by the orientation of the (100) normal f_{100} because of its hexagonal symmetry according to the equation[124,125]

$$f_c = -2f_{100} \qquad (59)$$

it is evident that the c-axis becomes preferentially oriented parallel to the streching direction. This is consistent with the increase in birefringence with time which has been discussed in the previous section.

This result is quite distinct from the crystal orientation which has been observed by Stein and his coworkers [29,30] for crosslinked polyethylene film crystallized from the oriented melt. They observed the a-axis orientation and the negative birefringence at low elongations which show that crystals are oriented with their c-axes perpendicular to the streching direction. Keller[26-28] and Krigbaum[31] observed in their similar experiments on crosslinked polyethylene that the maximum position of the a-axis distribution was changed from the meridian to a certain angle near the equator with increasing elongation ratio, and that the b-axis was preferentially oriented perpendicular to the streching direction all over the range of elongation. For this observation, Keller and his coworkers[26-28] have proposed the row structure in which the b-axis orientation is perpendicular to the stretching direction with the a- and c-axes randomly oriented around the b-axis, or with c-axis parallel to the stretching direction, depending upon the stress.

The results in this work are similar to those of Krigbaum and Roe on polychloroprene[118], of Yau and Stein[36,37]

on crosslinked natural rubber and of Andrews[20] on natural rubber. They all observed that the c-axes aligned toward the streching direction while the a- and b-axes are randomly distributed around the c-axis. As has beenpointed out in the previous section, the observation of the orientation of crystal is important to elucidate the nature of oriented crystal growth and its mechanism, and the subsequent morphology of crystallized network.

The orientation function was calculated using the method described in the section III.4. The variation of the orientation function at two crystallization temperatures 85 and 95°C as a function of the elongation ratio is shown in Figure 26. The orientation function is strongly dependent upon the crystallization temperature, but almost independent of the elongation ratio ($\alpha \leq 2.0$) used in this work. The c-axis orientation function becomes more positive indicating orientation more parallel to the stretching direction with decreasing crystallization temperature. At considerable lower temperature the stress required to maintain the original stretched length fell to zero in a short times. This may be attributed to the large orientation function of the crystal c-axis as well as the large amount of crystallinity developed in a short time.

The crystal orientation behaviour in the process of crystallization under stress may result from the thermodynamic effect of equilibrium crystallization base on the

segment orientation of amorphous network. According to the statistical treatment of a random long chain by Kuhn and Grun[8], the birefringence of a strained network is derived using a series expansion of the inverse langevin function as the equation

$$\Delta = n_1 - n_2$$

$$= N_c(b_1 - b_2)_s\left[\frac{1}{5}(\alpha^2 - 1/\alpha) + \frac{2}{175n_s}(6\alpha^4 + 2\alpha - \frac{8}{\alpha^2}) + \frac{6}{875n_s^2}(10\alpha^6 + 6\alpha^3 - \frac{16}{\alpha^3}) + ----\right] \qquad (60)$$

where N_c is the number of chains per unit volume and $(b_1 - b_2)_s$ is an anisotropy of polarizability of the stastical segment. If we use the segment orientation function which is given by the equation

$$f_s = (3\cos^2\theta_s - 1)/2 \qquad (61)$$

in order to describe the orientation of amorphous chains, then the birefringence of strained network may be also represented by the equation

$$\Delta = N_s(b_1 - b_2)_s f_s \qquad (62)$$

where N_s is the number of segment per unit volume. As a consequence, the Kuhn-Grun theory of Gaussian network chains which is given by the first term of eq.(60) predicts that the segment orientation function of Gaussian network chain is represented as the equation

$$f_s = \frac{1}{5}(N_c/N_s)(\alpha^2 - 1/\alpha) \qquad (63)$$

The value (N_c/N_s) is identical to the inverse value of the number of segment per chain. Since value (N_c/N_s) is able to be calculated experimentally using eq.(10), (11) and (12), one can calculate f_s as a function of the elongation ratio.

Considering a little increase in stiffness of the chain in the amorphous phase at the crystallization temperature, the number of segments per chain were determined as about 80 for both crystallization temperatures, 85 and 90 °C. Then eq. (63) is transformed to the equation

$$f_s = \frac{1}{400} (\alpha^2 - 1/\alpha) \qquad (64)$$

Using eq. (64) the value f_s of stretched network prior to the crystallization was calculated. The result is shown in Figure 26.

In this figure, theory shows that the orientation of the amorphous chain before the onset of crystallization is surprisingly lower than the crystal orientation function. How does such a high crystal orientation come from in the process of crystallization under stress?

This question has been studied by Krigbaum and Roe[118], assuming that the nucleation process controls the overall crystalline orientation distribution in the crystallized sample. They derived the orientation distribution function $W(\theta_s)$ for the segments of streched amorphous network at fairly low elongation[119].

$$W(\theta_s) = 1/2 + (1/4n_s)(3\overline{\cos^2\theta_s} - 1)(\alpha^2 - 1/\alpha) + \cdots \quad (65)$$

where θ_s is the angle which the segment makes with the stretching direction, and n_s is the number of statistical segmants per chain. Since the value $\overline{\cos^2\theta_s}$ is calculated from the equation

$$\overline{\cos^2\theta_s} = \frac{\int_0^{\pi} W \cdot \cos^2\theta_s \cdot \sin\theta_s \, d\theta_s}{\int_0^{\pi} W \cdot \sin\theta_s \cdot d\theta_s} \quad (66)$$

the value f_s is calculated from eq. (61). This gives the same equation as eq.(63) which was developed by Kuhn and Grün[8].

The crystal growth may be a consequence of repeated secondary nucleation on the surface of crystals and subsequent rapid growth in two dimensions[120-122]. The rate of nucleation may be expected to depend upon the segment orientation in the polymer melt. In the process of growth, the orientation of segments which diffuse from melt to crystal may be the same as that of segments in the nucleus upon which growth occurs.

Provided that the critical nucleus contains ν statistical segments whose alignment is in the same direction. If $P(\phi)d\phi$ is taken as the probability of finding a statistical segment in amorphous chain with its axis oriented in the range of angle $(\phi, \phi + d\phi)$, the rate of nucleation $R(\phi)$ may be represented by the equation

$$R(\phi) = K\left[P(\phi)\right]^{\nu} \tag{67}$$

where K is constant. Using eq.(65) for the function $P(\phi)$, Krigbaum and Roe[118] derived the orientation distribution function of the crystal c-axis.

$$f_c(\theta_s) = \frac{\left[w(\theta_s)\right]^{\nu}}{\int_0^{\pi}\left[w(\theta_s)\right]^{\nu}\sin\theta_s \cdot d\theta_s} \tag{68}$$

then

$$\overline{\cos^2\theta_c} = \int_0^{\pi} f_c(\theta_s)\cos^2\theta_s d\theta_s \tag{69}$$

In their derivation of eq.(68) and (69), they assumed that the orientation distribution of crystallites may be the same as the segment orientation distribution of the secondary nuclei which have been originated so far.

It is very interesting that the critical volume of nuleus which is represented by the value ν may affect the crystal growth in the oriented crystallization and the crystal orientation of subsequent crystalline networks. Since the crystal orientation is not appreciablly affected by the elongation in this work and also the segment orientation function f_s calculated theoretically is not much changed with elongation, the value ν may be almost constant according to eq.(68) and (69). But the change of the crystallization temperature may give rise to the change of the value ν because the crystal orientation function is affected by the crystallization temperature. According to the classical nucleation theory developed by Frankel[120],

the critical volume of the nucleus is expressed by the equation[121,122]

$$v^* = \frac{4\sigma_1\sigma_2 d}{h_f}\left(\frac{T_m}{T_m - T}\right)^2 \qquad (70)$$

where σ_1 and σ_2 is the interfacial free energy between crystal and its melt, h_f is the heat of fusion of crystal, d is the thickness of the nucleus on the crystal surface, T_m is the equilibrium melting temperature and T is the temperature at which nuclei are formed. As a consequence, the value γ may be decreased with decreasing crystallization temperature and may result in the increase in the crystal orientation function according to eq.(68) and (69).

5. Variation of crystallinity with elongation

As has been seen in the section IV.3, the birefringence of trans 1,4-polybutadiene in its stretched state increases as crystallization proceeds. It is important for studies of crystallization kinetics to know how much the increase in crystallinity will be reflected in the increase in the birefringence. In order to describe the birefringence change during crystallization, the effect of crystal orientation and that of the strained amorphous network have to be considered.

As has been discussed before, the total birefringence of crosslinked trans 1,4-polybutadiene during crystalliza-

tion under stress may be given by eq.(1)[42,43]. Since the crystal and amorphous orientation functions f_c and f_a is related to the crystal and amorphous birefringence values, Δ_c and Δ_a, respectively by eq.(2) and (3), the crystallinity at a given time after the onset of crystallization may be derived from eq.(1) as the following equation

$$X_c = \frac{\Delta - \Delta_a^o \cdot f_a}{\Delta_c^o \cdot f_c - \Delta_a^o \cdot f_a} \qquad (71)$$

where Δ_c^o and Δ_a^o are the intrinsic birefringence values of the crystalline and amorphous phases, respectively. Substituting eq.(5) into eq.(71), eq.(71) is transformed to eq.(72)

$$X_c = \frac{\Delta - C_T \cdot \sigma}{\Delta_c^o f_c - C_T \cdot \sigma} \qquad (72)$$

where C_T is the stress- optical coefficient of amorphous phase of this polymer at the crystallization temperature, and σ is the stress during crystallization. Thus, the crystallinity is represented as a function of stress and birefringence.

The determinations of values Δ_c^o, f_c and C_T have been discussed in the previous sections.

The crystallinity of this polymer was calculated from eq.(72) by the simultaneous measurement of stress during crystallization. The variation of crystallinity with time at the crystallization temperatures of 85, 90 and 95°C are shown in Figures 27, 28 and 29. At each cry-

stallization temperature, the crystallinity increases rapidly with increasing elongation ratio. The strain in the melt significantly effects the rate of crystallization. Gent[11,12] has observed a similar effect of the strain on the crystallizations of crosslinked natural rubber, trans-polyisoprene and trans-chloroprene. Andrews[20] has observed for natural rubber that the rate of growth of α-filaments is not appreciablly affected but the rate of their nucleation increases with increasing the strain.

As is seen from eq.(52), the crystallinity is a function of stress alone. The crystallinity calculated from eq.(52) using the value of stress is shown in Figures 30 and 31, together with the experimental values determined from eq.(72). The crystallinity at the same crystallization time (100 min at 90 and 95°C, and 30 min at 85°C) increases with increasing elongation ratio and with decreasing crystallization temperature. The crystallinity at 90 and 95 °C determined from eq.(72) is more than three times higher than those calculated from the Flory's equation. The crystallinity at 85°C is a little closer to the calculated value than that in the case of crystallization temperatures of 90 and 95°C. This tendency is consistent with the results of crystal orientation measurements in which the crystal orientation function increases with decreasing the crystallization temperature.

The effect of the crystallites as a filler which

has been discussed in the previous section is shown in the same figures. The difference from the crystallinity calculated from eq.(72) shows that the filler effect increases with increasing elongation ratio because the rate of crystallization is increased with elongation.

The growth of the crystalline phase of this polymer was measured from the increase in crystallinity calculated above.

When the nuclei appear randomly in space and then grow at a certain rate, the change in crystallinity with time may be described by the Avrami relation for the phase transformation[108-110].

$$X_c = X_\infty \left[1 - \exp(-k' t^n)\right] \qquad (73)$$

where X_c is the crystallinity at a given time, X_∞ is the crystallinity at the final state of crystallization, k' represents the rate constant of crystallization and n is the Avrami index, depending upon the mode of nucleation and crystal growth. For small amount of crystallinity, eq.(73) is reduced to the equation

$$X_c \simeq k'' t^n \qquad (74)$$

Then

$$\ln X_c = n \cdot \ln t + \ln k'' \qquad (75)$$

Eq.(74) corresponds to the case of free growth of crystal without impingement. The quantity $\ln X_c$ is plotted against $\ln t$ in Figures 32,33 and 34. The value n is observed to be about 0.7 - 1.0. This shows that the crystal growth may

be one-dimensional like the rod-like crystal growth. The value n was observed about 1.0 by Gent[11] for crosslinked natural rubber which was stretched at $\alpha = 3.0$.

The Avrami index n for homopolymer which contains the non-crystallizing units along its chain or for crosslinked polymer has been observed by several authors to be smaller than the theoretical value which is determined from the mode of crystal growth of pure homopolymer. Gent[103] observed $n = 1.8 \sim 2.5$ for the normal crystallization of crosslinked trans-isoprene instead of $n = 3.0$ for the uncrosslinked one. He also observed $n = 2.0$ for the crosslinked trans-chloroprene whose trans content is 93%[12]. These observation may result from the retardation of crystallization in the later stage. The crystal growth habit is not changed by the presence of chain irregularity. As a consequence, it may be impossible to describe the isothermal crystallization curve by a unique value of n as far as eq.(73) is used. Gornick and Mandelkern[111] have developed a theory which shows that the presence of small amount of non-crystallizing units causes a substantial retardation of crystallization as crystallization proceeds. In fact, the crystallization curve of branched polyethylene was observed to deviated appreciably from that expected from the Avrami equation[112,113]. It may be due to the presence of cis- and trans- isomers in this polymer that the plot of $\ln X_c$ versus $\ln t$ deviates from the linear relationship in this work.

6. The light scattering studies on the morphology of trans 1,4-polybutadiene

(1) Superstructure resulting from the crystallization without stress. The small angle light scattering patterns of trans 1,4-polybutadiene films crystallized without stress are shown in Figures 35,36 and 37. Light scattering patterns characteristic of three kinds of superstructure were observed, depending upon the crystallization condition. The film which was rapidly crystallized by quenching from the molten state to the dry ice-methanol temperature gave the 0°- 90° type H_V patterns and the 45° type V_V patterns shown in Figure 35. The 45° type H_V patterns shown in Figure 36 were observed for the film which was crystallized at $87^{\circ}C$ for 5 hours. This H_V pattern has same orientation of intensity distribution with respect to the polarization directions as that of a typical four-leaf clover pattern from polyethylene.[125,126] However, the intensity of scattered light decreases continuously with increasing scattering angle, rather than passing through a maximum.

Similar types of H_V scattering patterns havebeen presented by Stein and his coworkers[127-129] for polytetrafluoroethylene and polychlorotrifluoroethylene as a function of their crystallization conditions. These polymers exhibit two types of scattering patterns characteristic of two different orientations of optic axes with respect to the prin-

cipal dimension of the scattering structure. They also show 45° type H_V patterns at higher crystallization temperature and 0°- 90° type H_V patterns at lower crystallization temperatures. The 0°- 90° type H_V patterns are often observed for collagen materials.[130]

The polyethylene-type pattern is well understood and quantitatively explained on the basis of the scattering from an anisotropic sphere or disk in which the optic axis is perpendicular to the radius and orients helicoidaly about the radius.[125,126] Both sphere and disk models predict that the H_V scattering intensity rises to a maximum at some particular scattering angle characteristic of the size of the sphere or disk and approaches zero with increasing the scattering angle. This spherulitic model can not explain the experimentally observed scattering patterns obtained with and without deformation of polytetrafluoroethylene film.[131] The rod model has been examined for this kind of morphology by Stein and his coworkers.[132,133]

The amplitude of scattered light from a rod of length L and infinitesimal thickness may be represented by the equation

$$E' = C(\underset{\sim}{M},\underset{\sim}{Q}) \frac{\sin(kaL/2)}{(kaL/2)} \qquad (76)$$

where

$$a = (1 - \cos\theta)\sin\alpha\cos\phi - \sin\alpha\sin\phi\sin\theta\sin\mu - \cos\alpha\sin\theta\cos\mu \qquad (77)$$

which reduces to the equation

$$a = -\cos(\alpha - \mu)\sin\theta \tag{78}$$

for the case $\phi = 90^{\circ}$. The angles α and ϕ are the angular coordinates of the rod axis shown in Figure 38. The angle α is the tilt of the rod as measured from the Z-axis. The angles θ and μ are the scattering angle and azimuthal angle, respectively.

$\underset{\sim}{M}$ is the induced dipole moment and for anisotropic rods with optic axis lying along the rod axis

$$\underset{\sim}{M} = \frac{\delta\cdot(\tilde{E},\tilde{r})\tilde{r}}{r^2} + \alpha_2\underset{\sim}{E} \tag{79}$$

where $\underset{\sim}{r}$ is a vector along the rod to the scattering element and given as the following equation for the case $\phi = 90^{\circ}$.

$$\underset{\sim}{r} = r\,(\sin\alpha\cdot\underset{\sim}{j} + \cos\alpha\cdot\underset{\sim}{k}) \tag{80}$$

δ is the anisotropy

$$\delta = \alpha_1 - \alpha_2 \tag{81}$$

where α_1 and α_2 are the polarizabilities parallel and perpendicular to the rod.

For a distribution of rods where $N(\alpha)d\alpha$ are in the angular interval $(\alpha, \alpha + d\alpha)$ with no phase coherence among them, the total scattered intensity is expressed by the equation

$$I = KL^2\int_0^{2\pi}(\underset{\sim}{M}\cdot\underset{\sim}{O})^2 N(\alpha)\,\frac{\sin^2(kaL/2)}{(kaL/2)^2}\,d\alpha \tag{82}$$

where K is constant. For a random distribution, $N(\alpha) = N/2\pi$ where N is the total number of rods.

Since the vector $\underset{\sim}{O}$ for the V_V and H_V polarization are given by the equations, respectively

$$\underset{\sim}{O}_V = (-\sin\rho_1)\underset{\sim}{i} + (\cos\rho_1)\underset{\sim}{k} \tag{83}$$

$$\underset{\sim}{O}_H = (-\sin\rho_2)\underset{\sim}{i} + (\cos\rho_2)\underset{\sim}{j} \tag{84}$$

where $$\cos\rho_1 = \cos\theta/(\cos^2\theta + \sin^2\theta\cos^2\mu)^{\frac{1}{2}} \tag{85}$$

$$\cos\rho_2 = \cos\theta/(\cos^2\theta + \sin^2\theta\sin^2\mu)^{\frac{1}{2}} \tag{86}$$

then

$$(\underset{\sim}{M}\cdot\underset{\sim}{O})_{V_V} = E\cos\rho_1\cdot(\delta\cos^2\alpha + \alpha_2) \tag{87}$$

$$(\underset{\sim}{M}\cdot\underset{\sim}{O})_{H_V} = E\cos\rho_2\cdot(\delta\sin\alpha\cdot\cos\alpha) \tag{88}$$

If the optic axis does not lie along the rod axis but at an angle ω to it as shown in Figure 38, then α in eqs.(87) and (88) is replaced by $\alpha' = \alpha + \omega$

The intensities of V_V and H_V scattering are then calculated by substituting eqs.(87) and (88) into eq.(82). The calculated results are shown in Figure 35 and 36. The azimuthal dependence of the scattered intensities is a function of the angle ω. For $\omega = 45^\circ$, both H_V and V_V patterns in Figure 35 are quite consistent with the calculated results. The H_V pattern in Figure 36 is in good agreement with the calculated contour plot for $\omega \cdot 90^\circ$ but the V_V pattern does not fit. This may be because the V_V scattering pattern depends upon the choice of the values of α_1 and α_2.

If the spherulite has a disorder of structure or a sheaf-like structure in the initial stage of crystallization, an appreciable increase in intensity at small angles is observed.[134-136] It may be impossible in this case to distinguish this from the rod structure. When the spheru-

litic morphology is expected, the typical spherulitic pattern should appear as crystallization proceeds. However, the H_V pattern in Figure 36 was not changed with time, except though an increase in intensity.

In certain crystallization conditions in which the crystallization temperature is about 65°C, scattering patterns specific for spherulite superstructure were observed, superposed on the 0° - 90° type H_V pattern as shown in Figure 37. Comparing the scattering angles, it is seen that the size of spherulites is very much larger ($>5\mu$) than that of rods. The appropriately low crystallization temperature of about 65°C may give rise to the further growth of lamellae from the rod-like crystallites (Figure 36) to the spherulitic aggregates (Figure 37).

The rod-like structures giving the patterns shown in Figure 36 is smaller than the spherulitic structure (Figure 37) but is larger than the other rod-like structures obtained by quenching (Figure 35). The change in orientation of scattering patterns of both rod structures may depend upon how the small original crystal rods make the super rod in the process of crystallization. If this is the case, the optic axis must have the same orientation with respect to the axis of small crystal rods which compose the super rod, regardless of the principal dimension of super rods.

(2) Superstructure resulting from the stress-induced crystallization. The crosslinked sample films were kept in the streched state above the melting temperature for 10 min and then quenched in the same way as mentioned previously. Light scattering patterns of these quenched films measured at room temperature are shown in Figure 39. The stretching direction was set parallel to the polarization direction of the incident beam. Scattering patterns show the eight lobes for H_V polarization and the 45^o-type pattern for V_V polarization which is quite similar to that obtained for the unstretched, quenched film already shown in Figure 35.

A substantial difference of scattering pattern between the stretched (Figure 39) and the unstretched films (Figure 35) is the appearance of eight lobes in H_V scattering pattern. Both give the similar V_V patterns.

H_V scattering patterns have the same general appearance over whole range of elongation and show eight lobes. However, each lobe moves by a small amount toward the horizontal direction with increasing elongation.

When the crystallization proceeded for 3 hours at 97^oC after the stretched films were heated above melting temperature for 10 min, the light scattering patterns measured at the crystallization temperature were affected by the elongation ratio, as shown in Figure 40. The H_V pattern at low elongation is different from the eight lobe pattern of the stretched, quenched film. This might be attributable to

some change of superstructure due to the crystallization.

Both H_V and V_V scattering patterns of films crystallized at high temperature(87°C) at low elongation look like those expected from the deformed spherulitic superstructure in which deformation occurs in the horizontal direction. Since amorphous chains in the molten phase are stretched in the vertical direction before the crystallization takes place, it might be thought that the rate of crystal growth (which is the secondary nucleation on the crystal surface) is larger in the horizontal direction than in any other directions. As a consequence, crystals may grow in an ellipsoidal aggregate whose long axis is perpendicular to the stretching direction. This ellipsoid has a uniaxial symmetry about the stretching direction.

At high elongation, four new lobes appear for H_V polarization and the remaining four lobes become diffused. Such changes of scattering pattern due to the difference of strain may accompany the morphological change in the crystalline structure. However, the corresponding changes of the X-ray diffraction pattern and of the crystal orientation as a whole were not observed.

After crystallization in the oriented state for 3 hours, further crystallization occured upon cooling slowly to the room temperature in the same strained state. In this process, spontaneous extension of film length was observed, as has been discussed in the section IV.3. Light scattering patterns of these films are shown in Fig-

ure 41. These show an almost similar eight lobe pattern as those in Figure 39.

Both H_V and V_V scattering patterns at low elongation (Figure 40) are not changed by further crystallization due to cooling (See Figure 41). The significant change of light scattering by cooling at high elongation is the appearance of eight lobes with strong intensity.

From these observations of light scattering pattern alone, it is uncertain whether the eight lobes in Figure 41 may come from the superposition of the two kinds of morphologies which were observed by Stein and Rhodes for polyethylene film heat treated under strain.[137] The stretched, quenched film also shows the similar eight lobes pattern as has been seen above (Figure 39).

The amorphous polymer shows the light scattering pattern caused by the strain surrounding a void or an inclusion in a polymer. It was observed that new four lobes were emerged for H_V polarization as ethylene-propylene copolymer was stretched.[138] This might be attributable to the strain heterogeneity around crystallites. Cured natural rubber showed a weak H_V pattern due to the strain as well as intense cross streaks for V_V polarization due to oriented crystallites.[36,37] As a consequence, the contribution of strained amorphous polymer around crystllites may explain the eight lobe H_V pattern in this work.

Eight lobe H_V scattering patterns have been proposed

from the theoretical calculation of deformed spherulite by considering the twisting and tilting of the optic axis of the scattering element.[132,139] Scattering patterns are appreciably affected by the parameter K which describes the tilting angle β of the optic axis with respect to the radius and does not so much depend upon the twisting parameter η which describes the distribution of the optic axis about the radius.

As was pointed out previously, the crystal may not grow spherically when the amorphous chains in the molten state have an anisotropic orientation distribution. This is because the growth rates are different in the different directions. Then it may be assumed that the crystal aggregate resulting from the crystallization under uniaxial strain has an ellipsoidal shape.

The optic axis of the scattering element on the horizontal plane of this ellipsoid may be perpendicular to the radius to the scattering element. But the optic axis of other scattering element has some angle with respect to the radius. The optic axis of the scattering element in the vertical direction may be randomly distributed about the radius, but the scattering element on the horizontal plane has the preferential orientation distribution of the optic axis along the stretching direction.

By using the same procedure as van Aartsen's[139], the amplitude of scattering from the two-dimensional el-

lipsoid (a elliptical disk) is derived as the equation

$$E_{H_V} = \frac{C}{W^2}\left[\int_0^{2\pi} \frac{P\cdot\cos\{W\,Q\,\cos(\alpha-\mu)\}-1}{\cos^2(\alpha-\mu)}\,d\alpha + W\int_0^{2\pi}\frac{P\cdot Q\,\sin\{W\,Q\,\cos(\alpha-\mu)\}}{\cos(\alpha-\mu)}\,d\alpha\right] \quad (90)$$

where

$$C = (\alpha_1-\alpha_2)\,E_0\,A^2/2 \quad (91)$$

$$W = \left(\frac{2\pi}{\lambda}\right) A\,\sin\theta \quad (92)$$

$$P = (\cos^2\beta - \sin^2\beta\,\overline{\cos^2\omega}\,)\sin 2\alpha \quad (93)$$

$$Q = \epsilon\cdot\sin\alpha/(\cos^2\alpha + \epsilon^2\sin^2\alpha\,)^{\frac{1}{2}} \quad (94)$$

The value $\epsilon = B/A$ is the ratio of lengths of semi-minor and semi-major axes, which describes the ellipticity.

We do not know the orientation distribution of the optic axis in each scattering element of the ellipsoid resulting from the oriented crystallization. Assuming that angles β and ω are represented by the following equations, the scattered intensity was calculated.

$$\beta = 90^\circ\cdot\exp\left[-K\cdot\cos^2\alpha\cdot\epsilon^2/(1-\epsilon^2)\right] \quad (95)$$

$$g = 2\cdot\overline{\cos^2\omega}\;-1 = 1-\left[\exp-\eta\sin^2\alpha\cdot\epsilon^2/(1-\epsilon^2)\right] \quad (96)$$

The calculated results of H_V patterns which are given by the first quadrants of whole patterns are shown in Figure 43, together with the parameters of both tilting and twisting angles, K and η which were used for the calculations.

The distribution of the twisting angle ω about the radius does not affect the eight lobe pattern. The calculated pattern is much dependent upon the choice of tilting angle.

Experimental results shown in Figure 41 fit well to the calculated eight lobe pattern in Figure 43. By choosing a combination of parameters K and η, the deformed spherulitic patterns which were observed for the films crystallized at high temperature under low stress (Figure 40) are theoretically calculated as shown in Figure 43. The computer program for the calculations is given in Appendix IV.

Eqs.(95) and (96) may not be appropriate functions to describe the angles β and ω. It is still uncertain that the crystalline aggregate has an ellipsoidal shape. Because the change in morphology upon crystallization under stretching may be due to the distribution of nuclei, relative distance and direction to the adjacent nuclei and the anisotropy of growth rate of the crystal.

V. CONCLUSIONS AND FUTURE WORKS

1. Conclusions

The melting point of trans 1,4-polybutadiene was measured as 96°C which is considerably lower than the reported value of 148°C for the pure trans polymer.[74] This is due to the presence of the structural irregularity along the polymer chains such as cis- and vinyl- isomers. The variation of melting points due to the introduction of crosslinks was considered by Flory's theory. The depression of the melting point was attributed to the imperfection of crystallites due to the steric irregularity of segments around the crosslinking points. This was suggested from the observation of an increase in transparency of films with increasing crosslinking.

In the measurement of the stress-optical coefficient of the amorphous network of this polymer, a linear relationship between birefringence and stress was observed even in the range of strain where the stress-strain relation deviated from the Kuhn's kinetic theory of rubber elasticity for a simple extension. This suggested that the birefringence would be described by the Mooney-Rivlin type equation.

The optical anisotropy of segments $(b_1 - b_2)_s$ decreased with increasing temperature. This was thought to be due to the decrease in chain stiffness which might cor-

respond to the decrease in the length of segments.

The progress of crystallization in the stretched state was examined from the observation of the stress relaxation and the birefrigence increase with time. A calculation of crystallinity was performed applying the two-phase model for the total birefringence. Crystallization was accelerated by the increase in strain. The calculated crystallinity was two or three times larger than that calculated from the Flory's theory. This suggested that the slow stress relaxation might be due to the subsequent crystallites which were not perfectly oriented along the stretching direction. This was confirmed by the measurement of crystal orientation function by the X-ray method. The orientation function was dependent upon the crystallization temperature but was indepedent of the strain in the range of this work ($\alpha \leq 2.0$). The lower crystallization temperature brought about the higher crystal orientation.

The observed stress values were corrected for the filler effect of the crystallites. This correction became significantly important in the later stage of crystallization.

The variation of crystallinity as a function of time was examined using the Avrami relation for the phase transformation. The Avrami index n was observed 0.7 - 1.0. However,as the crystallization proceeded, variation of the Avrami index was observed. This is quite similar to the results for the crystallization of branched polyethylene

reported by Buchdall and his coworkers[112] and might be attributable to the delay of the rate of crystallization in the later stage because the components in molten state change their concentration with crystallization time.

The orientation functions of amorphous segments before the onset of crystallization were evaluated according to the statistical rubber elasticity theory. These values were surprisingly lower than the orientation functions of the subsequent crystallites. The high orientation function of crystallites was considered using the Krigbaum's treatment of the crystal growth process.

In the small angle light scattering measurement, three types of H_V scattering patterns were observed for the unstrained films. Two of these show rod-like structures, in which the optic axis is oriented at 45° or 90° with respect to the principal dimension of super rods. These patterns were quite consistent with the theoretically calculated results. The other is a four-leaf clover pattern specific for the spherulitic superstructure, which was observed at the crystallization temperature of about $65^{\circ}C$.

Films crystallized at high temperature under stress and then observed at this crystallizing temperature gave different scattering patterns from the above ones. At low stress, the H_V pattern look like that of deformed spherulitic superstructure. But at high stress, new cross streaks

appear near the horizontal direction, superposed on the previous pattern.

On the other hand, strained, quenched films measured at room temperature showed an eight lobe pattern for H_V polarization in the whole range of strain ($\alpha \leq 2.0$). As was mentioned in the section IV.6, eight lobes are theoretically expected from the certain choice of tilting angle and twisting angle of the optic axis of scattering element with respect to the radius of the ellipsoidal aggregates. Since the amorphous chain is very strained near the crystallites, this strain inhomogeneity may give rise to the additional scattering pattern. It is still uncertain in this work whether the strain inhomogeneity is responsible for the eight lobe H_V pattern.

2. Future works

Since the Flory's theory is based on the perfect alignment of segments in crystallites parallel to the stretching direction, it was not able to describe the experimental data on oriented crystallization of this work. His theory may be further developed by considering the crystals tilted at a certain angles (θ, ϕ) with respect to the stretching direction. If this is the case, the decrease in the displacement length of chain due to a single segment in these crystals may be given by the equations

$$x = l \cdot \sin\theta \cos\phi \tag{97}$$

$$y = l \cdot \sin\theta \sin\phi \tag{98}$$

$$z = l \cdot \cos\theta \tag{99}$$

where θ and ϕ are the angular coordinates of this segment, and l is the length of segment. Since crystals are distributed uniaxially aroud the stretching direction, trigonometric functions of angle ϕ are defined as average values.

$$\overline{\sin\phi} = \overline{\cos\phi} = 0$$

$$\overline{\sin^2\phi} = \overline{\cos^2\phi} = \tfrac{1}{2}$$

Consequently, the equilibrium stress may be represented by some function of angle θ, which may explain the data of this work.

The photometric measurement of small angle light scattering during crystallization with and without strain which was originally planned, was not performed because the hot cell for this experiment was not completed in time. The intensity change of light scattering with time may help us measure the change in the size of growing crystals (rods and spherulites). It is proposed to measure the effect of strain and temperature on the crystal growth rate, which will be compared with results obtained in this work.

As has been observed previously, crystallization is expected to depend appreciably upon the average degree of

orientation of amorphous chains produced by elongation in the molten state. The lower the average length of chains M_c, the greater the average degree of alignment of amorphous segments resulting from a given elongation, according to eq.(63) for the segment orientation function of amorphous chains. As a consequence, the degree of crosslinking may affect appreciably the rate of crystallization under stress. However, the introduction of crosslinks increases the structural irregularity along the chain and then may decrease the crystallinity in the final state of crystallization. On the other hand, on increasing the content of cis -isomer, the melting point of copolymer decreases according to eq.(29) which results in amorphous rubber-like properties at room temperature. Thus the crystallization will set in at lower temperature.

The variation of the degree of crosslinking and the concentration of trans content will change the crystallization rate at a given temperature and at a given elongation. The studies of these effects may be quite important from the point of view of the actual applications of rubber-like materials in the vibrational or constantly elongated state.

Thus, the dynamic X-ray studies of the crystallization may show many interesting effects of the frequence of vibration on the rate of crystallization, because this experimental condition is much closer to that of the actual

vibrational usage of rubber-like materials.

There exists other method to study the rate of oriented crystallization. If one can measure the volume contraction resulting from the crystallization under stress by the dilatometer and others, it will be possible to investigate the kinetics of this crystallization using the same relation between the crystallinity and the volume contraction as that of normal crystallization.

A P P E N D I X I

Theoretical calculation of the birefringence of trans 1,4 - polybutadiene crystals (high temperature form)

Natta and his coworkers[48] have reported from X-ray diffraction studies on crystalline trans 1,4-polybutadiene that the high temperature form (modification II) has a hexagonal crystal system and that the chain conformation is a zigzag structure of planar butadiene units, in which one monomer unit is involved in each repeat distance. The repeat distance is 4.68 $\mathring{A}$, measured along the zigzag axis. The rotational angle of the CH_2-CH_2 bond about the adjacent CH_2=CH bond is about 80°. The chain conformation of this form is illustrated in Figure 44.

The Z-axis is taken as C-axis of crystal, and the x- and y-axes as two perpendicular axes to the C-axis. If $P_{\parallel}$ is the chain polarizability parallel to the C-axis and $P_{\perp}$ is the average polarizability perpendicular to the C-axis, then $P_{\parallel}$ and $P_{\perp}$ are expressed by the equations

$$P_{\parallel} = P_Z \qquad (A1)$$

$$P_{\perp} = (P_x + P_y)/2 \qquad (A2)$$

The polarizability along the x-axis P_x may be calculated by using the equation

$$P_x = (b_1 - b_2)_{cc} \sum_{i=1}^{3} (\cos^2\theta^i_{cc} + b^i_{2_{cc}})$$

$$+ (b_1 - b_2)_{c=c} \cos^2 \theta_{c=c} + b_{2_{c=c}}$$

$$+ (b_1 - b_2)_{CH} \sum_{i=1}^{6} (\cos^2 \theta_{CH}^{i} + b_{2_{CH}}^{i}) \quad (A3)$$

P_y and P_z will be calculated from the similar equations. P_x , P_y and P_z of the monomer unit in the crystal of trans 1,4-polybutadiene were calculated in this procedure using the values of bond polarizabilities, given by Denbigh.[47] Results of this calculation are shown in Table 2.

The refractive index of trans 1,4-polybutadiene crystals may be calculated from the Lorentz-Lorenz equation

$$\frac{\bar{n}_2 - 1}{\bar{n}_2 + 2} = \frac{4\pi}{3} \bar{P} \quad (A4)$$

Where $\bar{n}$ is the average refractive index and $\bar{P}$ is the average unit cell polarizability per unit volume, which is given by the equation

$$\bar{P} = (P_{\parallel} + 2P_{\perp})/3V_c \quad (A5)$$

where V_c is the unit cell volume, determined as 96.3×10^{-24} cm^3.

As has been mentioned in the section II, the relationship between the birefringence and the difference in principal polarizability may be obtained by differentiating eq.(A4).

$$\Delta_c^o = (n_{\parallel} - n_{\perp})$$
$$= \left(\frac{2\pi}{9} \right) \frac{(n^2 + 2)^2}{\bar{n}} \frac{(P_{\parallel} - P_{\perp})_c}{V_c} \quad (A6)$$

Since the number of butadiene units per unit cell is unity, then

$$(P_{\parallel} - P_{\perp})_c = 1x(P_{\parallel} - P_{\perp}) = 21.2x10^{-24} cm^3 \quad (A7)$$

Substituting the values of V_c , $(P_{\parallel} - P_{\perp})_c$ and $\bar{n}$, the intrinsic birefringence of trans 1,4-polybutadiene crystals was calculated as 0.183 cm . For the calculation of a more accurate value of Δ_c^o , one should consider the internal field effect by a dipolar interaction of neighboring bonds.[140,141]

A P P E N D I X II

The computer program for correction of the diffracted X-ray intensities

```
10  PROGRAM ANGEL
15  DIMENSION E(150),B(150),C(150),D(150)
20  DO 30 I=1,71
25  READ,E(I)
30  CONTINUE
35  DO 45 I=1,71
40  READ,B(I)
45  CONTINUE
50  PI=3.141596
55  CABS=3.84
60  B=.084
65  WAVE=1.54
66  EI=756.
67  BI=701.
70  ANG1=25.*180.*PI
75  AK=SIN(ANG1)/WAVE
80  AK2=AK*AK
85  POL1=2./(1.+COS(2.*ANG1)**2)
90  ABS1=EXP(-CABS*B*(1.-1./COS(ANG1)))*COS(ANG1)
95  DI=BI-EI
100 DI=DI*POL1*ABS1
105 FAH1=0.38*EXP(-4.67*AK2)+0.62*EXP(-63.65*AK2)
110 FAC1=2.64*EXP(-0.97*AK2)+3.76*EXP(-23.52*AK2)
115 FINC1=0.6*(1.-FAH1)+0.4*(6.-FAC1)
120 CINC=DI/FINC1
125 DO 170 I=1,71
126 TEST1=I-11
127 IF(TEST1) 128,126,131
128 AI=I-1
129 ANG=(10.+0.5*AI)/360.*PI
130 GO TO 140
131 TEST2=I-61
132 IF(TEST2) 133,133,136
133 YI=I-11
134 ANG=(15.+0.2*YI)/360.*PI
135 GO TO 140
136 ZI=I-61
137 ANG=(25.+0.5*ZI)/360.*PI
140 YK=SIN(ANG)/WAVE
145 YK2=YK*YK
150 FAH=0.38*EXP(-4.67*YK2)+0.62*EXP(-63.65*YK2)
155 FAC=2.64*EXP(-0.97*YK2)+3.76*EXP(-23.52*YK2)
160 FINC=0.6*(1.-FAH)+0.4*(6.-FAC)
165 C(I)=CINC*FINC
170 CONTINUE
```

```
200 DO 255 I=1,71
201 IES11=I-11
202 IF(IES11) 203,203,204
203 AI=I-1
204 BANG=10.+0.5*AI
205 GO TO 225
206 IES12=I-61
207 IF(IES12) 208,209,211
208 AI=I-11
209 BANG=15.+0.2*AI
210 GO TO 225
211 AI=I-61
212 BANG=25.+0.5*AI
225 BANG=BANG/180.*3.1
230 COSH=COS(BANG)
235 COSHSQ=COSH*COSH
240 FOL=2./(1.+COSHSQ)
245 X=1./COSH
246 ABS=(ABS*LN(1.-X)/(EXP((ABS*L*(1.-X))-1.)
250 D(I)=FOL*ABS*(E(I)-E(I))-C(I)
255 CONTINUE
260 PRINT 265
265 FORMAT(1X,5HBANGG,10X,4HCINT,10X,5HINCOR)
270 DO 295 I=1,71
271 IES11=I-11
272 IF(IES11) 273,273,274
273 AI=I-1
274 BANGG=10.+0.5*AI
275 GO TO 285
276 IES12=I-61
277 IF(IES12) 278,279,281
278 AI=I-11
279 BANGG=15.+0.2*AI
280 GO TO 285
281 AI=I-61
282 BANGG=25.+0.5*AI
285 PRINT 290,BANGG,D(I),C(I)
290 FORMAT(1X,F6.2,5X,2F10.2)
295 CONTINUE
300 END
30  ENDFILE6
```

A P P E N D I X III

The computer program for the calculation of orientation function of (100) normals:

```
10 PROGRAM ARAT2
15 DIMENSION EC(50),EA(50),DC(50),DA(50),D(50)
20 DO 30 I=1,19
25 READ,EC(I),EA(I)
30 CONTINUE
35 READ,EC,EA
40 READ,AINCC,AINCA
45 PI=3.141596
50 CAES=3.64
55 L=0.046
60 BANG1=20.7
65 BANGC=BANG1/180.*PI
70 BANG2=18.6
75 BANGA=BANG2/180.*PI
80 COSC2=COS(BANGC)*COS(BANGC)
85 COSC1=COS(BANGC/2.)
90 COSA2=COS(BANGA)*COS(BANGA)
95 ANG1=BANGC/2.
100 ANG2=BANGA-ANG1
105 X=1./COS(ANG1)
110 Y=1./COS(ANG2)
115 FOL1=2./(1.+COSC2)
120 FOL2=2./(1.+COSA2)
125 ABS1=EXP(-CAES*L*(1.-1./COSC1))*COSC1
130 ABS2=CAES*L*(X-Y)*EXP(-CAES*D)/X/(EXP(-CAES*D*Y)-EXP(-CAES*L*X))
135 DO 155 I=1,19
140 DC(I)=FOL1*ABS1*(EC(I)-EC)-AINCC
145 DA(I)=FOL2*ABS2*(EA(I)-EA)-AINCA
150 D(I)=DC(I)-DA(I)
155 CONTINUE
160 DELAZ=5./180.*PI
165 DEL=DELAZ/2.
170 SUM0=0.
175 SUM1=0.
180 SUM2=0.
185 DO 285 I=1,19
190 AI=I-1
195 AZM=DELAZ*AI
200 SINAZ=SIN(AZM)
205 SIN2=SINAZ*SINAZ
210 COSAZ=COS(AZM)
215 U=I-1
220 IF(U) 225,235,225
225 V=I-19
```

```
250 IF(
255 SUM
265 SUM
270 SUM
280 SUM
285 CONTINUE
290 FAC=SUM2/SUM0
295 F=(3.*FAC-1.)/2.
300 PRINT 305
305 FORMAT(1X,5HLANG1,10X,5HLANG2)
310 PRINT 315,LANG1,LANG2
315 FORMAT(1X,F5.2,10X,F5.2)
320 PRINT 325
325 FORMAT(1X,3HIN1,10X,4HIN11,7X,4HIN12)
330 DO 345 I=1,19
335 PRINT 340,L(I),DC(I),DA(I)
340 FORMAT(1X,F10.2,5X,F10.
345 CONTINUE
350 PRINT 355,F
355 FORMAT(1X,2HF=,F5.3)
360 END
365 ENDFILE
```

A P P E N D I X IV

The computer program of the calculation of light scattering patterns for ellipsoidal aggregates

```
10 PROGRAM AK
15 ANIS=0.003
20 POL1=0.002
25 POL2=-0.001
30 WIN=1.
35 DELW=1.
40 WMAX=15.
45 UIN=0.
50 DELU=10.
55 UMAX=90.
60 EPSIL=0.6
65 NALP=100
70 AK=0.4
75 RAN=1.
80 EZ=90.
85 PI=3.14159
90 PRINT 95
95 FORMAT(3X,4HANIS,9X,4HPOL1,9X,4HPOL2,9X,5HEPSIL,7X,2HAK,8X,3HRAN)
100 PRINT 105,ANIS,POL1,POL2,EPSIL,AK,RAN
105 FORMAT(1X,F10.5,3X,F10.5,3X,F10.5,5X,F5.2,5X,F5.2,5X,F5.2)
110 PRINT 115
115 FORMAT(3X,3HWIN,10X,4HDELW,9X,4HUMAX,9X,2HEZ,9X,4HNALP)
120 PRINT 125,WIN,DELW,UMAX,EZ,NALP
125 FORMAT(1X,F7.2,8X,F5.2,7X,F6.2,9X,F5.2,6X,I4)
130 PRINT 135
135 FORMAT(18X,2HHV,11X,2HVV,9X,7HLOG(HV),8X7HLOG(VV))
145 W=WIN
150 PRINT 155,W
155 FORMAT(1X,2HW=,F5.2)
160 W2=W*W
165 U=UIN
170 UX=U/180.*PI
175 ALPN=NALP
180 DEALP=2.*PI/ALPN
185 EZ1=EZ/180.*PI
190 C1=10.**5*ANIS/EPSIL/W2
195 C2=10.**5*POL2/EPSIL/W2
200 SUMH1=0.
205 SUMH2=0.
210 SUMV1=0.
215 SUMV2=
220 SUMV3=0.
225 SUMV4=0.
```

```
230 DO 430 I=1,NALF
235 IALF=1
240 X=X
245 ALF=I*DELALF
250 SINAL=SIN(ALF)
255 SINAL2=SINAL*SINAL
260 SIN2AL=SIN(2.*ALF)
265 COSAL=COS(ALF)
270 COSAL2=COSAL*COSAL
275 AO=ALF+OA
280 COSAO=COS(AO)
285 COSAO2=COSAO*COSAO
290 EPS2=EPSIL*EPSIL
295 R=EPSIL/SQRT(COSAL2+EPS2*SINAL2)
300 Q=T*COSAQ
305 QR=Q*R
310 D=D1*EXP(-XK*(1.-EPS2)/EPS2*COSAL2)
315 COSD=COS(D)**2
320 SIND=SIN(D)**2
325 G=1.-EXP(-XAO*(1.-EPS2)/EPS2*SINAL2)
330 FH=SINIAL*(COSD-SIND*(1.+G)/2.)
335 FV=EPS2*COSAL2*SIND*SINAL2*(1.+G)/2.
340 IF(QR-.5) 360,345,360
345 X=-(Q*R)**2/2.
350 Y=Q*R
355 GO TO 375
360 X=(COS(QR)-1.)/COSAO2
365 Y=SIN(QR)/COSAO
370 AHV=FH*X*DEALF
375 BHV=FH*R*Y*DEALF
380 SUMH1=SUMH1+AHV
385 SUMH2=SUMH2+BHV
390 AVV=FV*X*DEALF
395 BVV=FV*R*Y*DEALF
400 CVV=X*DEALF
405 DVV=R*Y*DEALF
410 SUMV1=SUMV1+AVV
415 SUMV2=SUMV2+BVV
420 SUMV3=SUMV3+CVV
425 SUMV4=SUMV4+DVV
430 CONTINUE
435 AMTH=C1/2.*(SUMH1+SUMH2*W)
440 HV=AMTH*AMTH
445 AMTV=C1*(SUMV1+W*SUMV2)+C2*(SUMV3+W*SUMV4)
450 VV=AMTV*AMTV
455 HVL=ALOG(HV)
460 VVL=ALOG(VV)
465 PRINT 470,Q,HV,VV,HVL,VVL
470 FORMAT(1X,F7.3,3X,2E13.5,2E15.5)
475 OPEN FILE
480 TEMP=OMAX
```

```
485 IF(I5)175,175,490
490 IKSI=W-WMAX
495 IF(IKSI)500,510,510
500 W=W+DELW
505 GO TO 150
510 END
515 ENTRY
```

B I B L I O G R A P H Y

1. J. E. Field, J. Appl. Phys., 12, 23 (1941)
2. T. Thiessen and R. Wittstadt, Z. Physik. Chem., 41, 33 (1938)
3. H. Feuchter, Kautschuk, 2, 260, 282 (1926)
4. L. R. G. Treloar, Trans. Faraday Soc., 37, 84 (1941)
5. L. R. G. Treloar, Trans. Faraday Soc., 36, 538 (1940)
6. S. D. Gehman and J. E. Field, J. Appl. Phys., 10, 564 (1939)
7. W. Kuh, Kolloid Z., 76, 258 (1936)
8. W. Kuhn and F. Grun, Kolloid Z., 101, 248 (1942)
9. L. R. G. Treloar, Trans. Faraday Soc., 43, 277 (1947)
10. L. R. G. Treloar, Trans. Faraday Soc., 43, 284 (1947)
11. A. N. Gent, Trans. Faraday Soc., 50, 521 (1954)
12. A. N. Gent, J. Polymer Sci., 3, 3787 (1965)
13. J. J. Arlman and J. M. Goppel, Appl. Sci. Res., A2, 1 (1951)
14. K. H. Meyer and C. Ferri, Helv. Chim. Acta, 18, 570 (1935)
15. L. A. Wood and F. C. Roth, J. Appl. Phys., 15, 781 (1944)
16. M. Mooney and W. E. Woltstenholme, Ind. Eng. Chem., 44, 335 (1952)
17. A. V. Tobolsky and G. M. Brown, J. Polymer Sci., 17, 547 (1955)

18. P. J. Flory, J. Chem. Phys., 15, 397 (1947)

19. W. H. Smith and C. P. Saylor, Nat. Bur. Stds. J. Res., 21, 257 (1938)

20. E. H. Andrews, Proc. Roy. Soc., London, A277, 562 (1964)

21. P. J. Flory, Ind. Eng. Chem., 38, 417 (1946)

22. E. C. Bernhardt, Processing of Thermoplastic Materials, Reinhold, New York, 1959.

23. H. Wakeham and W. P. Virgin, Textile Res. J., 26, 177 (1956)

24. Y. Sakurada and L. Rebenfeld, J. Appl. Polymer Sci., 10, 637 (1966)

25. G. Caroti and J. H. Dusenbury, J. Polymer Sci., 22, 399 (1956)

26. A. Keller and M. J. Marchin, J. Macromol. Sci., B1, 41 (1967)

27. M. J. Hill and A. Keller, J. Macromol. Sci., B3, 153 (1969)

28. M. J. Hill and A. Keller, J. Macromol. Sci., B5, 591 (1971)

29. T. T. Li, R. J. Volungis and R. S. Stein, J. Polymer Sci., 20, 199 (1956)

30. J. T. Judge and R. S. Stein, J. Appl. Phys., 32, 2357 (1961)

31. W. R. Krigbaum and R. J. Roe, J. Chem. Phys., 41, 737 (1964)

32. E. S. Clark, SPE Journal, 23, 46 (1967)

33. E. S. Clark, ACS Papers, Organic Coatings and Plastics Chemistry, 32, 19 (1972)

34. W. Yau, K. Sasaguri, and R. S. Stein, ONR Technical Report, No. 54, 1963, Univ. of Mass., Amherst.

35. G. Kraus and J. T. Gruver, ACS Polymer Preprint, 13, (2), 891 (1972)

36. W. Yau and R. S. Stein, Polymer Letters, 2, 231 (1964)

37. W. Yau and R. S. Stein, J. Polymer Sci., A2, 6, 1 (1968)

38. J. J. Arlman, Appl. Sci. Res., A1, 347 (1949)

39. J. M. Goppel and J. J. Arlman, Appl. Sci. Res., A1, 3, 18 (1949)

40. H. G. Kilian, Kolloid Z., 183, 1 (1962)

41. P. H. Hermans and A. Weidinger, J. Polymer Sci., 4, 709 (1949)

42. R. S. Stein and F. H. Norris, J. Polymer Sci., 21, 381 (1956)

43. R. S. Stein, J. Polymer Sci., 32, 327, 335 (1958)

44. F. A. Battlheim and R. S. Stein, J. Polymer Sci., 27, 567 (1958)

45. L. R. G. Treloar, Trans. Faraday Soc., 50, 881 (1954)

46. D. A. Keedy, J. Powers and R. S. Stein, J. Appl. Phys., 31, 1911 (1960)

47. K. G. Denbigh, Trans. Farady Soc., 36, 936 (1940)

48. G. Natta and P. Corrandini, Nuovo Cimento, 15, Suppl., 1, 9 (1960)

49. M. Mooney, J. Appl. Phys., 19, 434 (1948)

50. R. S. Rivlin, in Rheology, Vol I., F. R. Eirich, Ed., Academic Press, New York, 1956

51. D. W. Saunders, Trans. Faraday Soc., 53, 860 (1957)

52. M. Fukuda, G. L. Wilkes and R. S. Stein, J. Polymer Sci., A2, 9, 1417 (1971)

53. T. Ishikawa and K. Nagai, Polymer J.(Japan), 1, 116 (1970)

54. I. Ya. Poddubnyi, Ye. G. Erenburg, and M. A. Yeremina, Vysokomol. Soedin., A10, 1381 (1968)

55. J. Furukada, S. Yamashita, T. Kotani and M. Kawashima, J. Appl. Polymer Sci., 13, 2527 (1969)

56. D. Morero, Chem. and Ind., 41, 758 (1958)

57. D. A. Keedy, R. J. Volungis and H. Kawai, Rev. Sci. Instr., 32, 415 (1961)

58. L. R. G. Treloar, The Physics of Rubber Elasticity, Oxford Univ. Press, 2nd ed., 1967

59. R. S. Stein, H. Kawai, T. Itoh and D. A. Keedy, Polymer Letters, 2, 1075 (1964)

60. H. P. Klug and L. E. Alexander, X-ray Diffraction Procedures, John Wiley, New York, 1954, chap. 11

61. R. S. Stein, J. Powers and S. Hoshino, ONR Technical Report No. 33, Project No. 356-378, Univ. of Massachusetts, Amherst, Mass., 1961

62. S. Krimm and A. V. Tobolsky, J. Polymer Sci., 7, 57 (1951)

63. International Tables for X-Ray Crystallography, Vol. III, Kynoch Press, Birmingham, England, 1962, p. 202

64. Ibid., Vol. III, 1962, p.162

65. N. S. Gingrich, Rev. Mod. Phys., 15, 90 (1943)

66. N. S. Gingrich, Rev. Mod. Phys., 15, 781 (1943)

67. D. A. Keedy, J. Power and R. S. Stein, J. Appl. Phys., 31, 1911 (1960)

68. M. B. Rhodes, D. A. Keedy and R. S. Stein, J. Polymer Sci., 62, 73 (1962)

69. M. Baccaredda and E. Butta, J. Polymer Sci., 51, 39 (1961)

70. G. Natta, M. Pegoraro and L. Szilagiji, Chim. e. Ind., 49, (1) 7 (1967)

71. J. Kalal, E. Zudkova, O. Hasek and I. Picova, Sb. Khimikotekhnologichesogo institute v Prage, C9, 37 (1966)

72. T. Tatsumi, T. Fukushima, K. Imada and M. Takayanagi, J. Macromol. Sci., B1, 459 (1967)

73. Y. Baba, K. Tamura, and R. Fujishiro, Repts. Progr. Polymer Phys. Japa, 10, 267 (1967)

74. G. Natta and G. Moraglio, Rubber Plastic Age, 44, 42 (1963)

75. L. Mandelkern, Crystallization of Polymers, MacGraw-Hill, New York, 1964, p.74

76. P. J. Flory, Trans. Faraday Soc., 51, 848 (1955)

77. P. J. Flory, J. Chem. Phys., 17, 223 (1949)

78. D. E. Roberts and L. Mandelkern, J. Am. Chem. Soc., 82, 1091 (1960)

79. W. Kuhn, E. Peterli and H. Majer, Z. Elektrochem., 62, 296 (1958)

80. W. Kuhn and H. Majer, Angew. Chem., 68, 345 (1956)

81. L. Mandelkern, D. E. Roberts, J. C. Halpin and F. F. Price, J. Am. Chem. Soc., 82, 46 (1960)

82. P. J. Flory, J. Am. Chem. Soc., 78, 5222 (1956)

83. A. N. Gent, J. Polymer. Sci., 18, 321 (1955)

84. A. N. Kuhn, Kolloid Z., 68, 2 (1934)

85. J. Wang and E. Guth, J. Chem. Phys., 20, 1144 (1952)

86. H. M. James and E. Guth, J. Chem. Phys., 11, 455 (1943)

87. P. J. Flory and and J. Rehner, Jr., J. Chem. Phys., 11, 512 (1943)

88. W. Kuhn, J. Polymer Sci., 1, 380 (1946)

89. T. Ishikawa and K. Nagai, Polymer J. (Japan) 1, 116 (1970)

90. R. J. Volungis and R. S. Stein, J. Chem. Phys., 23, 1179 (1955)

91. A. N. Gent and V. V. Vickroy, J. Polymer Sci., A2, 5, 47 (1967)

92. T. Ishikawa and K. Nagai, J. Polymer Sci., A2, 7, 1123 (1963)

93. D. W. Saunders, Trans. Faraday Soc., 52, 1414 (1956)

94. K. J. Smith and D. Puett, J. Appl. Phys., 37, 346 (1966)

95. L. Mullins, J. Appl. Polymer Sci., 2, 1 (1959)

96. S. M. Gumbrell, L. Mullins and R. S. Rivlin, Trans. Faraday Soc., 49, 1495 (1953)

97. A. N. Gent, Macromolecules, 2, 262 (1969)

98. G. S. Whitby, J. Phys. Chem., 36, 198 (1932)

99. R. S. Stein, F. H. Holmes and A. V. Tobolsky, J. Polymer Sci., 14, 443 (1954)

100. R. S. Stein and A. V. Tobolsky, Textile Res. J., 18, 201, 302 (1948)

101. L. E. Nielsen and R. Buchdahl, J. Chem. Phys., 17, 839 (1949)

102. H. Peukert, Kunstoffe, 41, 154 (1951)

103. A. N. Gent, J. Polymer Sci., 4, 447 (1966)

104. L. E. Nielsen and F. D. Stockton, J. Polymer Sci., A1, 1955 (1963)

105. K. Baba, M. S. Thesis, Univ. of Massachusetts, Amherst, 1972

106. E. Guth, J. Appl. Phys., 16, 20 (1945)

107. H. M. Smallwood, J. Appl. Phys., 15, 758 (1944)

108. M. Avrami, J. Chem. Phys., 7, 1103 (1939)

109. M. Avrami, J. Chem. Phys., 8, 212 (1940)

110. M. Avrami, J. Chem. Phys., 9, 177 (1941)

111. F. Gornick and L. Mandelkern, J. Appl. Phys., 33,

907 (1962)

112. R. Buchdahl, R. L. Miller and S. Newman, J. Polymer Sci., 36, 215 (1959)

113. A. Kovacs, Ric. Sci., Suppl. A, 25, 668 (1955)

114. R. Nagao, Polymer, 10, 175 (1969)

115. F. Danusso, Polymer, 8, 281 (1967)

116. S. F. Bermudez and J. M. G. Fatou, European Polymer J., 8, 575 (1972)

117. K. Suehiro and M. Takayanagi, J. Macromol. Sci., B4(1), 39 (1970)

118. W. R. Krigbaum and R. J. Roe, J. Polymer Sci., A, 2, 4391 (1964)

119. R. J. Roe and W. R. Krigbaum, J. Appl. Phys., 35, 2215 (1964)

120. J. Frenkel, Kinetic Theory of Liquids, Oxford Univ. Press, 1964, p. 413

121. F. P. Price, J. Polymer Sci., 42, 49 (1960)

122. F. P. Price, SPE Trans., 151 (1964)

123. R. J. Roe, J. Appl. Phys., 36, 2024 (1965)

124. Z. W. Wilchinsky, Advances in X-Ray Analysis, Vol. 6, Plenum Press, New York, 1963, p.231

125. R. S. Stein and M. B. Rhodes, J. Appl. Phys., 31, 1873 (1960)

126. R. S. Stein, M. B. Rhodes, R. K. Wilson and S. N. Stidham, Pure Appl. Chem., 4, 219 (1962)

127. M. B. Rhodes and R. S. Stein, J. Polymer Sci., 62

S84 (1962)

128. M. B. Rhodes and R. S. Stein, Polymer Letters, 1, 663 (1963)

129. G. G. Adams and R. S. Stein, J. Polymer Sci., A2, 6, 31 (1968)

130. A. L. Nguyen, B. T. Vu, and G. L. Wilkes, ACS Polymer Preprints, 13(2), 1007 (1972)

131. M. B. Rhodes, Ph. D. Thesis, Univ. of Massachusetts, Amherst, 1966

132. R. S. Stein, P. Erhardt, J. J. van Aartsen, S. Clough and M. B. Rhodes, J. Polymer Sci., C(13), 1 (1966)

133. M. B. Rhodes and R. S. Stein, J. Polymer Sci., A2, 7, 1539 (1969)

134. R. S. Stein and W. Chu, J. Polymer Sci., A2, 8, 1137 (1970)

135. M. Motegi, T. Oda, M. Moritani and H. Kawai, Polymer J. (Japan), 1, 209 (1970)

136. C. Picot, R. S. Stein, M. Motegi, and H. Kawai, J. Polymer Sci., A2, 8, 2115 (1970)

137. M. B. Rhodes and R. S. Stein, J. Appl. Phys., 32, 2344 (1963)

138. K. Baba, MS Thesis, Univ. Of Massachusetts, Amherst, 1972

139. J. J. van Aartsen and R. S. Stein, J. Polymer Sci., A2, 9, 295 (1971)

140. R. L. Rowell and R. S. Stein, J. Chem. Phys., 47,

2985 (1967)

141. R. S. Stein, J. Polymer Sci., A2, 7, 1021 (1969)

C A P T I O N S F O R T A B L E S

1. The length of the a-axis of trans 1,4-polybutadiene unit cell.
2. Values of trans 1,4-polybutadiene chain polarizability in the high temperature crystal form.

C A P T I O N S F O R F I G U R E S

1. The orientation of lamellae in molded bars of polyoxymethylene (from E. S. Clark[32])
2. Schematic diagram of lamella orientation of polyethylene due to the crystallization under stress (from A. Keller[27].)
3. Schematic diagram of the apparatus for the simultaneous measurements of birefringence and stress.
4. The geometry of the experimental system for orientation function measurement by X-ray diffraction method.
5. The coordinate system for the calculation of orientation function of the (100) normals.
6. The experimental system for photographic light scattering.
7. The variation of the melting temperature with the trans content.
8. The variation of the melting temperature with the molecular weight of network chain.
9. The variation of the quantity $(T_m^o - T_m)/T_m$ with $1/M_c$.
10. The stress-strain relations for the amorphous network in simple extension.
11. Mooney-Rivlin plots at 110°C for various degrees of crosslinking.
12. The variation of the birefringence with stress at 110 °C for various degrees of crosslinking.
13. The variation of the stress optical coefficient with

temperature.

14. The variation of the optical anisotropy of the statistical segment $(b_1 - b_2)_s$ with temperature.
15. The stress relaxation with time during crystallization at 85°C.
16. The stress relaxation with time during crystallization at 90°C.
17. The stress relaxation with time during crystallization at 95°C.
18. The variation of the birefringence with time during crystallization at 85°C.
19. The variation of the birefringence with time during crystallization at 85°C.
20. The variation of the birefringence with time during crystallization at 90°C.
21. The variation of the birefringence with time during crystallization at 90°C.
22. The variation of the birefringence with time during crystallization at 95°C.
23. The variation of the birefringence with time during crystallization at 95°C.
24. The variation of the X-ray diffraction intensities at various temperatures with Bragg angle.
25. The X-ray diffraction patterns of the crystallized films with and without strain.
26. The variation of the orientation function with elon-

gation ratio at two crystallization temperatures.

27. The variation of the crystallinity with time during crystallization under stress at 85°C.

28. The variation of the crystallinity with time during crystallization under stress at 90°C.

29. The variation of the crystallinity with time during crystallization under stress at 95°C.

30. The comparison of the crystallinity calculated from eq.(72) in this work (80°C) with that from the Flory's theory, and the correction for filler effect.

31. The comparison of the crystallinity calculated from eq.(72) in this work (90 and 95°C) with that from the Flory's theory, and the correction for filler effect.

32. Avrami plots for the crystallization under various strains at 85°C.

33. Avrami plots for the crystallization under various strains at 90°C.

34. Avrami plots for the crystallization under various strains at 95°C.

35. The H_V and V_V light scattering patterns from the quenched films without strain, and the calculated scattering patterns for rod-like aggregates ($\omega = 45^\circ$).

36. The H_V and V_V light scattering patterns from the films under the crystallization without strain at high temperature (87°C), and the calculated scat-

Table 1 The length of the a-axis of trans 1,4-poly-butadiene unit cell ($\mathring{A}$)

Modification	Natta[48]	Takayanagi[117]	This work
Low temperature form	4.68	4.60	4.64
High temperature form	4.88	4.95	4.98

Table 2 Values of trans 1,4-polybutadiene chain polarizability (high temperature form) ($\times 10^{24}$ cm^3)

P_x	P_y	P_z	$P_{\parallel} - P_{\perp}$
65.9	69.4	88.9	21.2

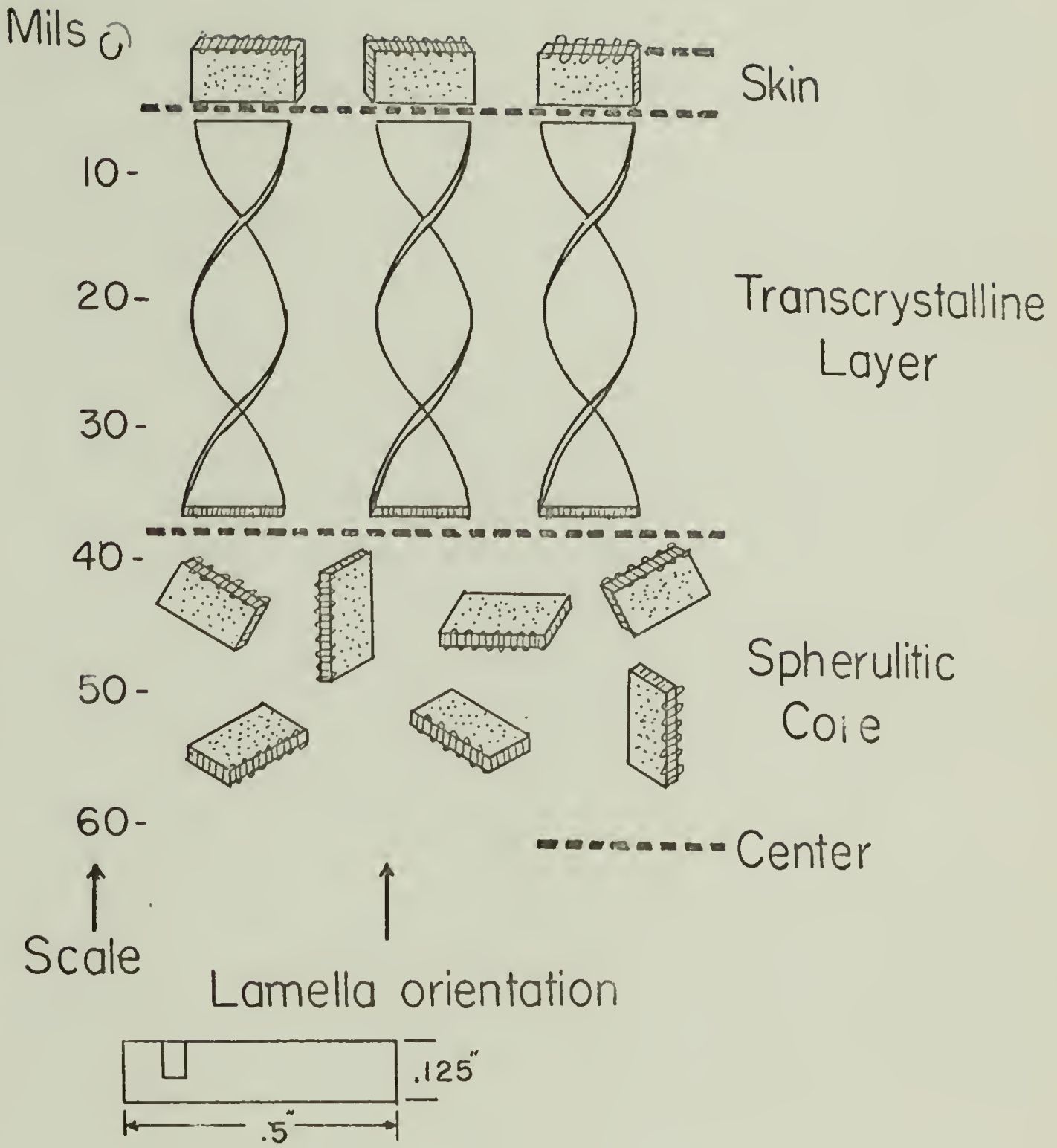
Mils
0
10-
20-
30-
40-
50-
60-
Skin
Transcrystalline Layer
Spherulitic Core
Center
Scale
Lamella orientation
.125"
.5"
Cross section of bar

FIG. 1

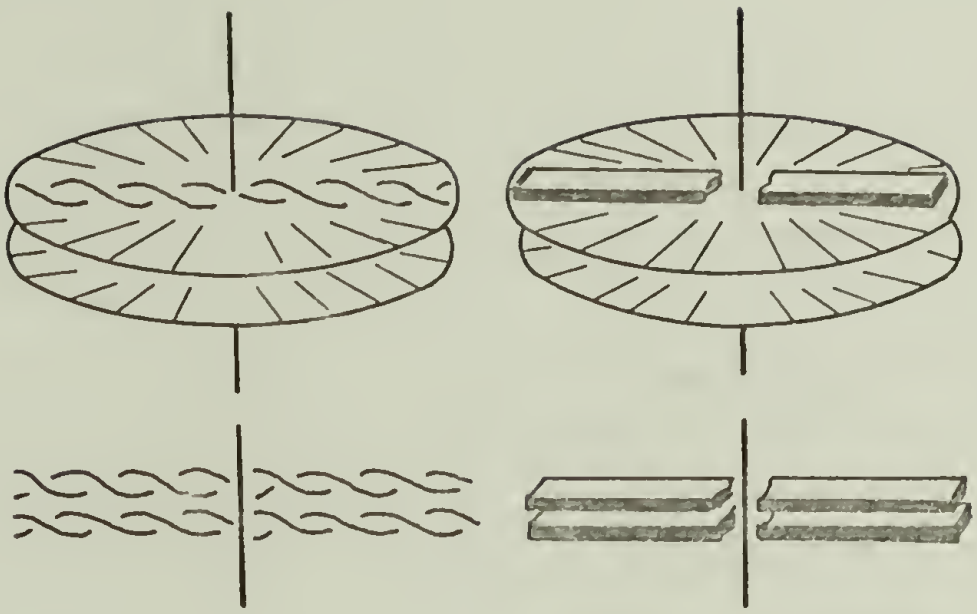

FIG. 2

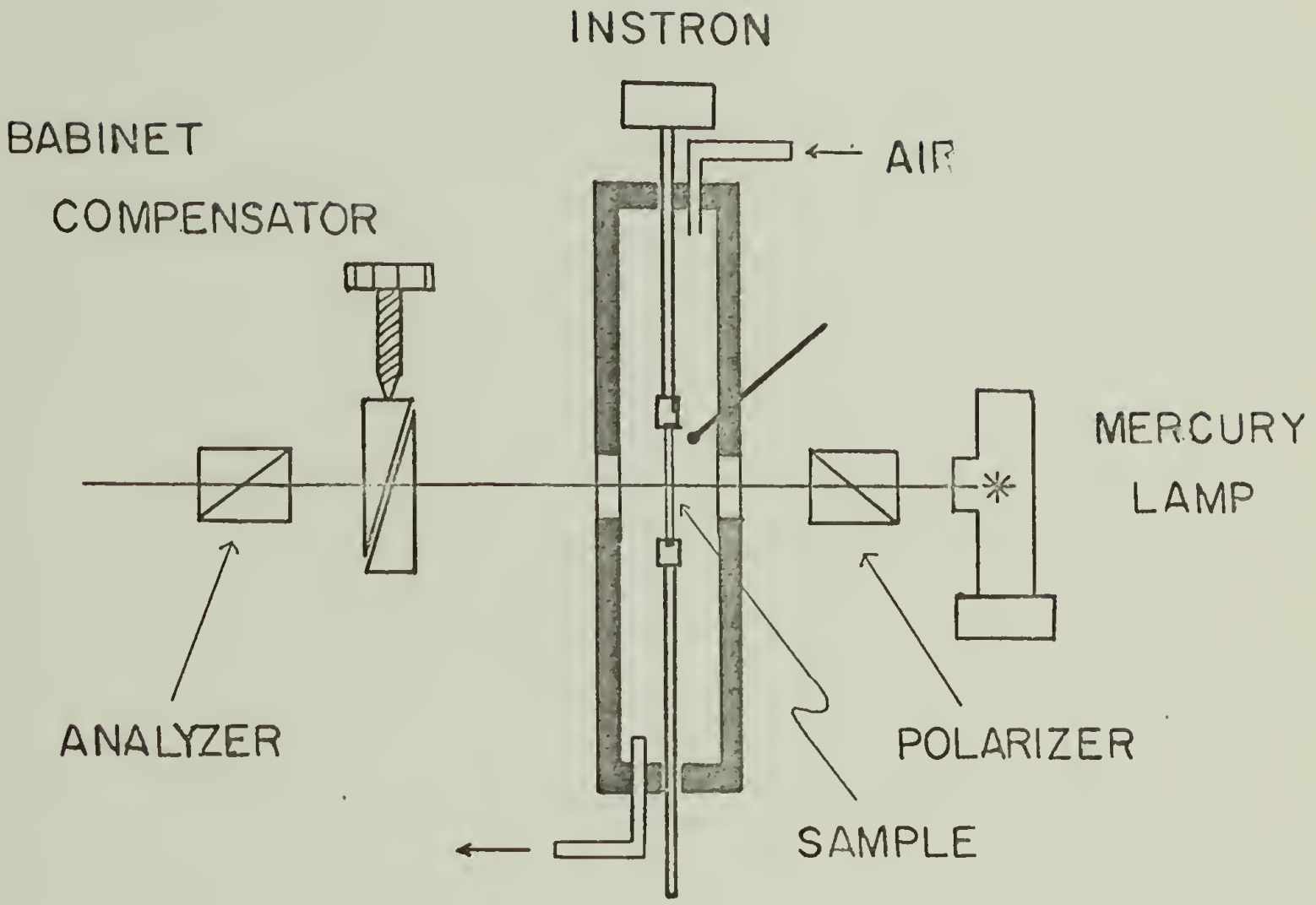
INSTRON
BABINET
COMPENSATOR
AIR
MERCURY
LAMP
ANALYZER
POLARIZER
SAMPLE

FIG. 3

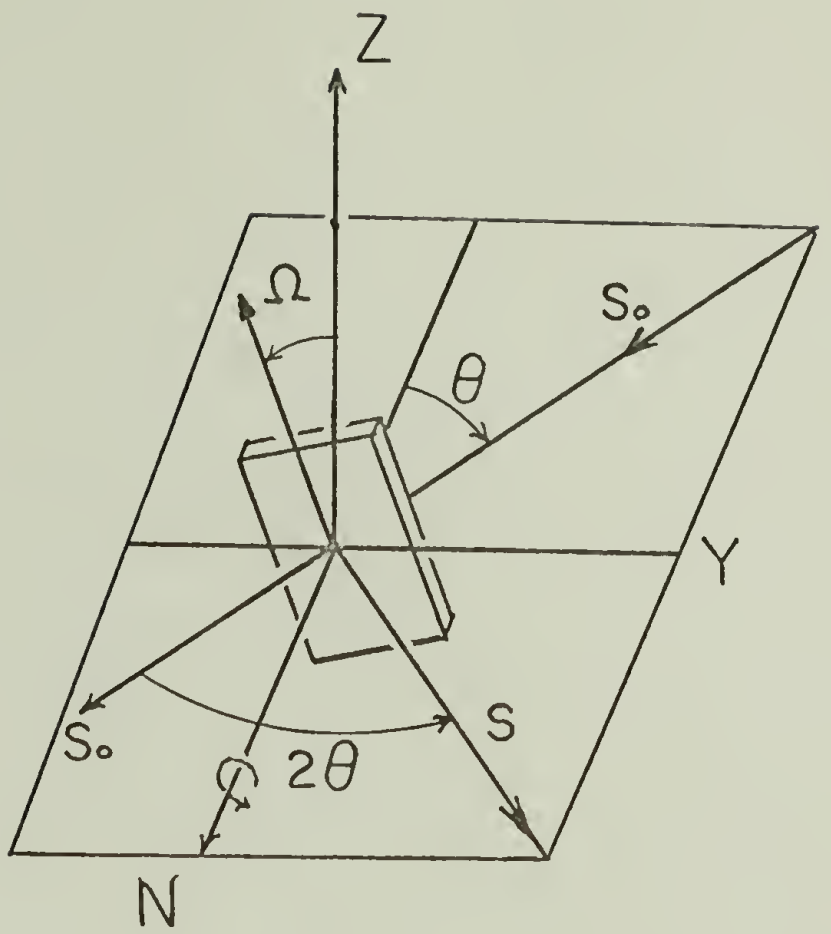

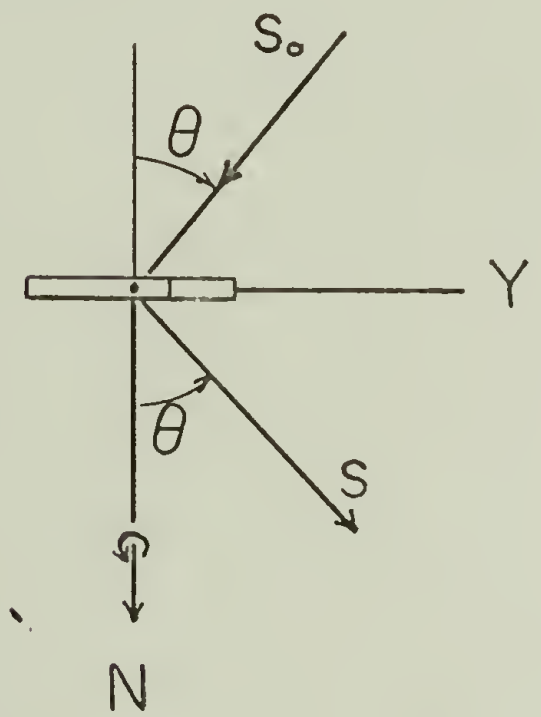

FIG. 4

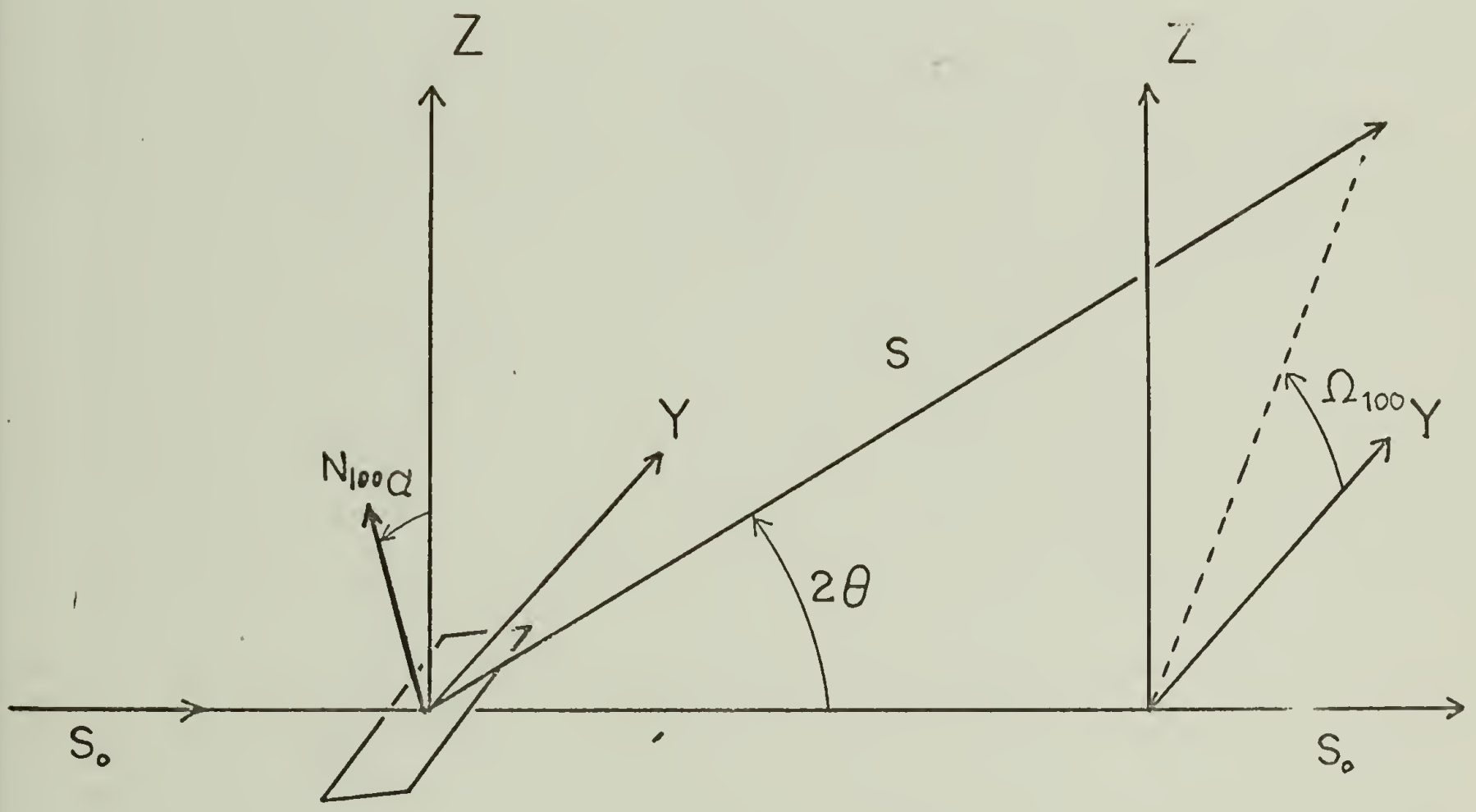

FIG. 5

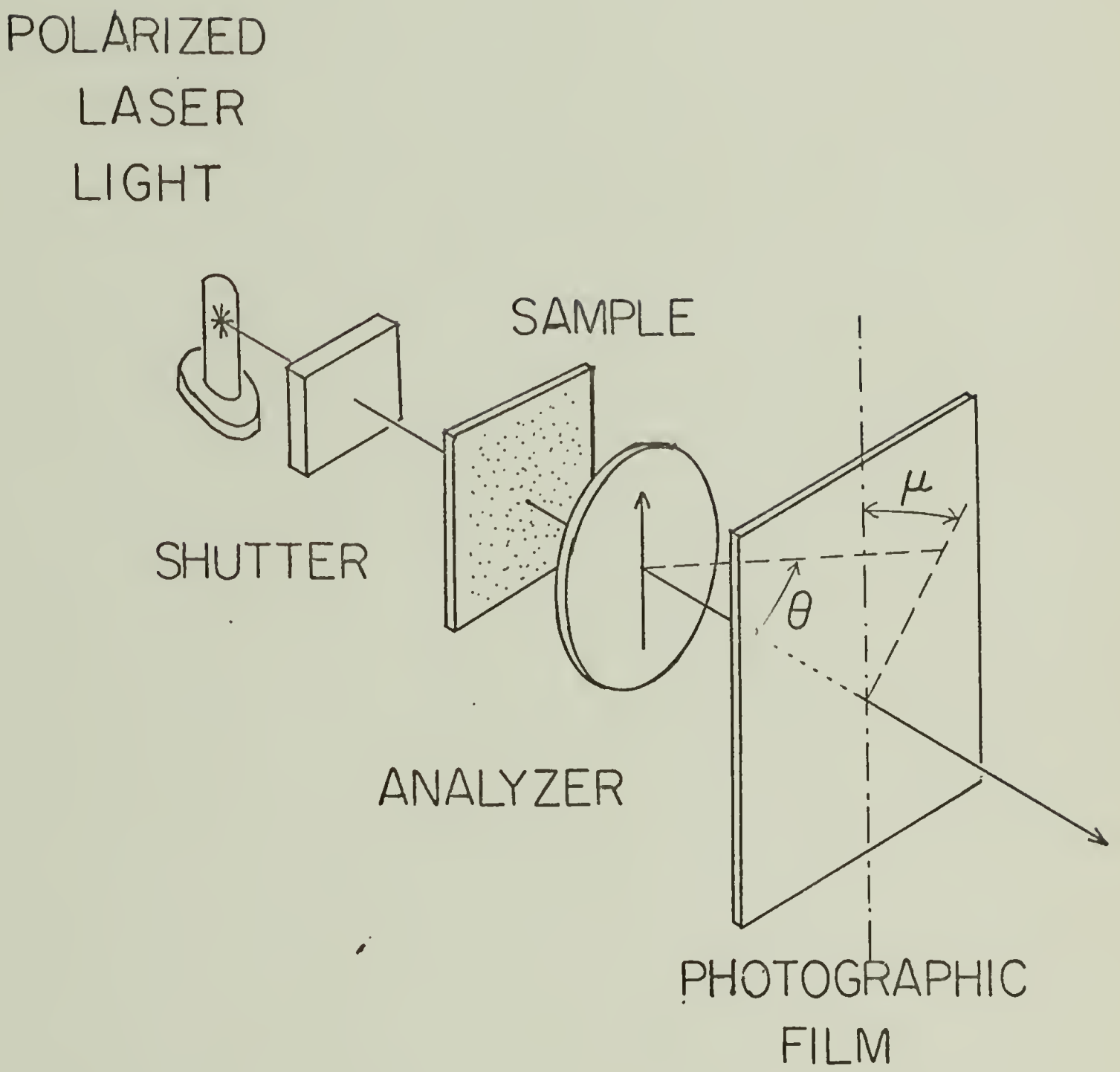
POLARIZED
LASER
LIGHT
SAMPLE
SHUTTER
ANALYZER
μ
θ
PHOTOGRAPHIC
FILM

FIG. 6

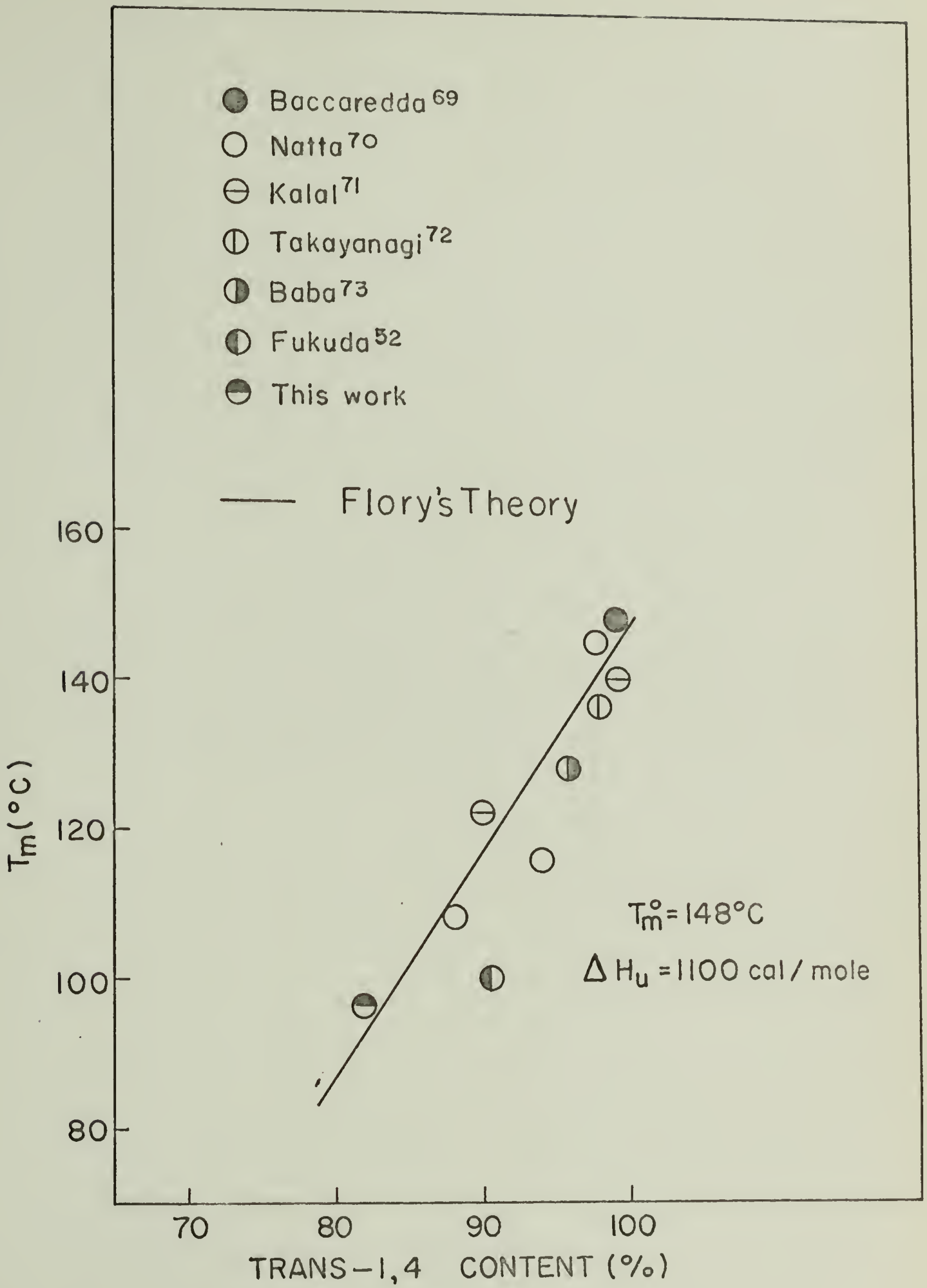
Baccaredda 69
Natta 70
Kalal 71
Takayanagi 72
Baba 73
Fukuda 52
This work
Flory's Theory
160
140
120
100
80
T_m(°C)
T_m^o=148°C
ΔH_u =1100 cal / mole
70
80
90
100
TRANS-1,4 CONTENT (%)

FIG. 7

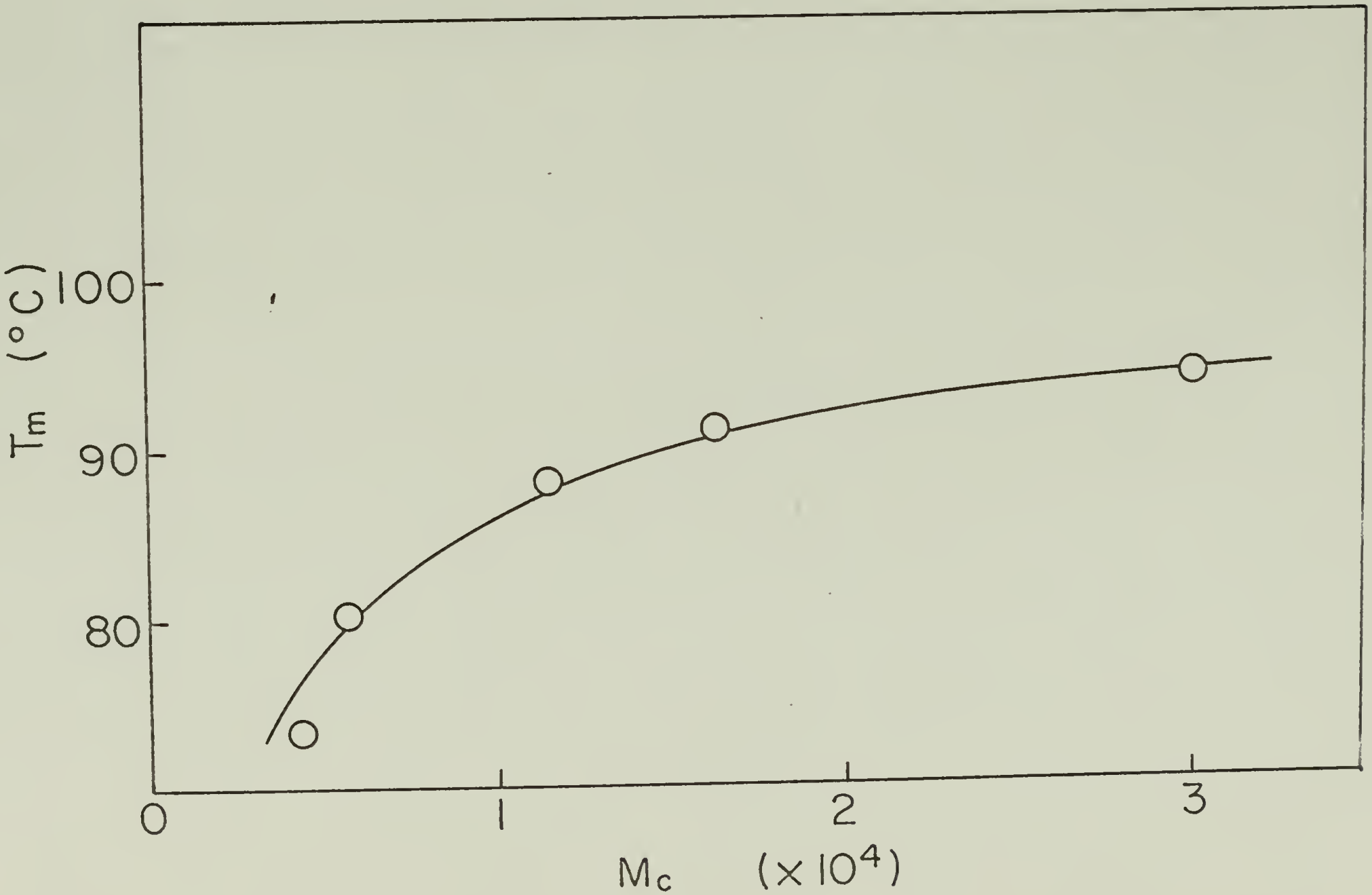

FIG. 8

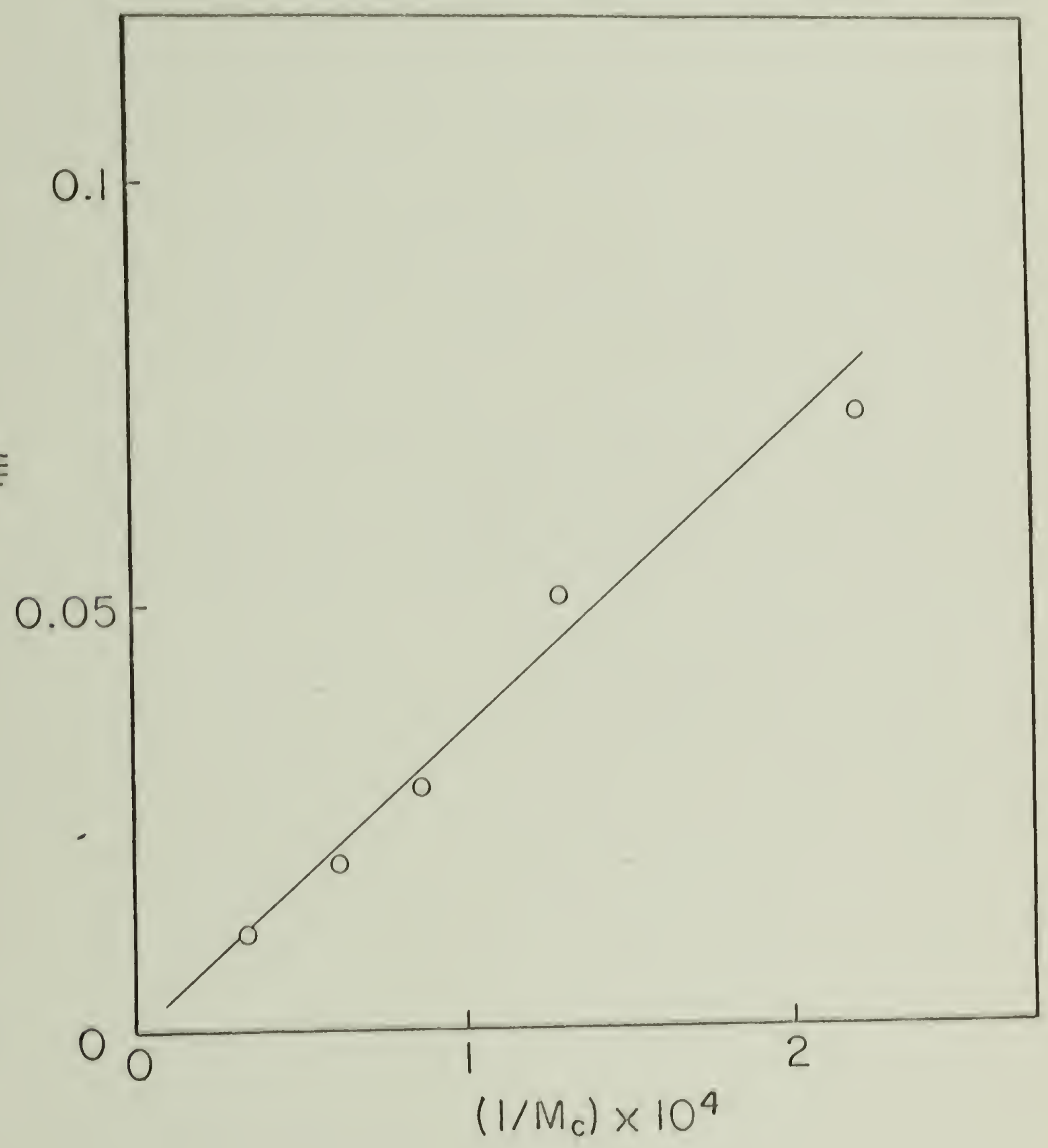

FIG. 9

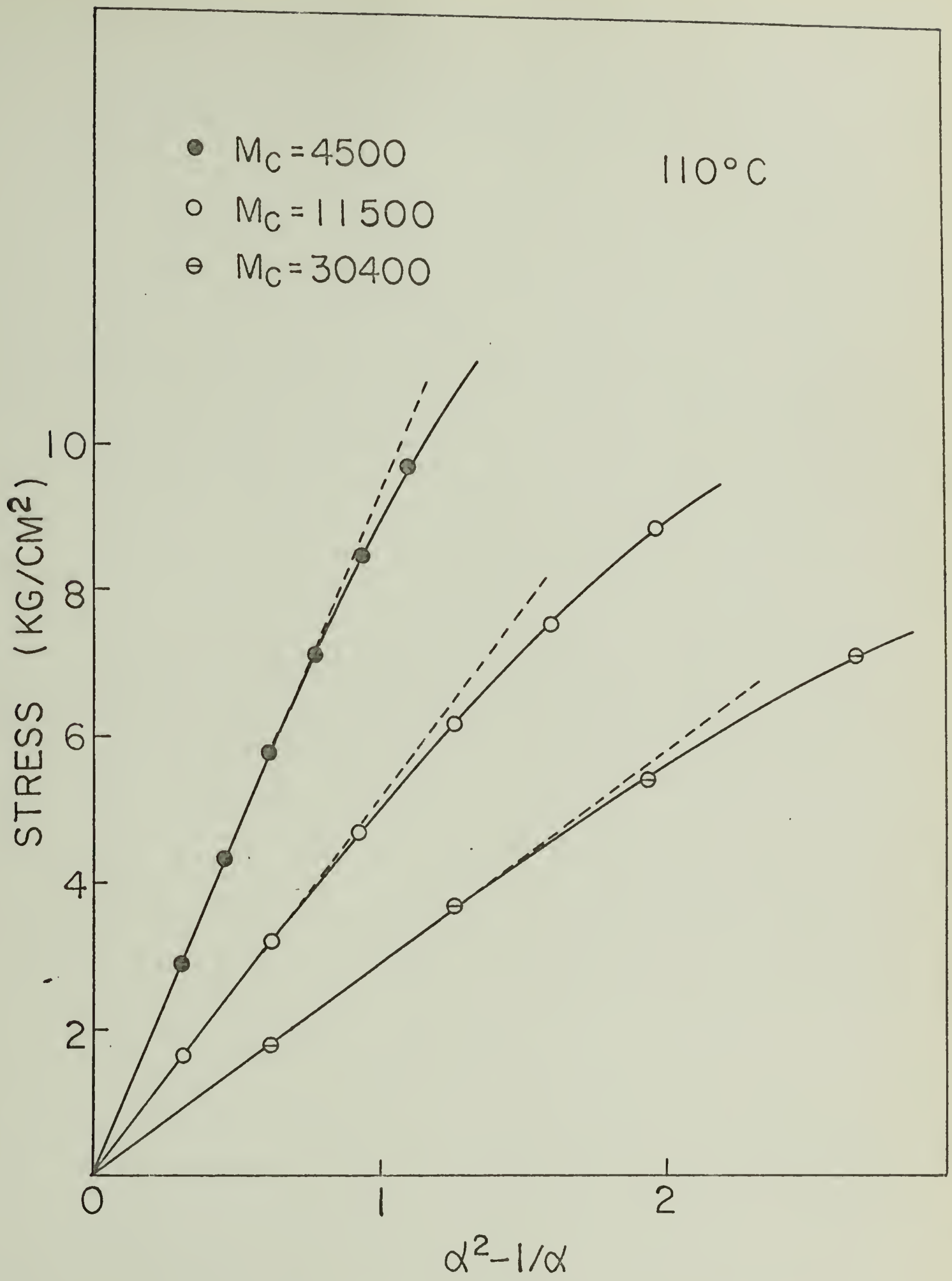
$M_c = 4500$
$M_c = 11500$
$M_c = 30400$
110°C
STRESS (KG/CM²)
0
2
4
6
8
10
0
1
2
$\alpha^2 - 1/\alpha$

FIG. 10

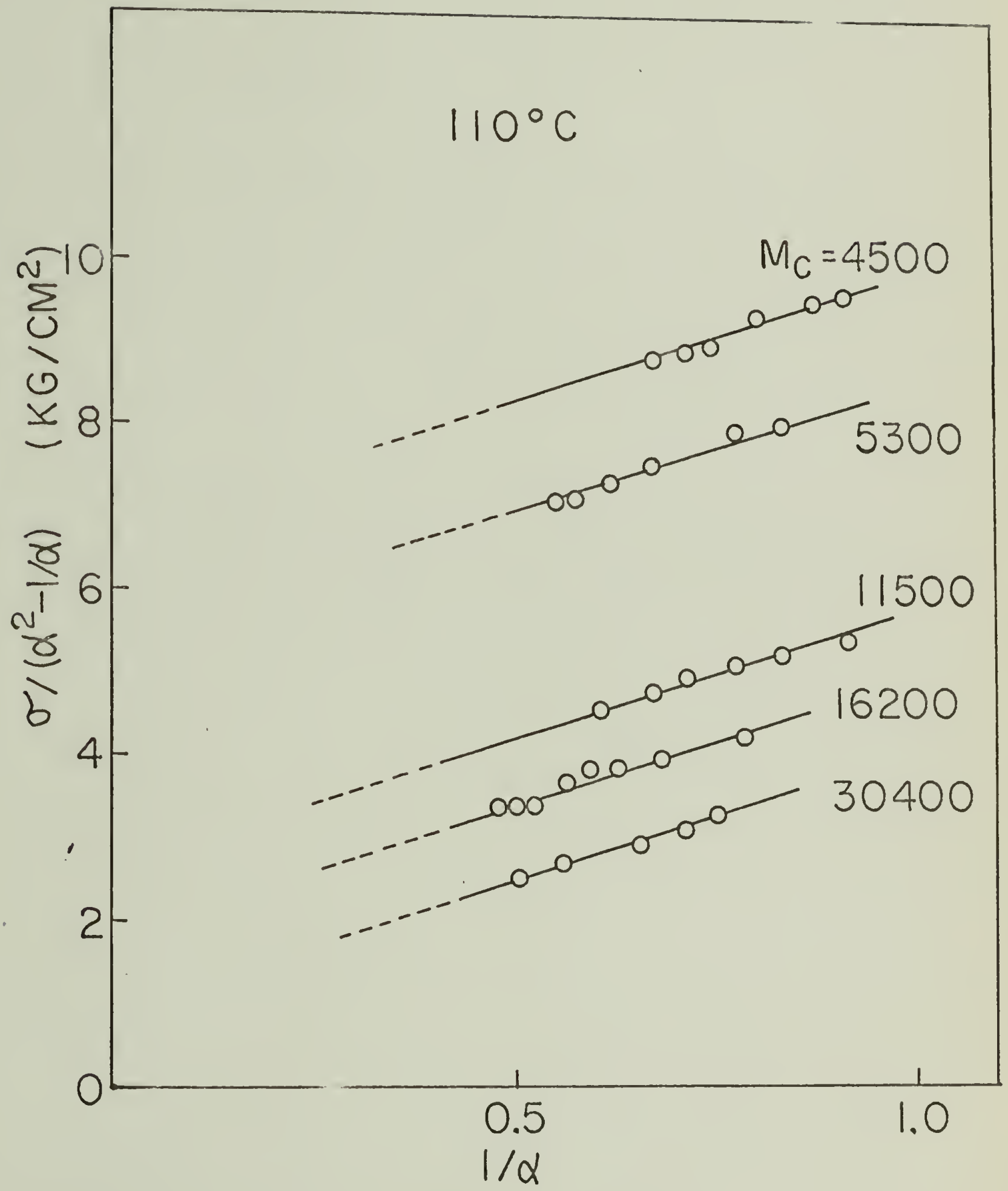
110°C
M_c=4500
5300
11500
16200
30400
$\sigma/(\alpha^2-1/\alpha)$ (KG/CM^2)
0
2
4
6
8
10
0.5
1.0
1/α

FIG. 11

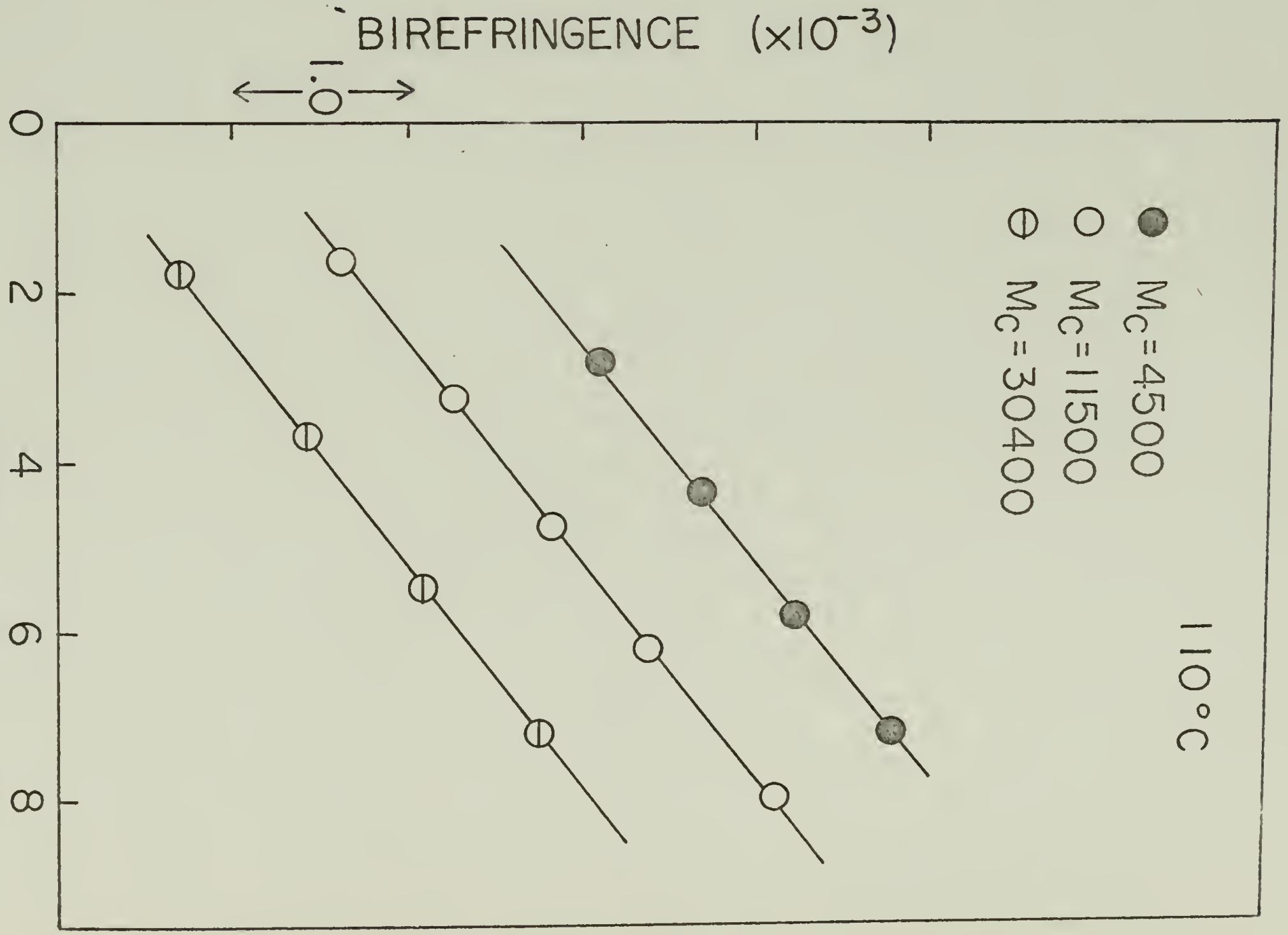
BIREFRINGENCE (×10⁻³)
0
2
4
6
8
STRESS (KG/CM²)
Mc=4500
Mc=11500
Mc=30400
110°C

FIG. 12

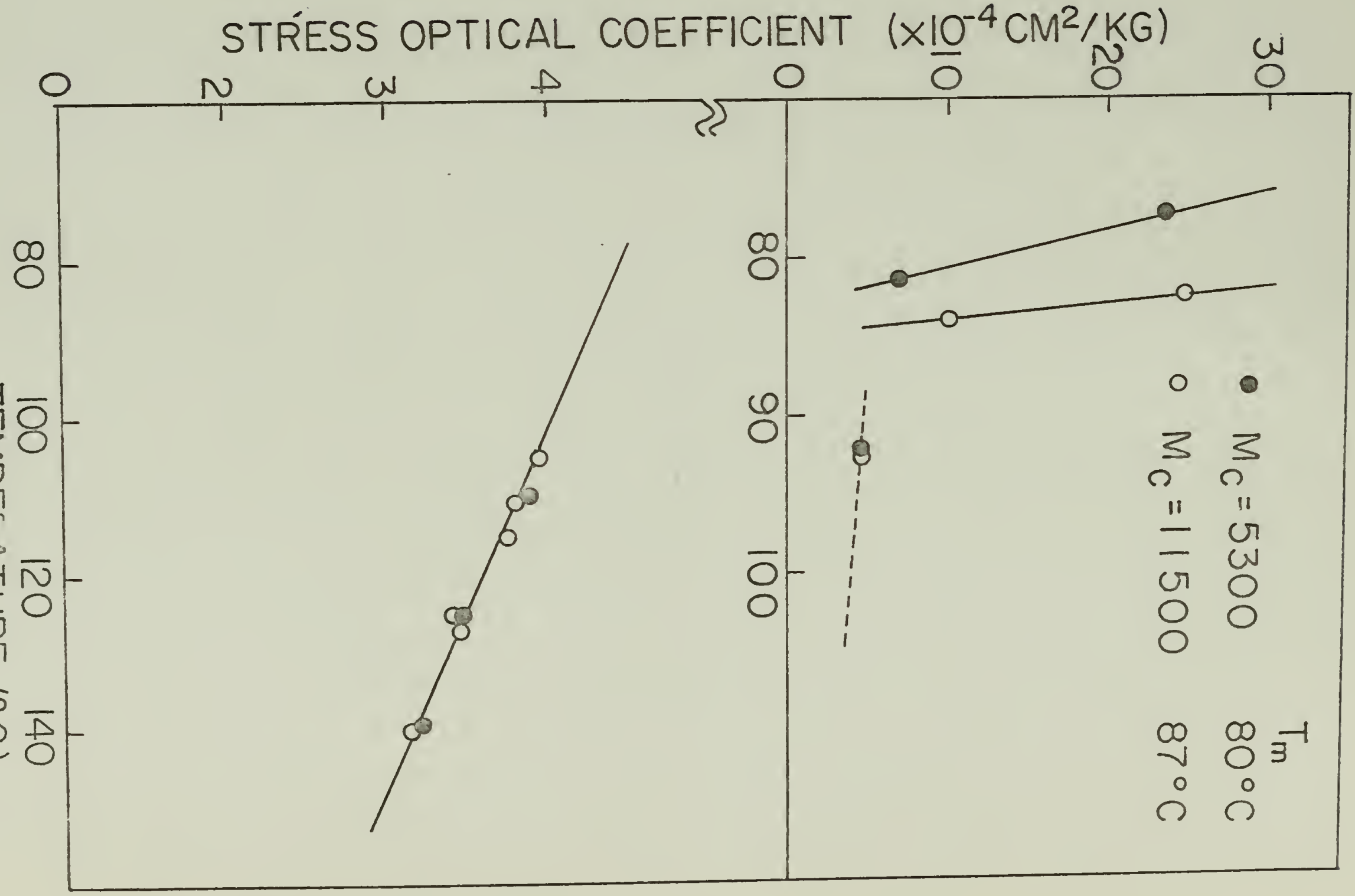
STRESS OPTICAL COEFFICIENT (x10⁻⁴ CM²/KG)
0
2
3
4
0
10
20
30
80
90
100
TEMPERATURE (°C)
100
120
140
• Mc=5300 Tm 80°C
° Mc=11500 87°C

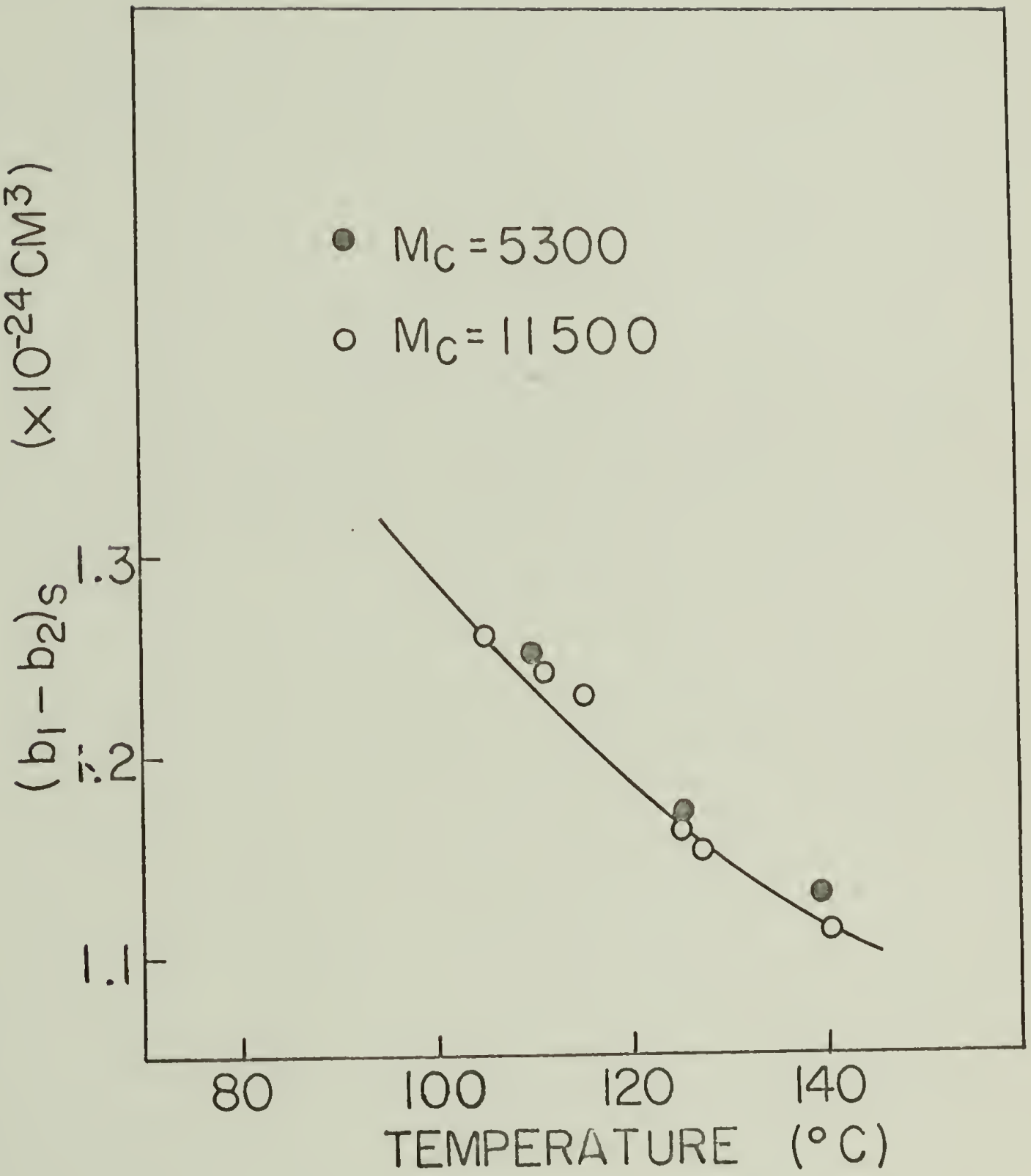
$(b_1 - b_2)_S$ (×10⁻²⁴ CM³)
1.3
1.2
1.1
80
100
120
140
TEMPERATURE (°C)
● M_C = 5300
○ M_C = 11500

FIG. 14

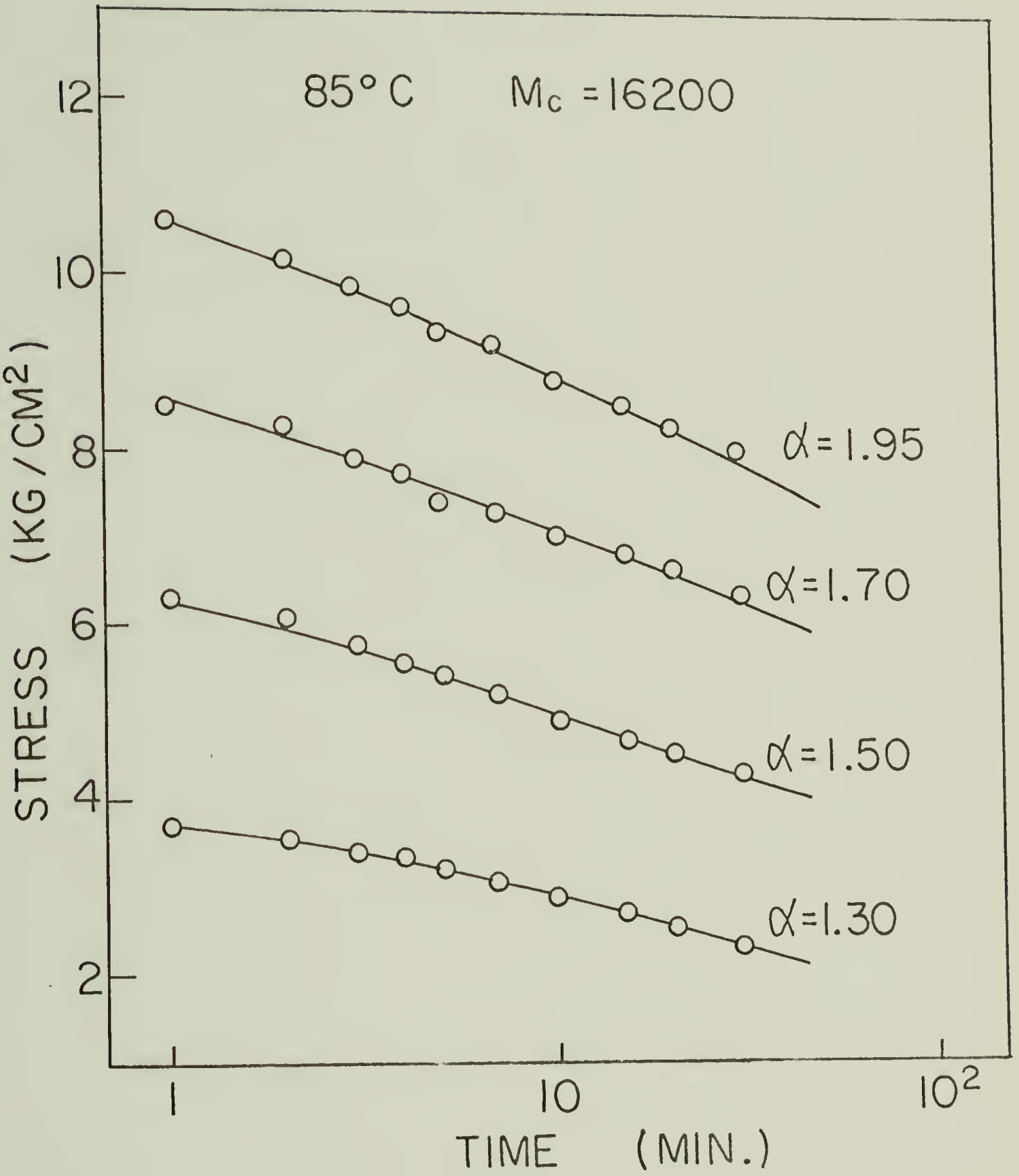
85° C
M_c = 16200
12
10
8
6
4
2
STRESS (KG/CM²)
α = 1.95
α = 1.70
α = 1.50
α = 1.30
1
10
10²
TIME (MIN.)

FIG. 15

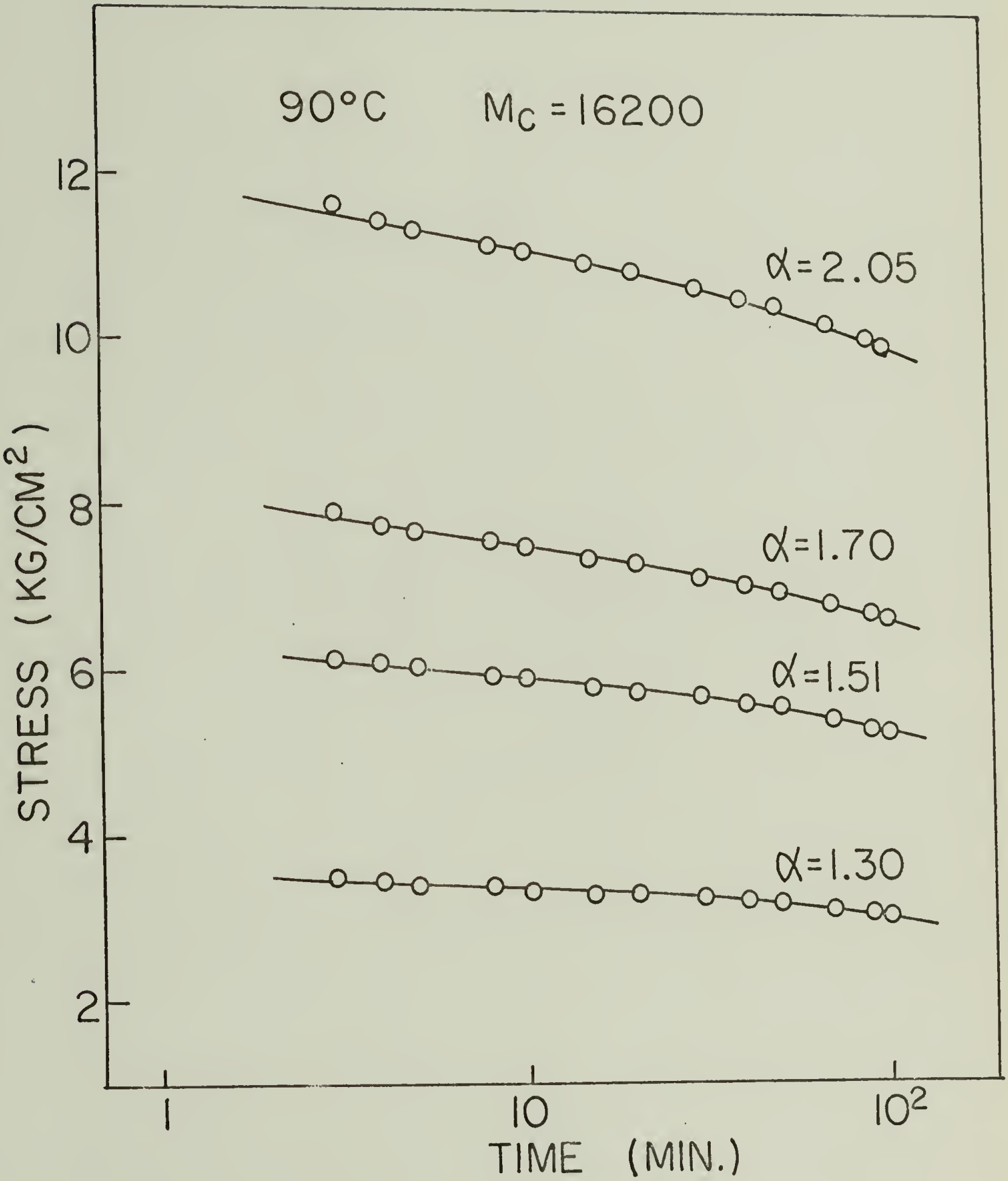
90°C
M_c = 16200
α = 2.05
α = 1.70
α = 1.51
α = 1.30
STRESS (KG/CM²)
12
10
8
6
4
2
1
10
10²
TIME (MIN.)

FIG. 16

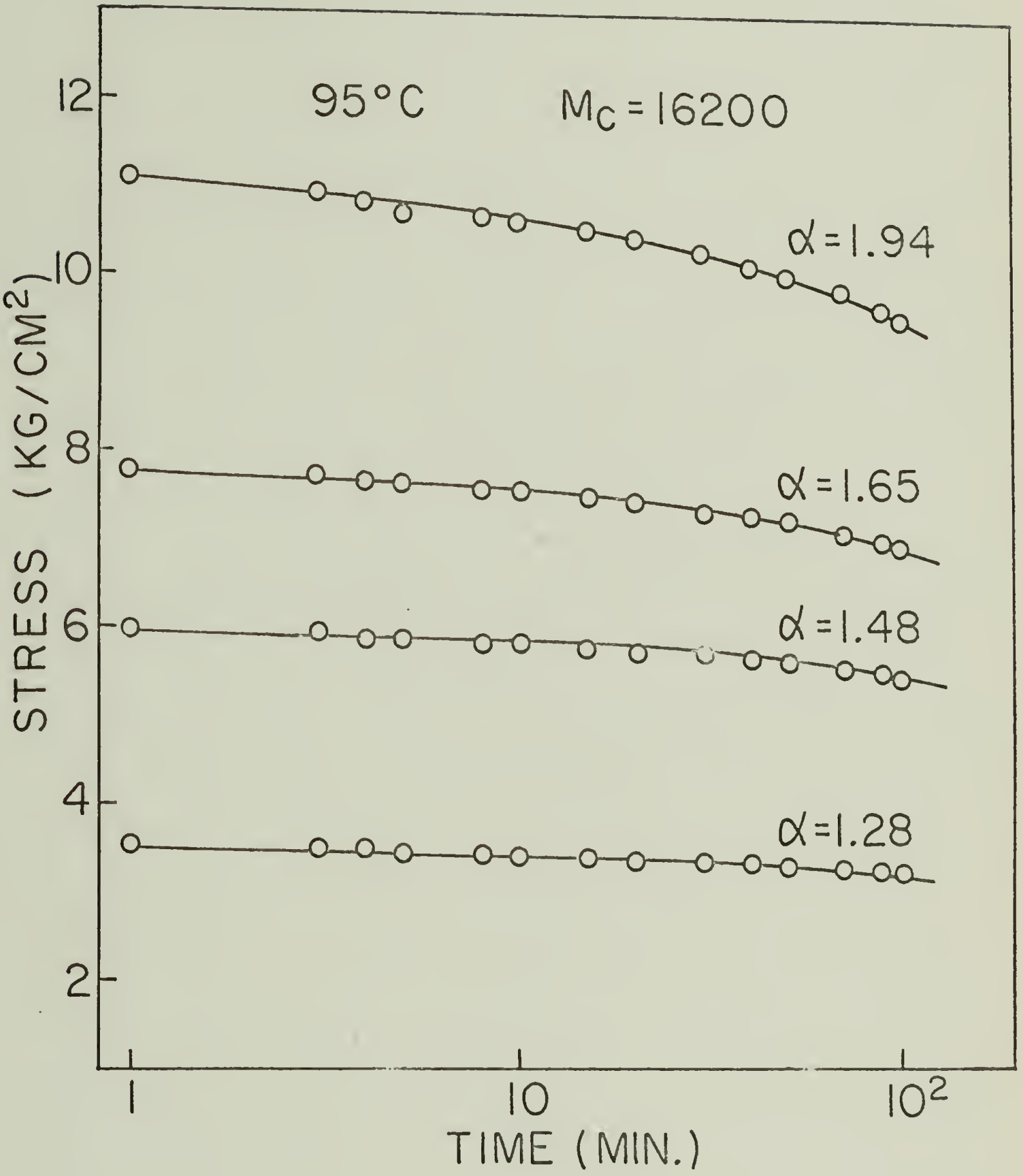
95°C
M_C = 16200
α = 1.94
α = 1.65
α = 1.48
α = 1.28
STRESS (KG/CM²)
12
10
8
6
4
2
1
10
10²
TIME (MIN.)

FIG. 17

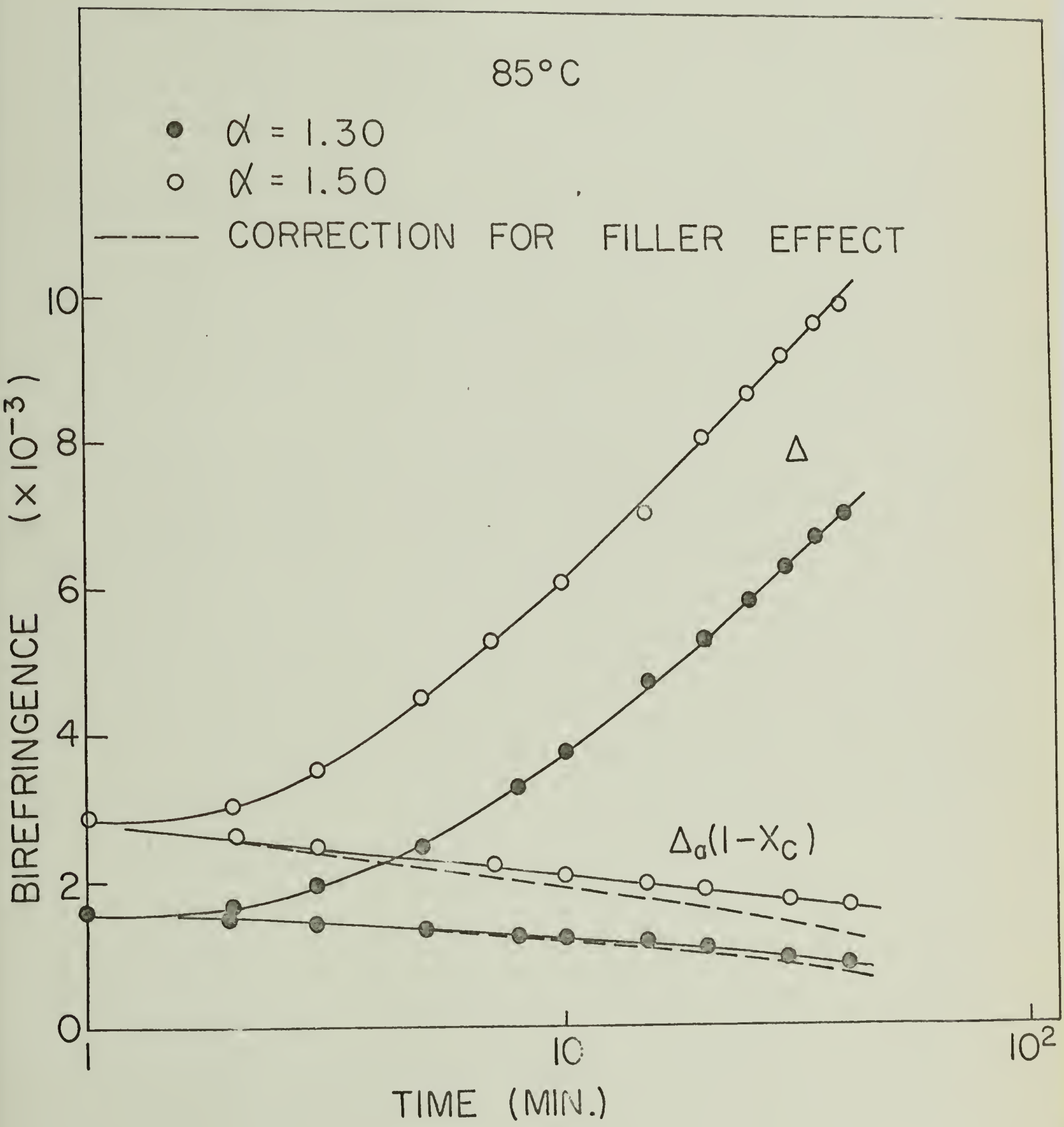
85°C
α = 1.30
α = 1.50
CORRECTION FOR FILLER EFFECT
BIREFRINGENCE (X 10⁻³)
0
2
4
6
8
10
1
10
10²
TIME (MIN.)
Δ
Δa(1-Xc)

FIG. 18

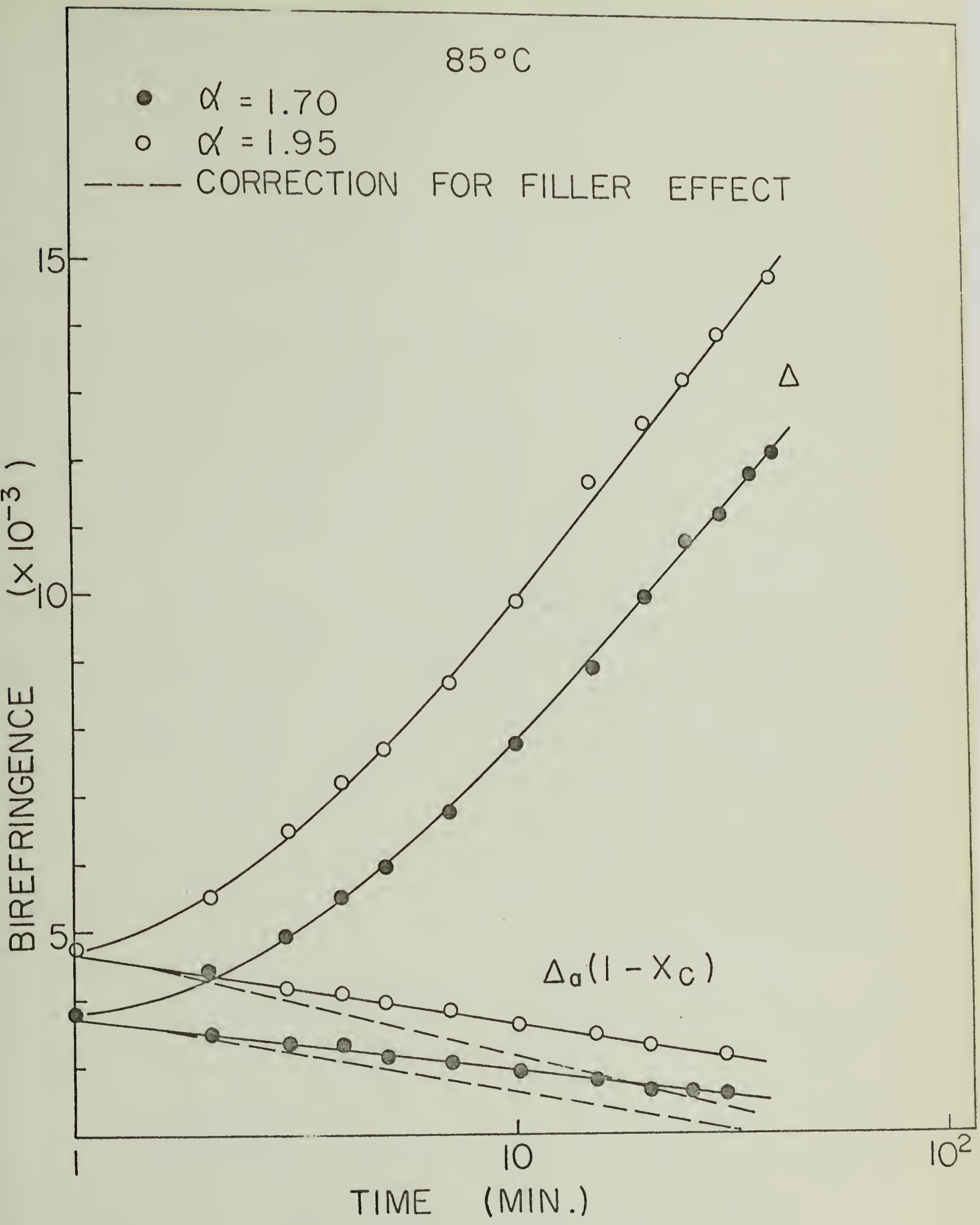
85°C
α = 1.70
α = 1.95
CORRECTION FOR FILLER EFFECT
BIREFRINGENCE (X 10⁻³)
15
10
5
Δa(1 - Xc)
1
10
10²
TIME (MIN.)

FIG. 19

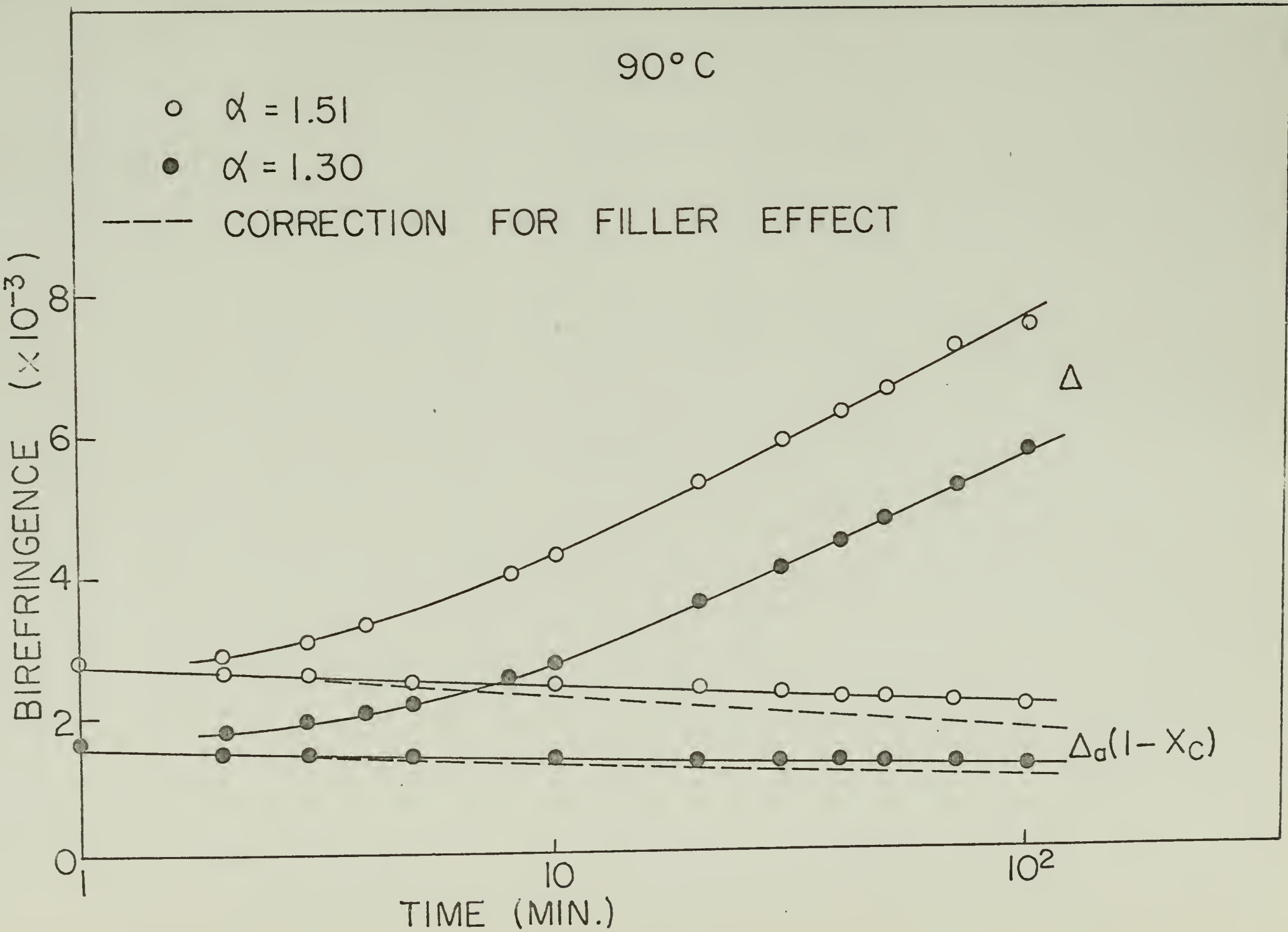
90° C
α = 1.51
α = 1.30
CORRECTION FOR FILLER EFFECT
BIREFRINGENCE (×10⁻³)
0
2
4
6
8
1
10
10²
TIME (MIN.)
Δ
Δa(1 − Xc)

FIG. 20

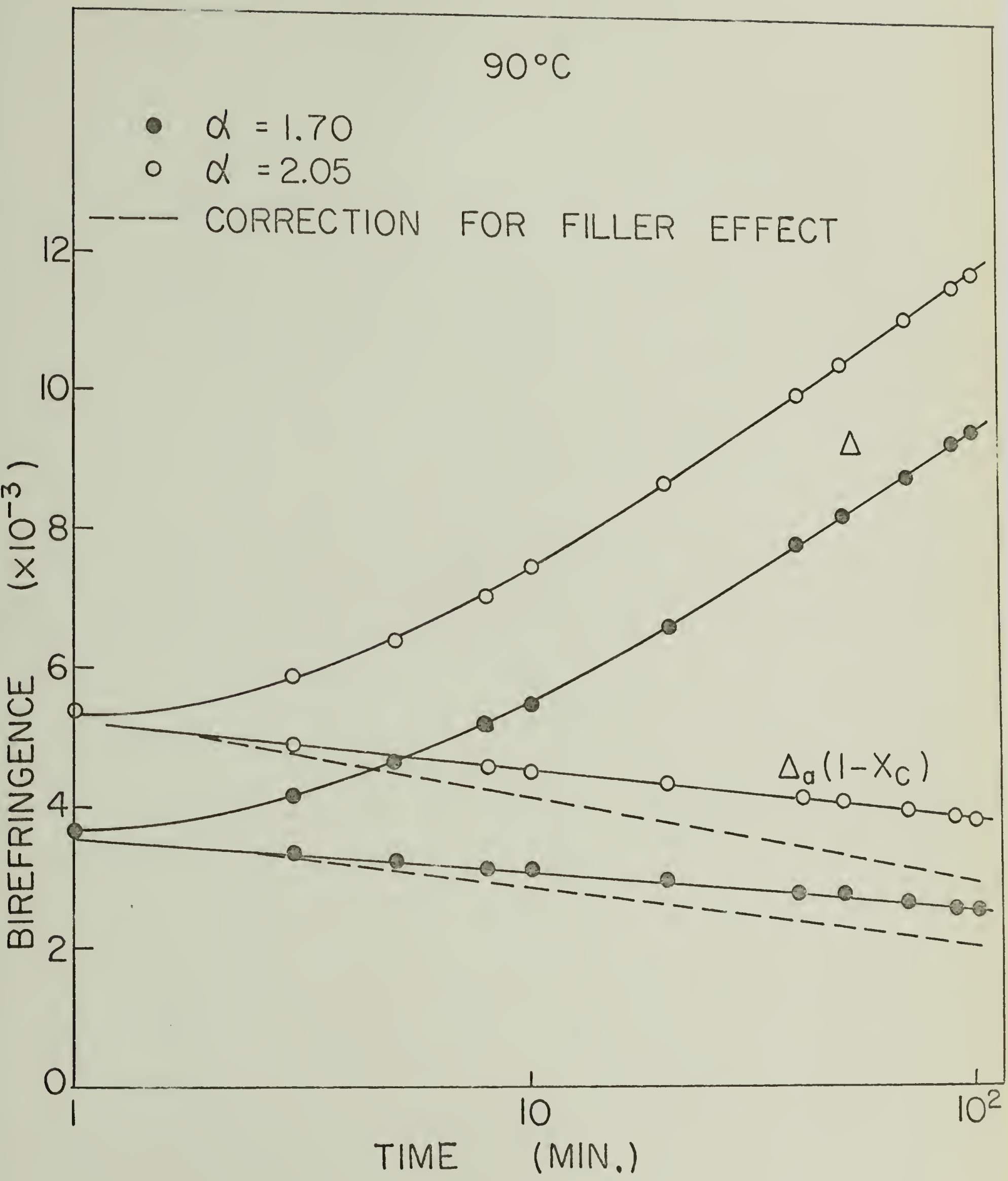
90°C
α = 1.70
α = 2.05
CORRECTION FOR FILLER EFFECT
BIREFRINGENCE (×10⁻³)
0
2
4
6
8
10
12
Δ
Δa(1-Xc)
1
10
10²
TIME (MIN.)

FIG. 21

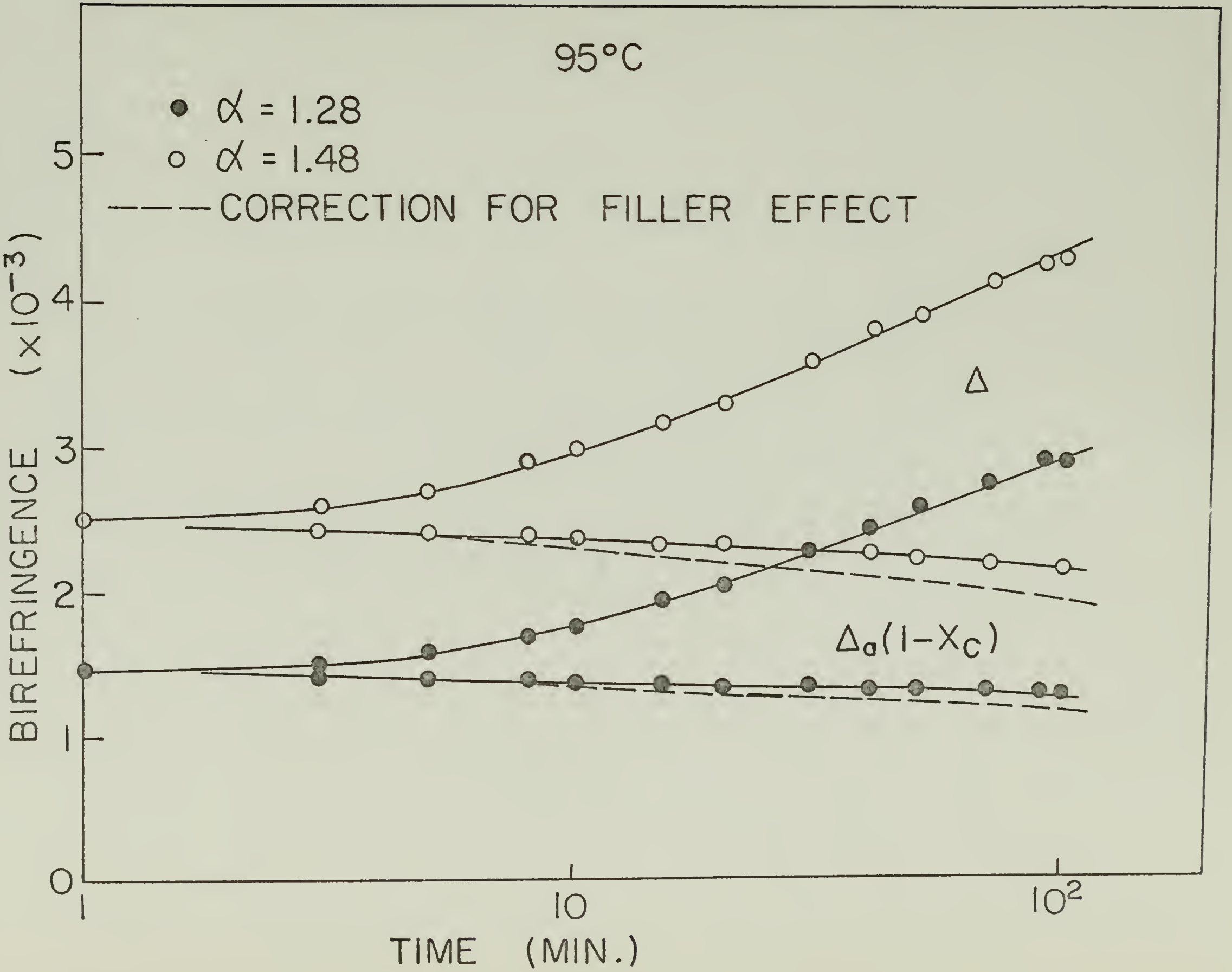
95°C
α = 1.28
α = 1.48
CORRECTION FOR FILLER EFFECT
BIREFRINGENCE (×10⁻³)
0
1
2
3
4
5
Δ
Δa(1-Xc)
1
10
10²
TIME (MIN.)

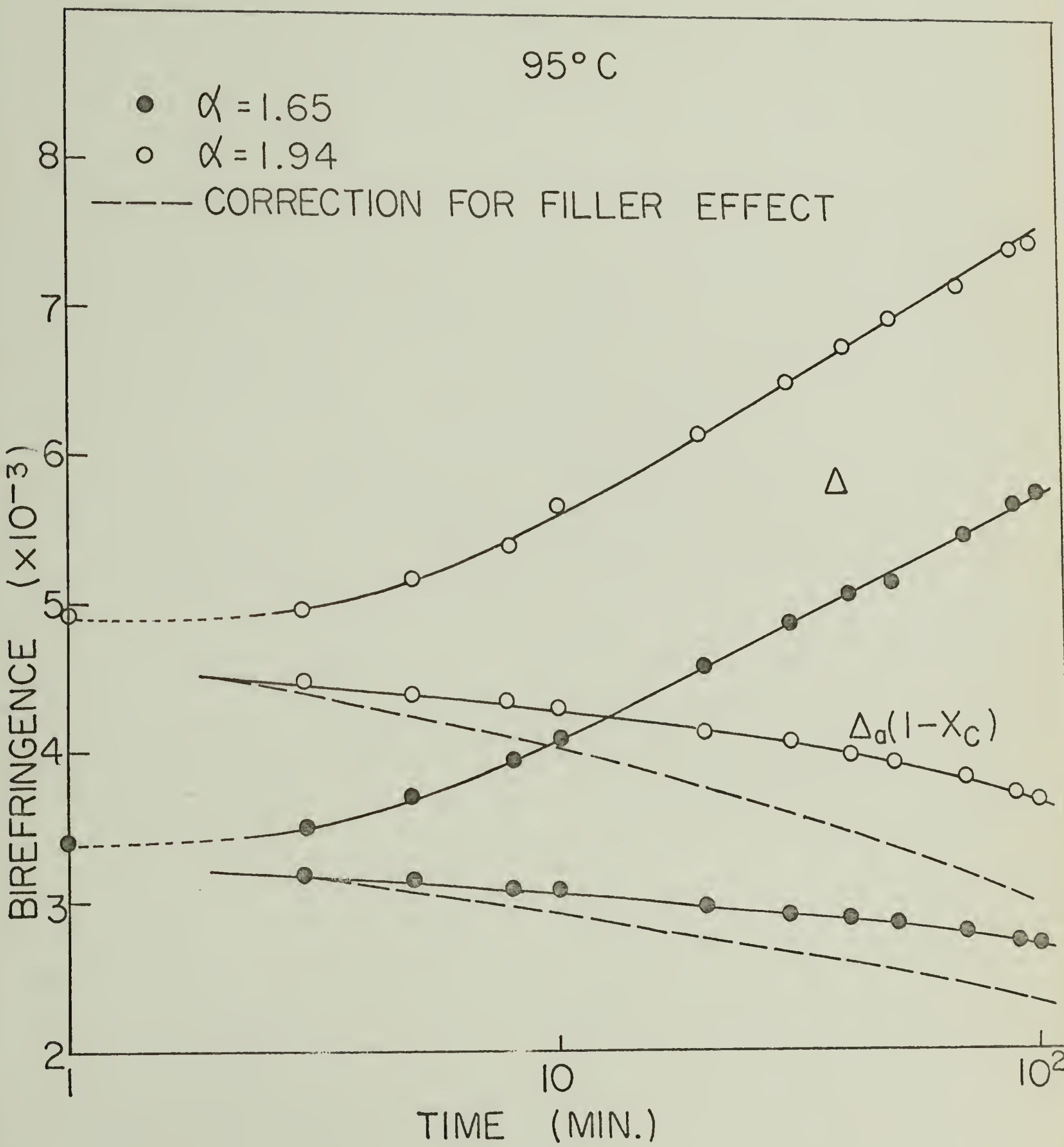
95° C
α = 1.65
α = 1.94
CORRECTION FOR FILLER EFFECT
BIREFRINGENCE (X10-3)
8
7
6
5
4
3
2
Δ
Δa(1-Xc)
1
10
10²
TIME (MIN.)

FIG. 23

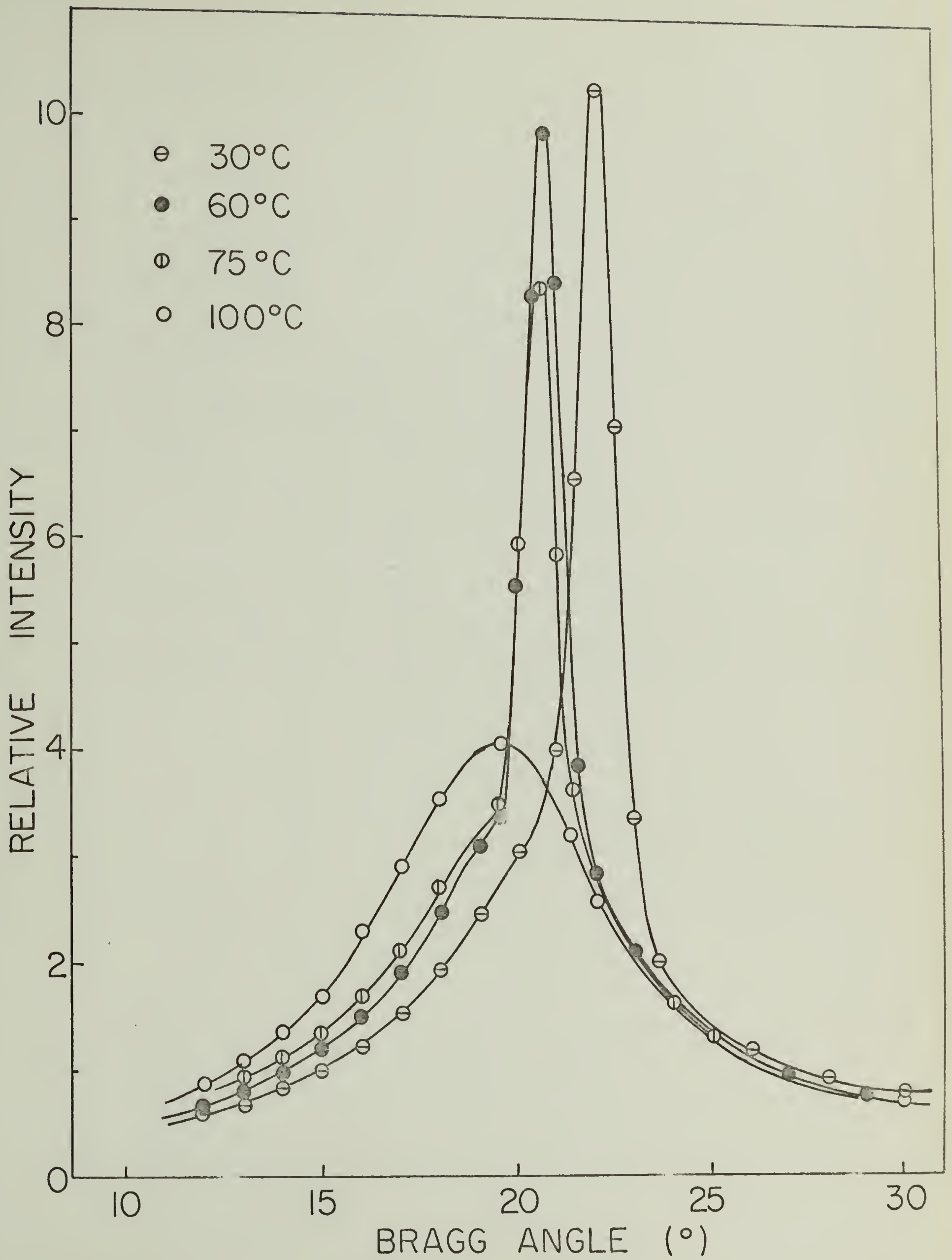
30°C
60°C
75°C
100°C
RELATIVE INTENSITY
0
2
4
6
8
10
10
15
20
25
30
BRAGG ANGLE (°)

FIG. 24

85 °C

105 °C

S.D.

5 HOURS 85 °C

$\alpha = 1.90$

FIG. 25

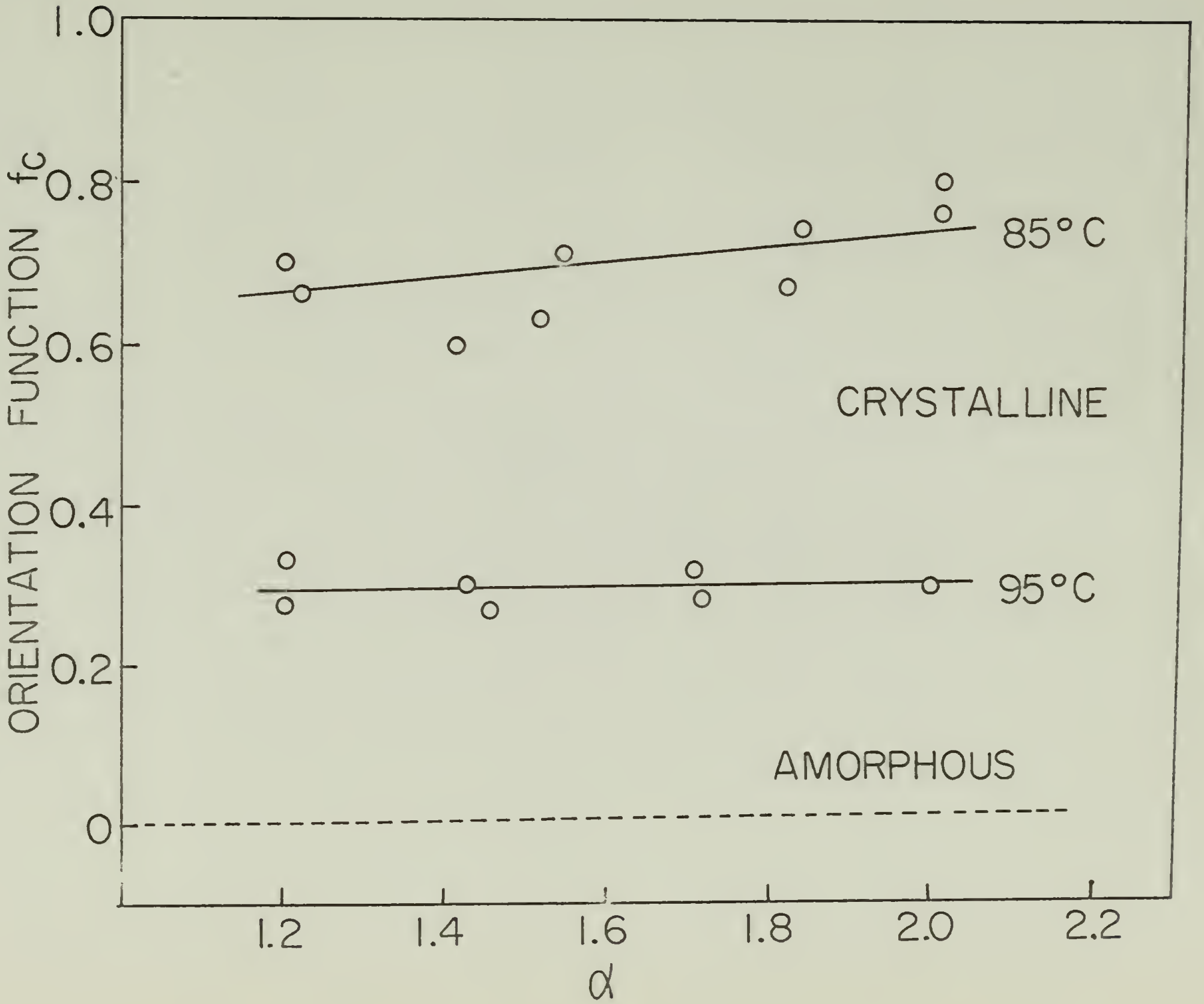
1.0
0.8
0.6
0.4
0.2
0
ORIENTATION FUNCTION f_c
85°C
CRYSTALLINE
95°C
AMORPHOUS
1.2
1.4
1.6
1.8
2.0
2.2
α

FIG. 26

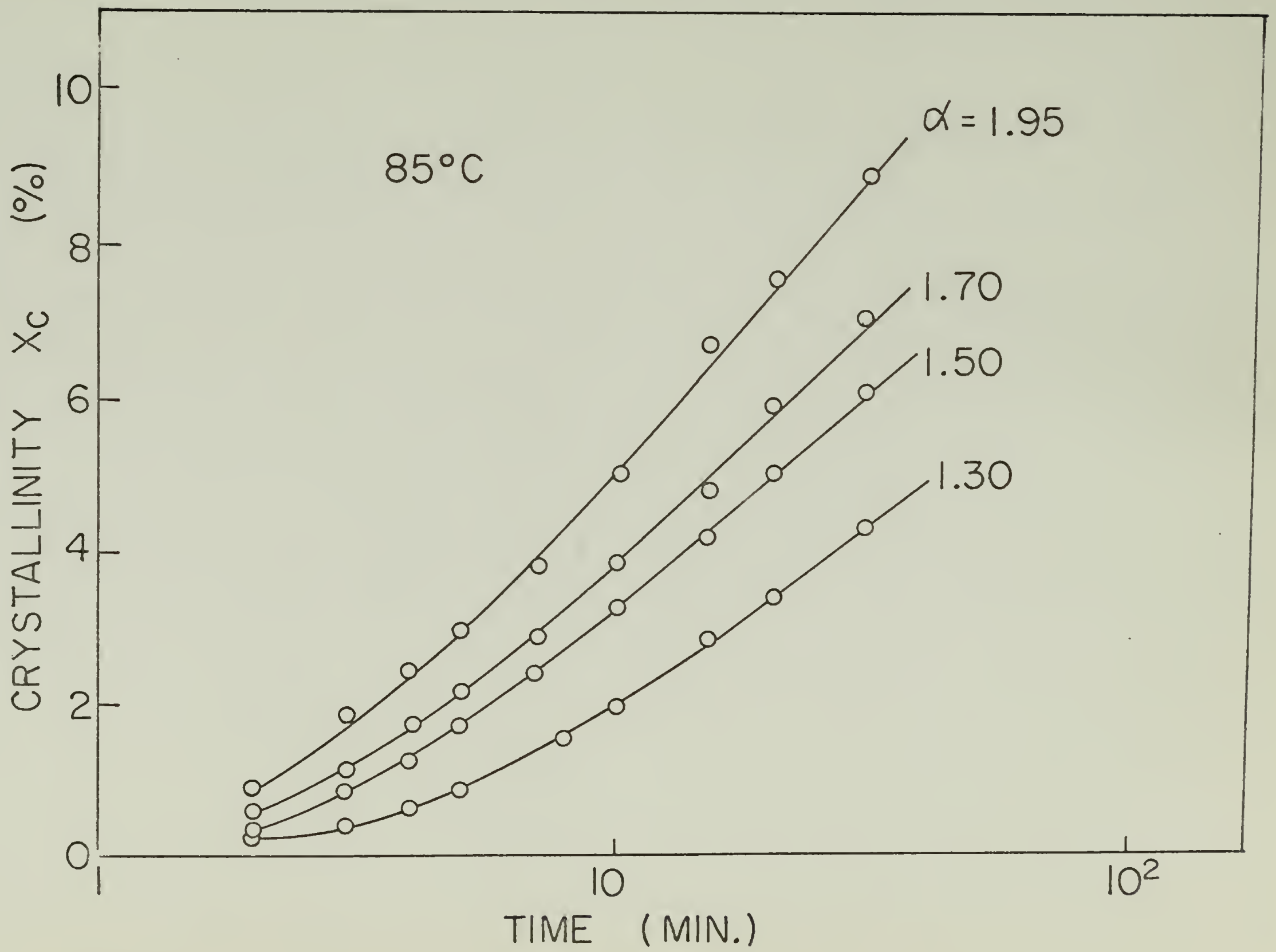
85°C
α = 1.95
1.70
1.50
1.30
CRYSTALLINITY Xc (%)
0
2
4
6
8
10
10
10²
TIME (MIN.)

FIG. 27

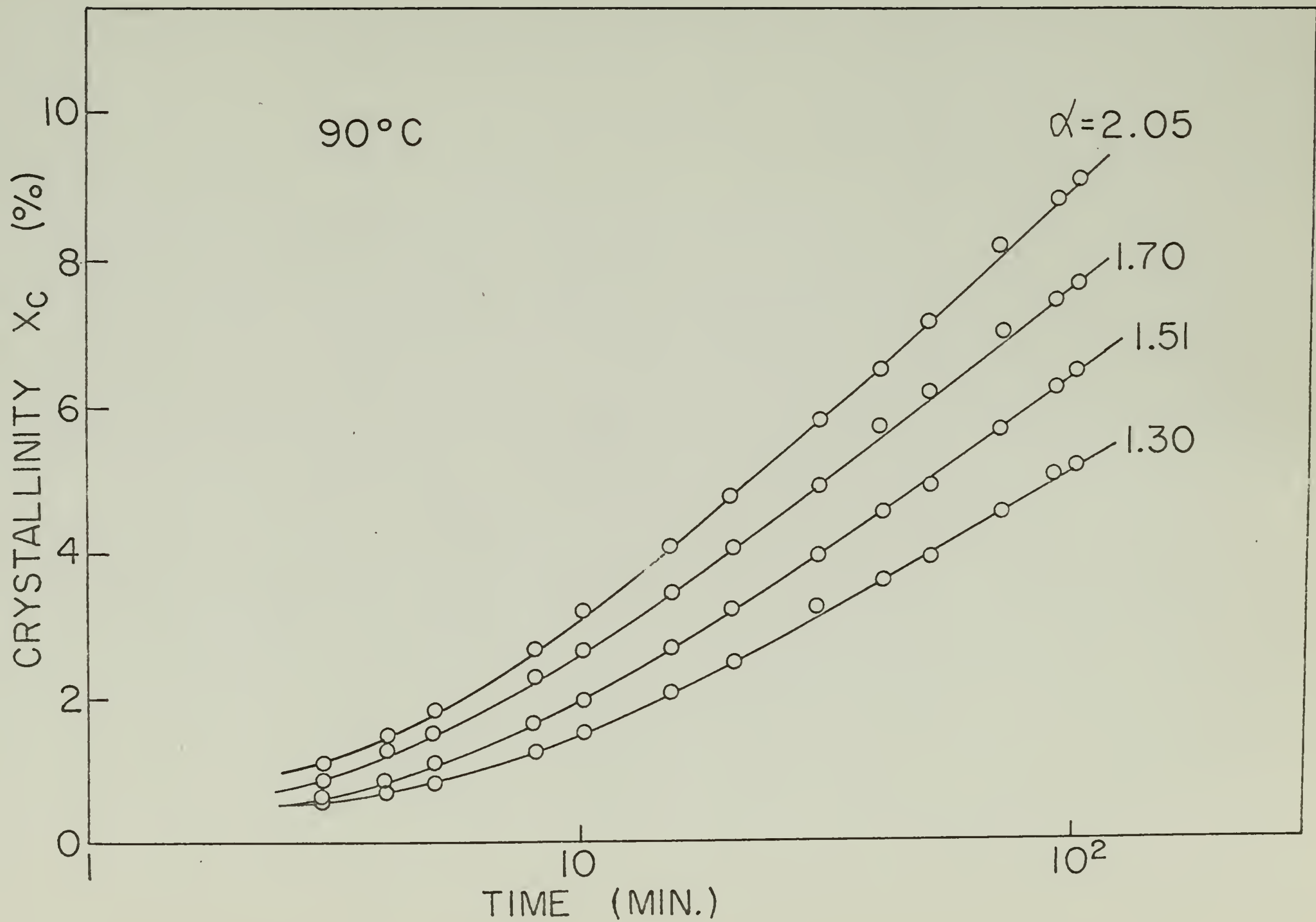
90°C
α=2.05
1.70
1.51
1.30
CRYSTALLINITY X_C (%)
0
2
4
6
8
10
10
10^2
TIME (MIN.)

FIG. 28

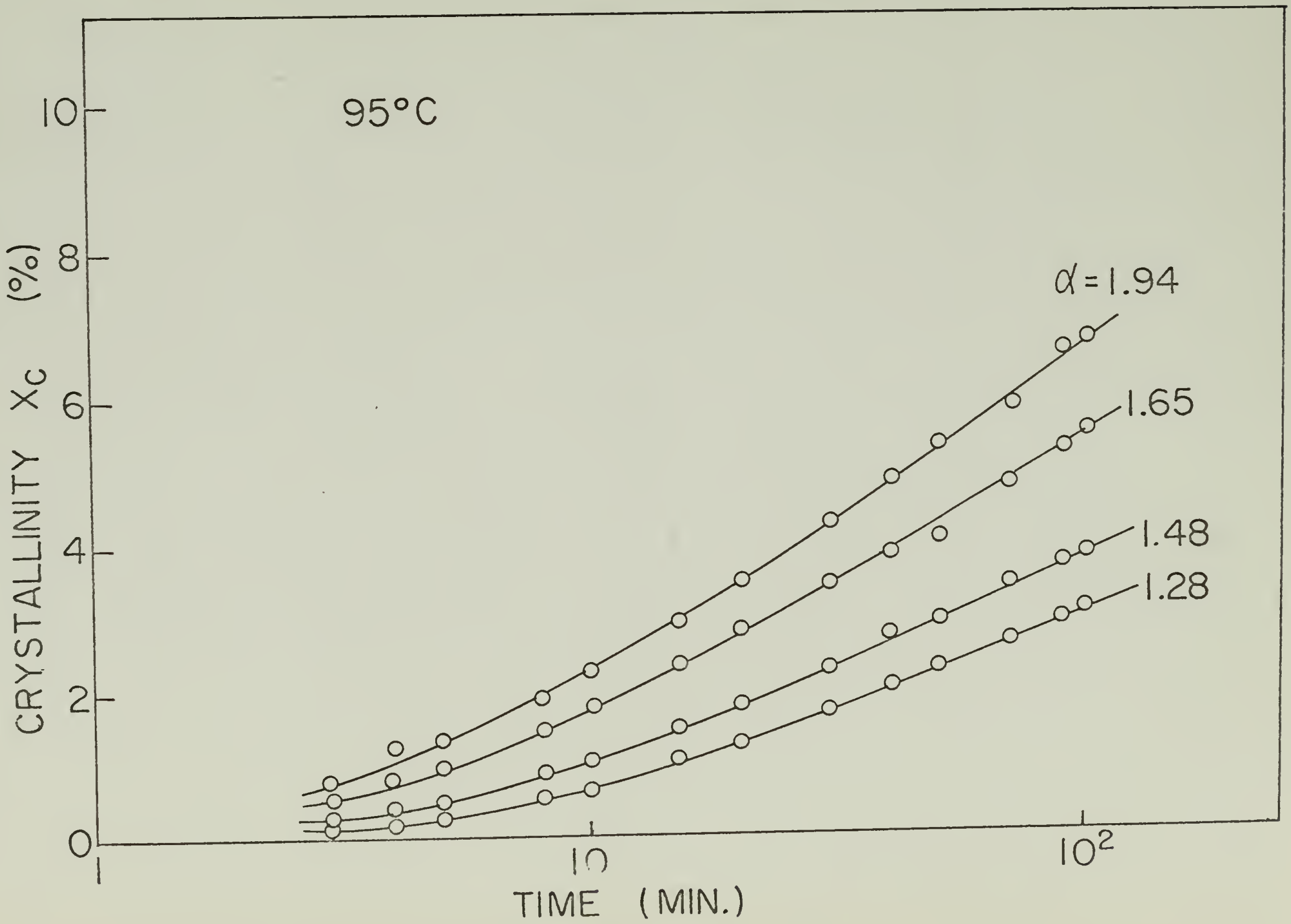
95°C
CRYSTALLINITY X_c (%)
0
2
4
6
8
10
α=1.94
1.65
1.48
1.28
10
10^2
TIME (MIN.)

FIG. 22

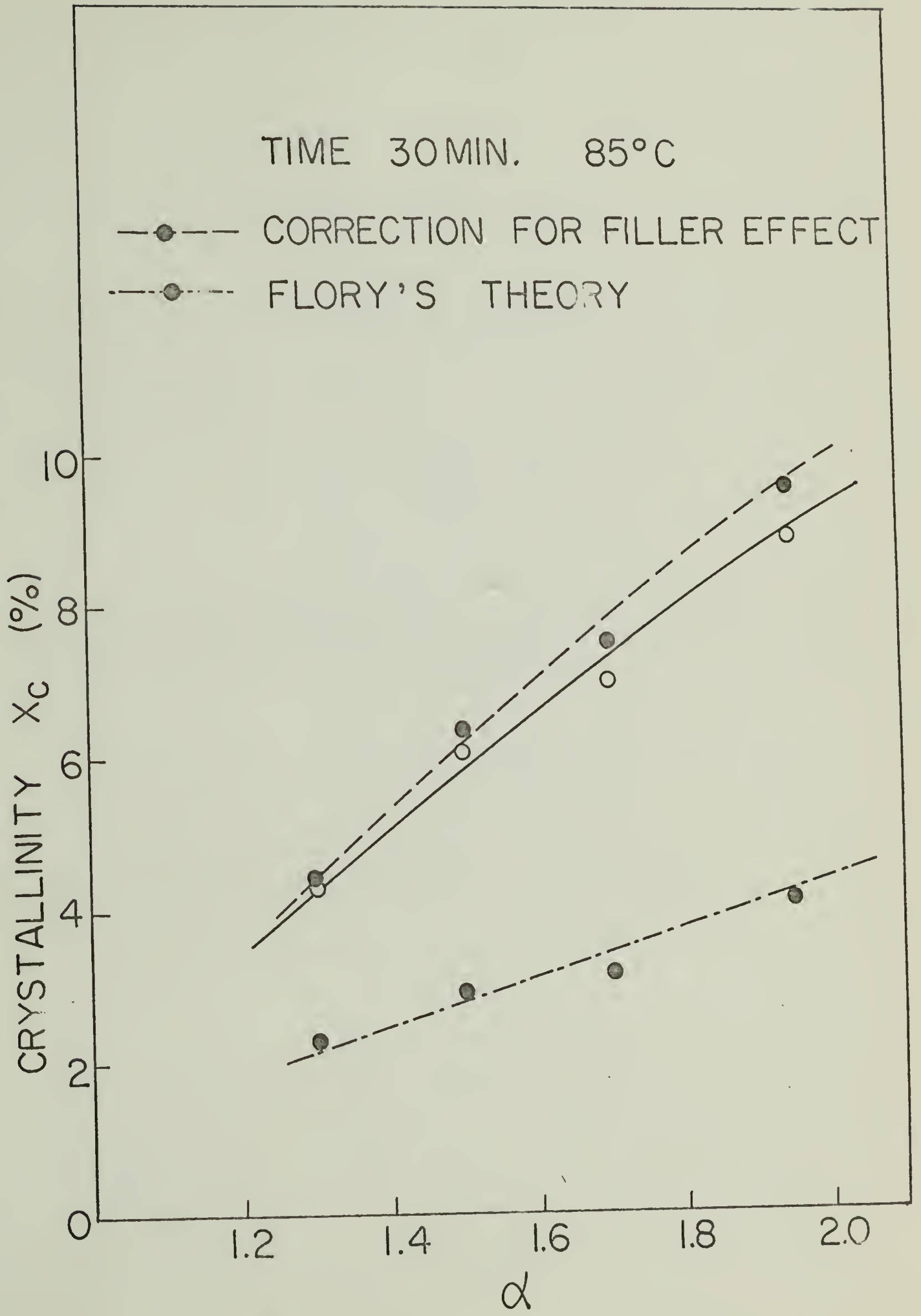
TIME 30 MIN. 85°C
CORRECTION FOR FILLER EFFECT
FLORY'S THEORY
CRYSTALLINITY Xc (%)
0
2
4
6
8
10
1.2
1.4
1.6
1.8
2.0
α

FIG. 30

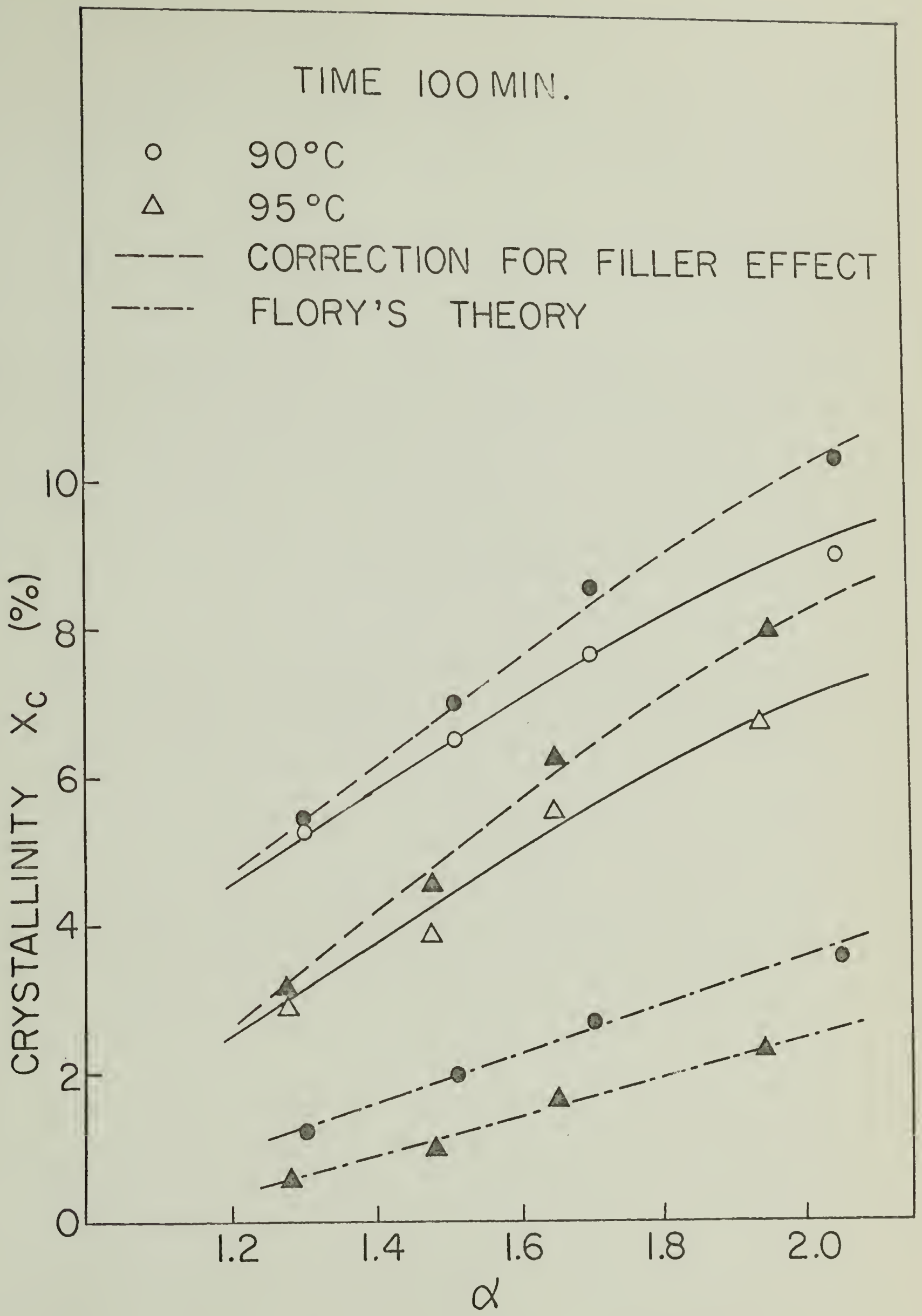
TIME 100 MIN.
90°C
95°C
CORRECTION FOR FILLER EFFECT
FLORY'S THEORY
CRYSTALLINITY Xc (%)
0
2
4
6
8
10
1.2
1.4
1.6
1.8
2.0
α

FIG. 31

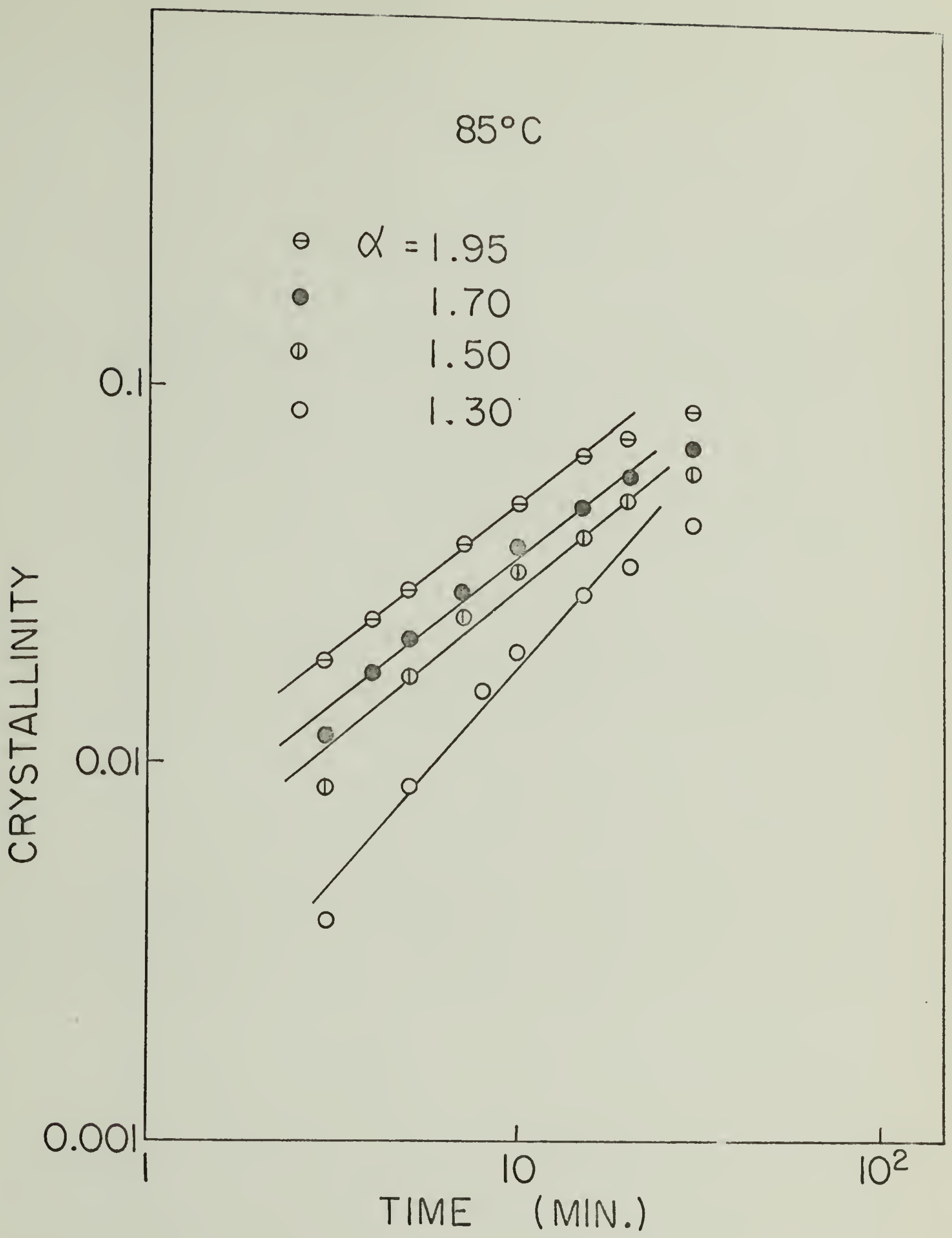
85°C
α = 1.95
1.70
1.50
1.30
0.1
0.01
0.001
CRYSTALLINITY
1
10
10²
TIME (MIN.)

FIG. 32

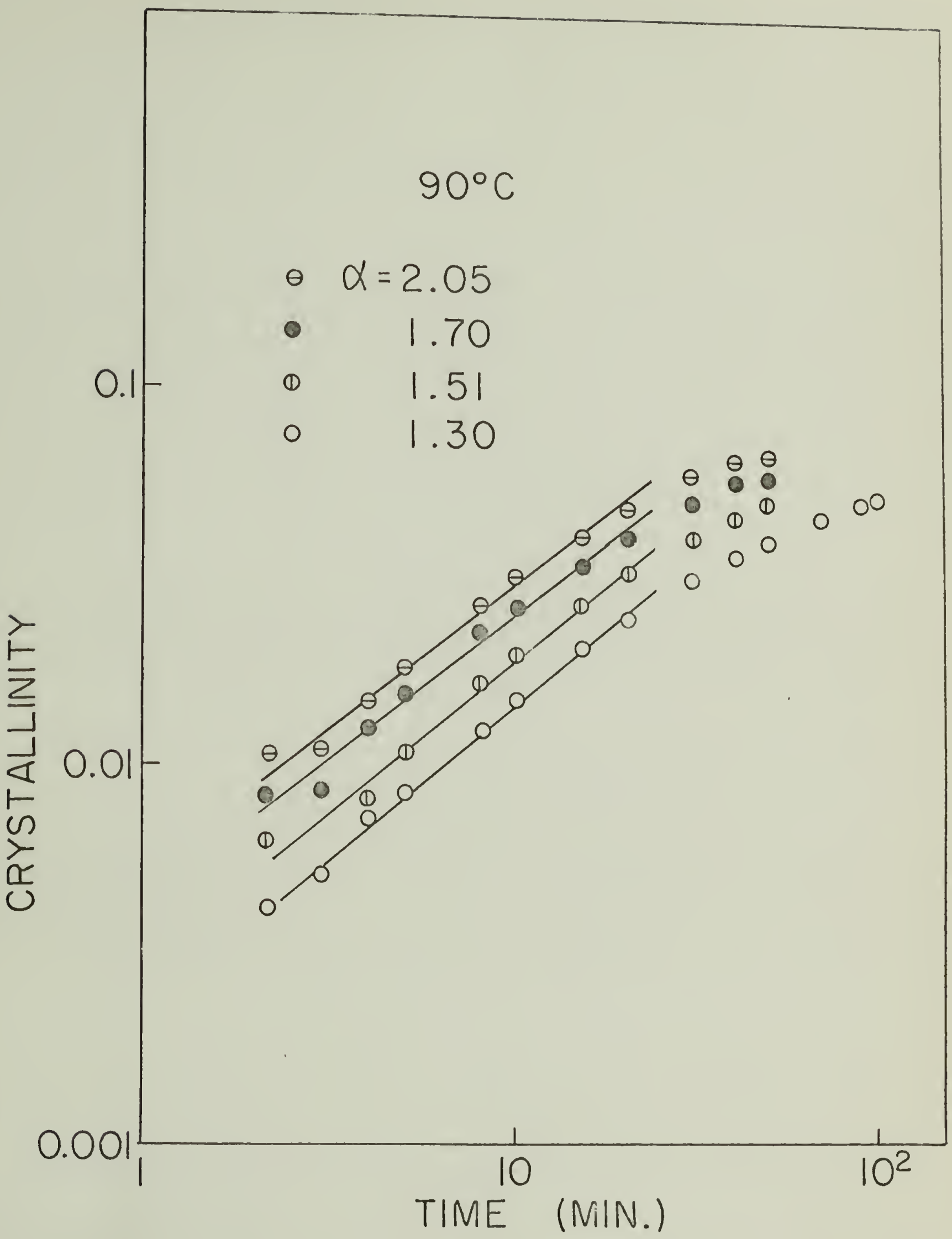
90°C
α = 2.05
1.70
1.51
1.30
0.1
0.01
0.001
CRYSTALLINITY
1
10
10²
TIME (MIN.)

FIG. 33

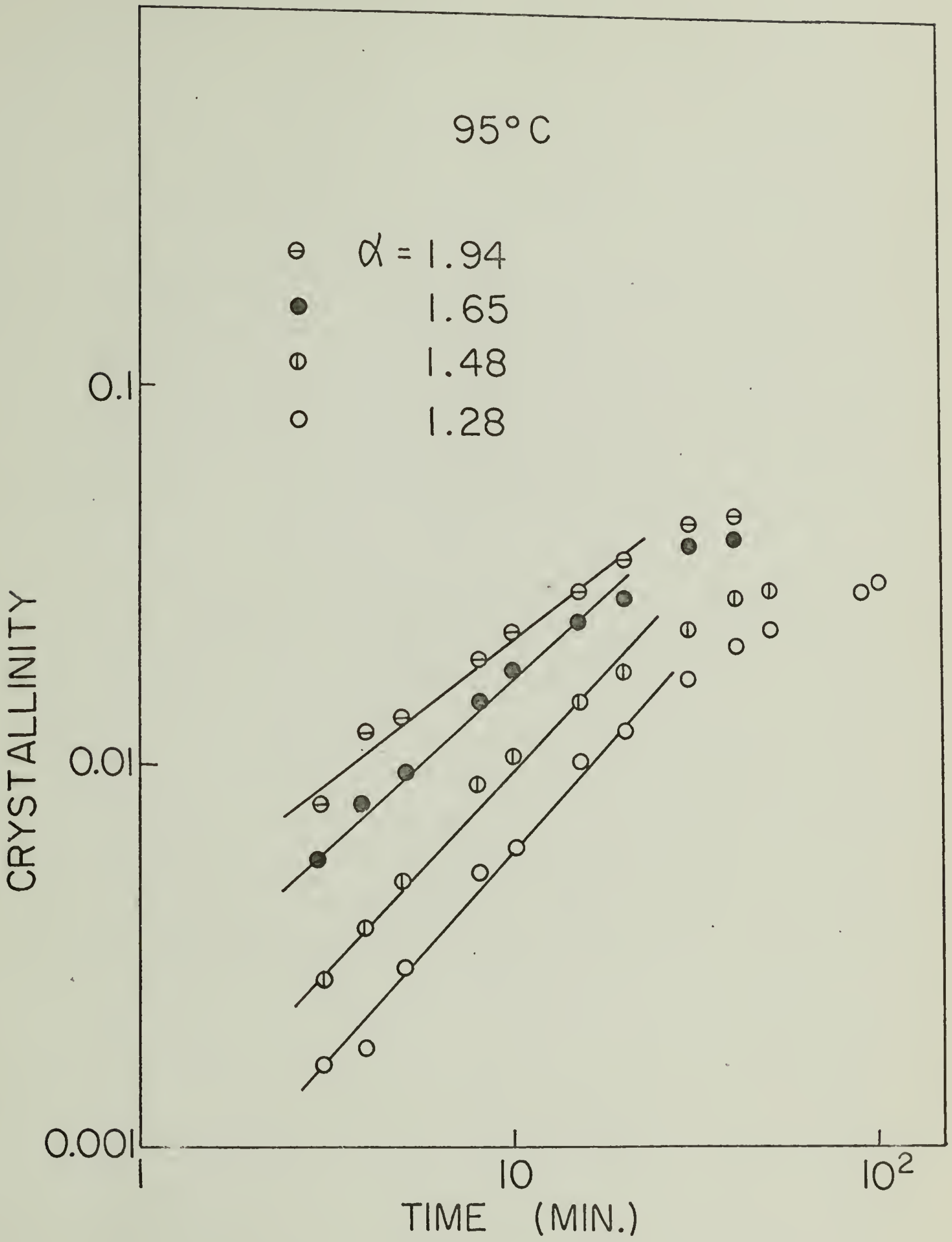
95° C
α = 1.94
1.65
1.48
1.28
0.1
0.01
0.001
CRYSTALLINITY
10
10²
TIME (MIN.)

FIG. 34

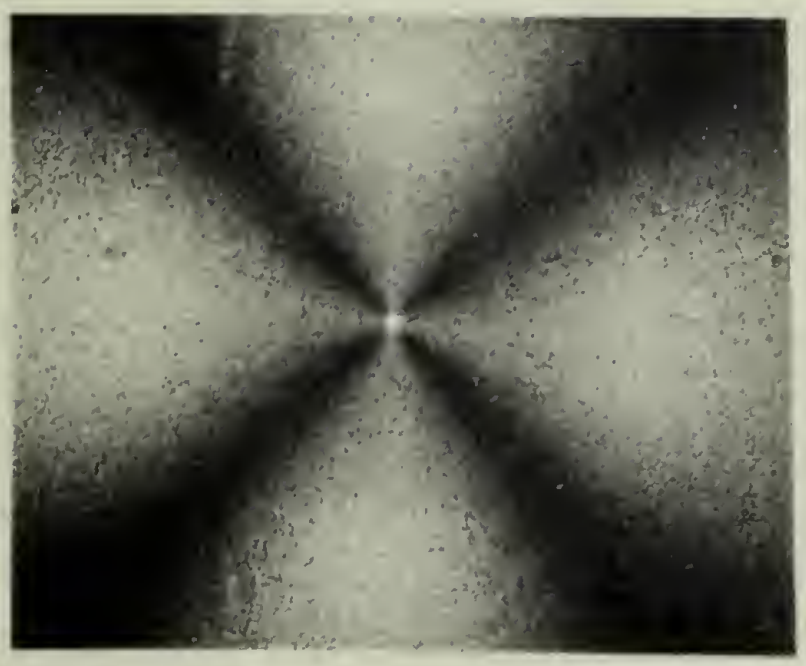

H_V

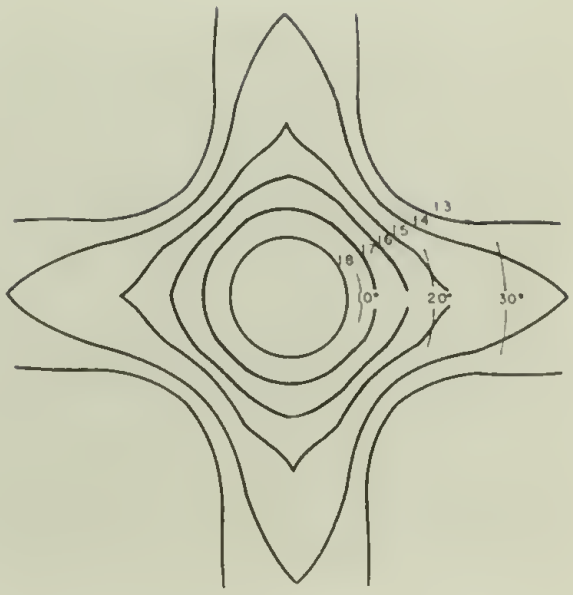

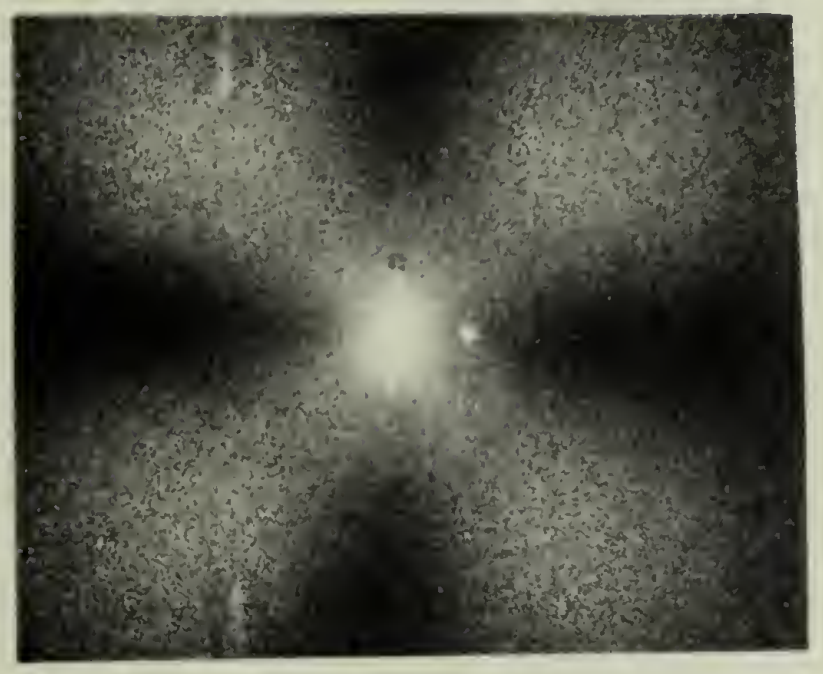

V_V

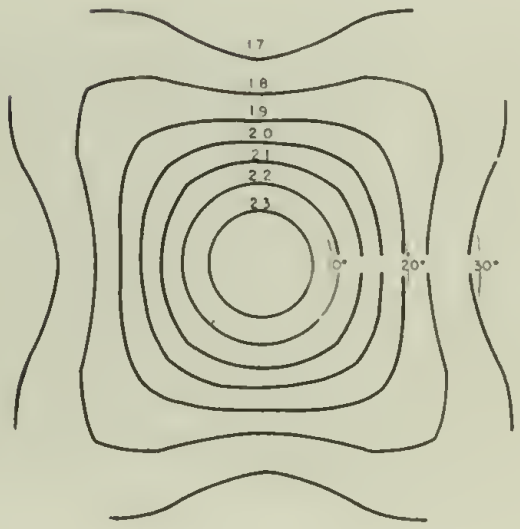

FIG. 35

H_V

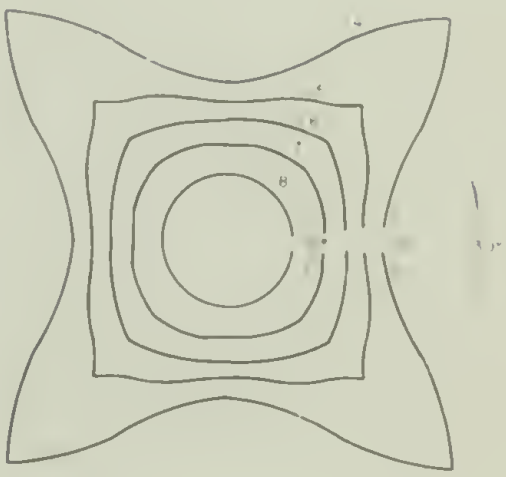

V_V

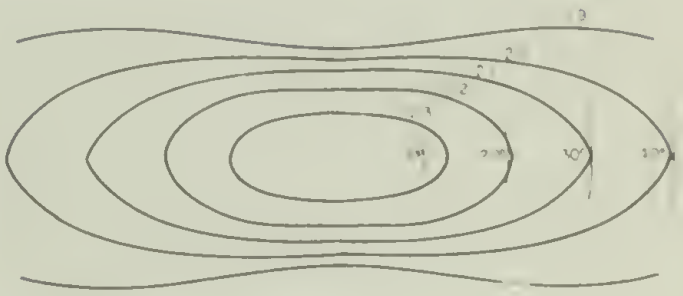

85 °C.

FIG. 36

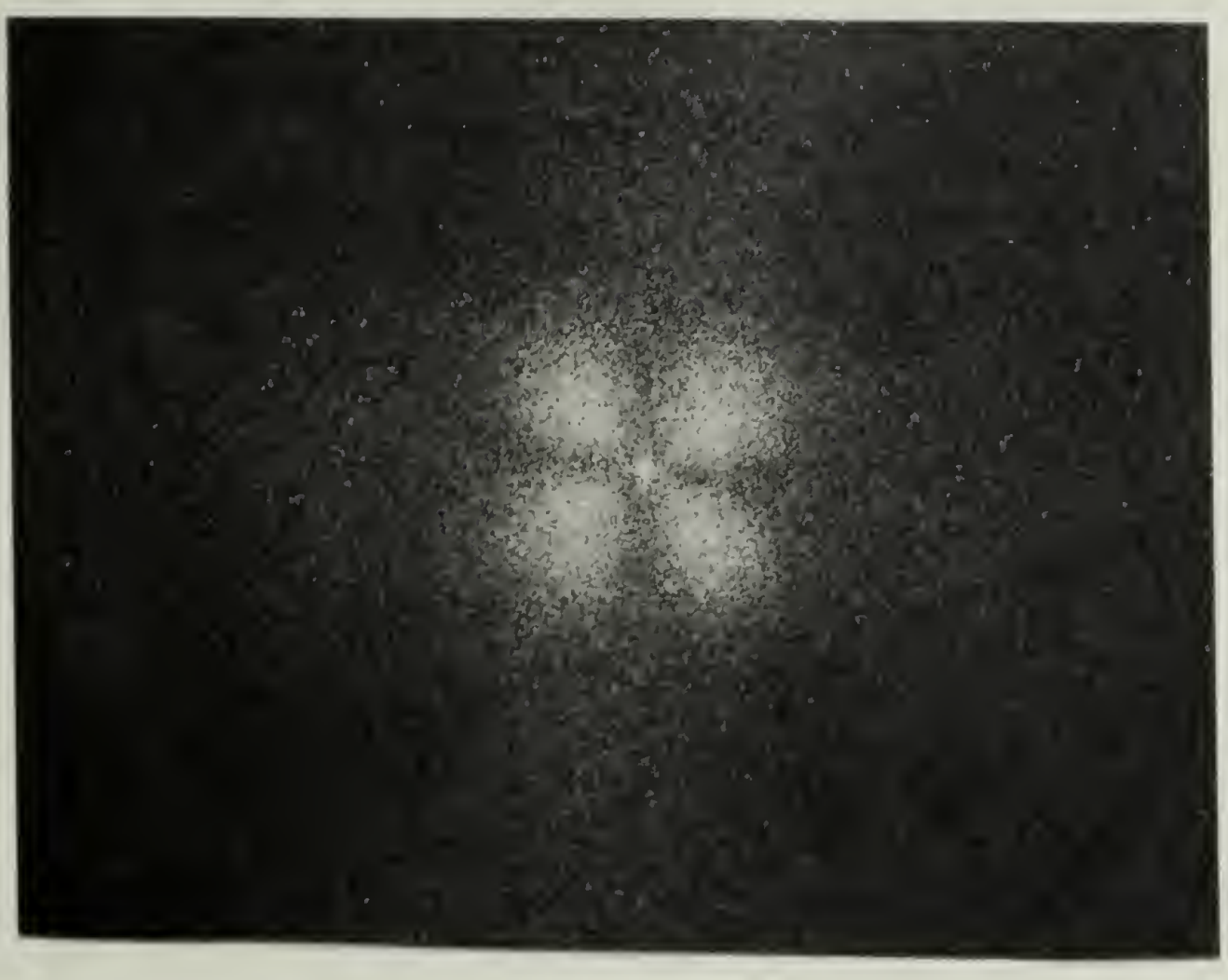

H_V

V_V

FIG. 37 65°C

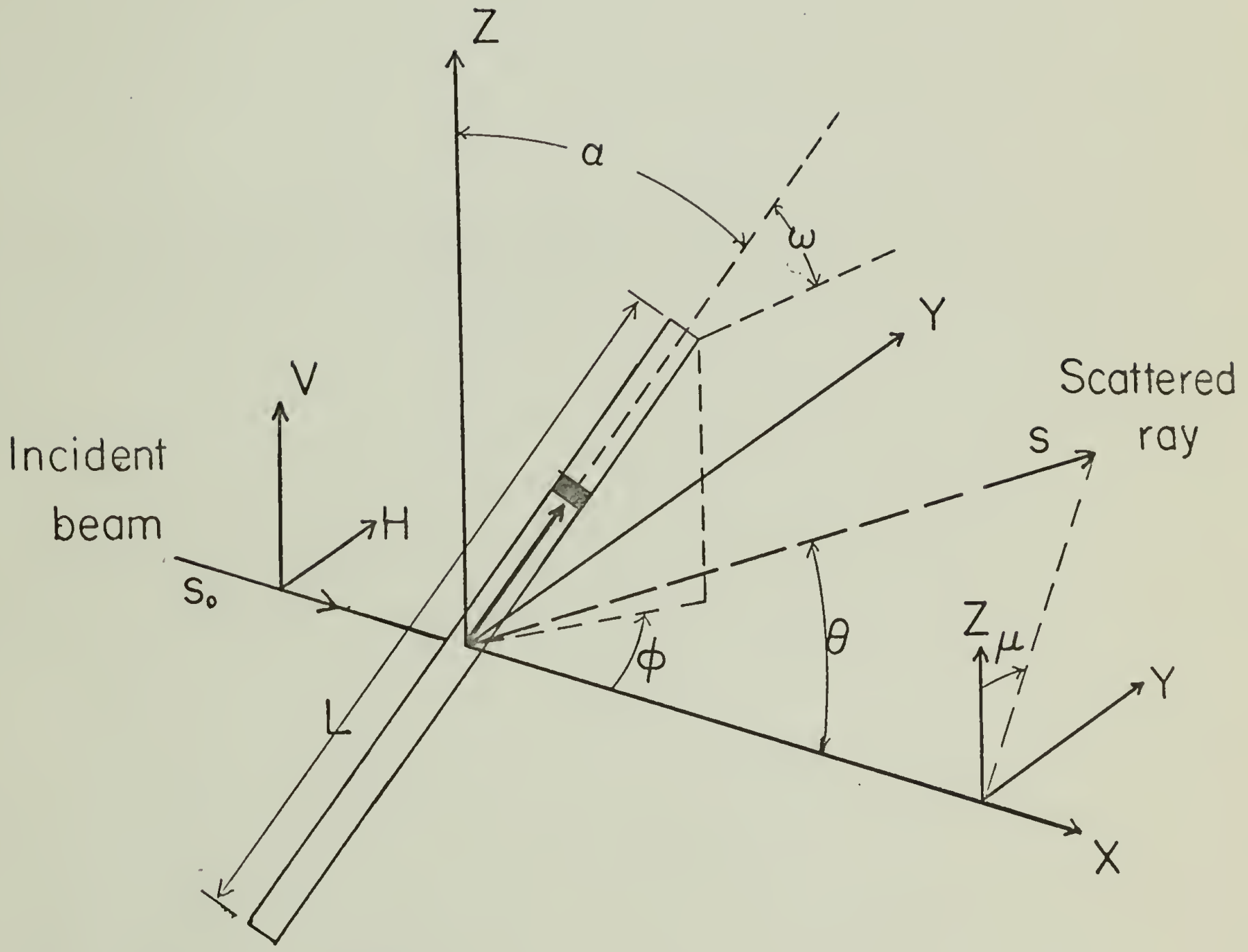

FIG. 38

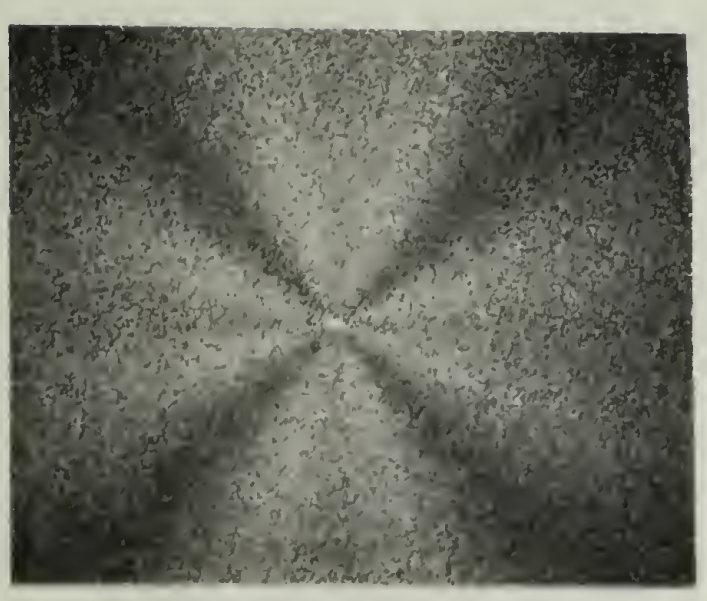

H_V $\alpha = 1.30$

V_V

S.D.

H_V $\alpha = 1.60$

V_V

H_V $\alpha = 1.90$

FIG. 39

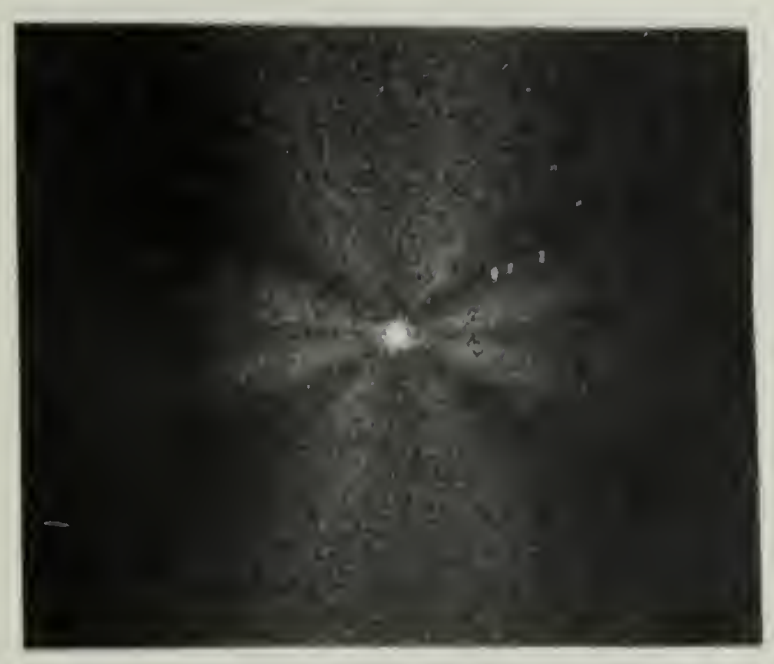

H_V

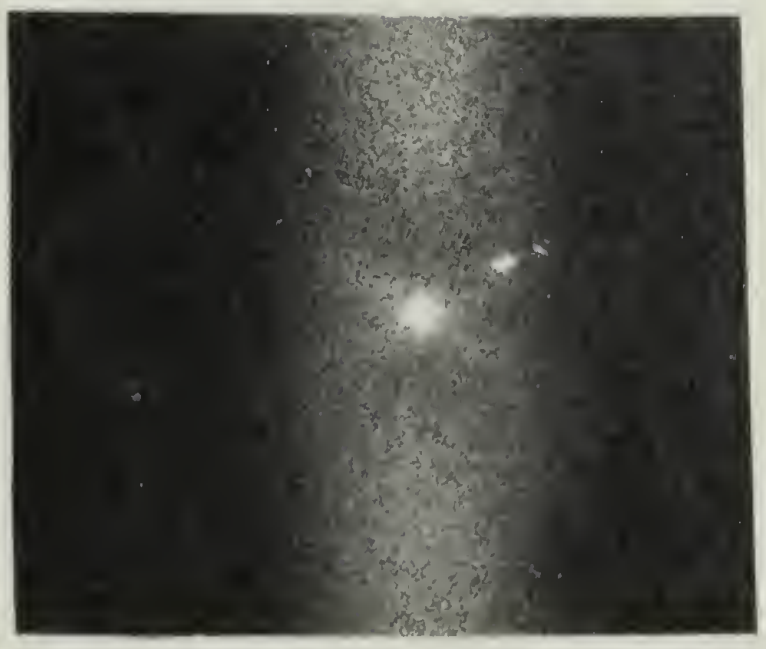

V_V

$\alpha = 1.30$

S.D.

H_V

V_V

$\alpha = 1.80$

87 °

FIG. 40

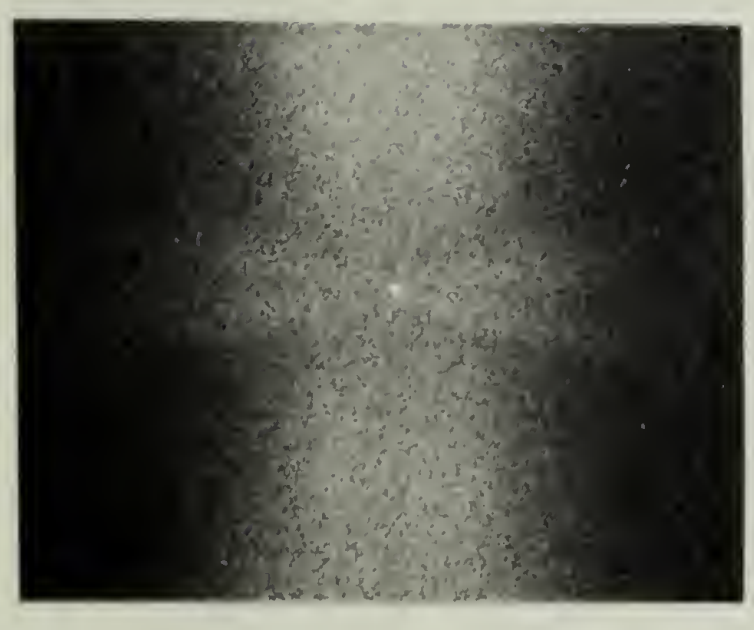

V_V

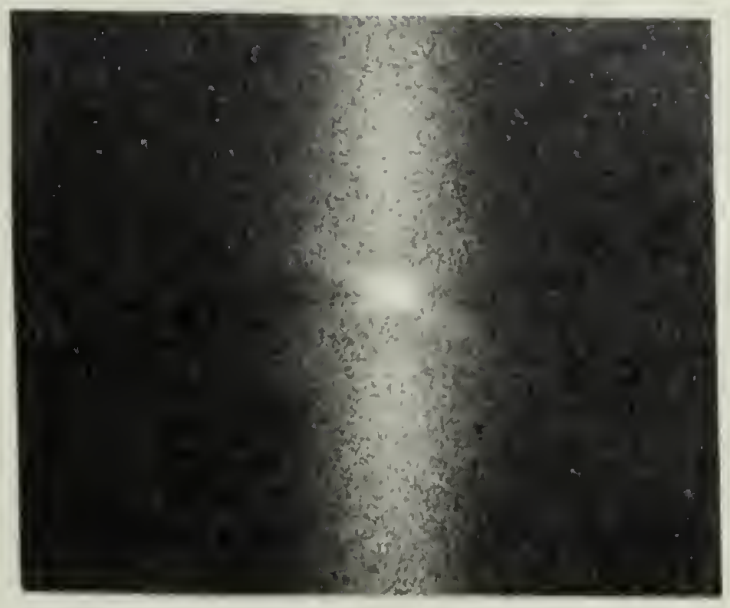

V_V

$\alpha = 1.30$

S.D.

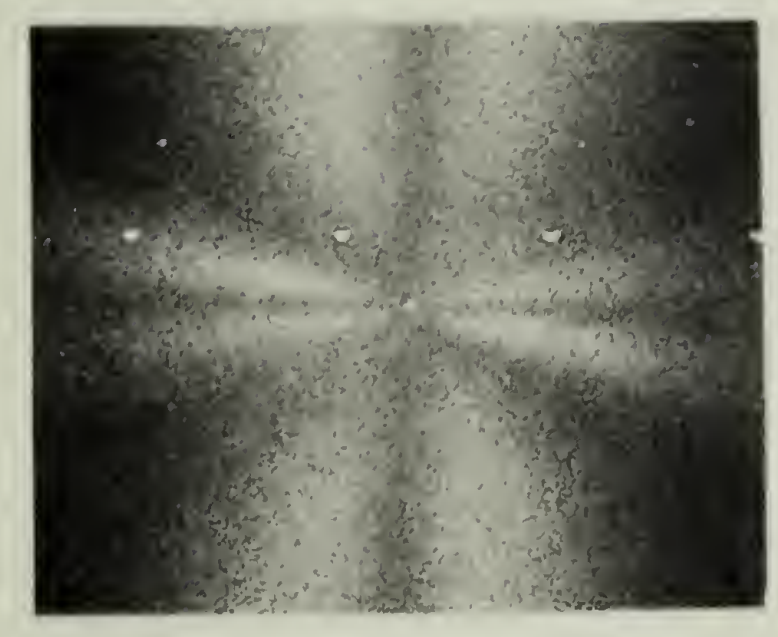

V_V

V_V

$\alpha = 1.60$

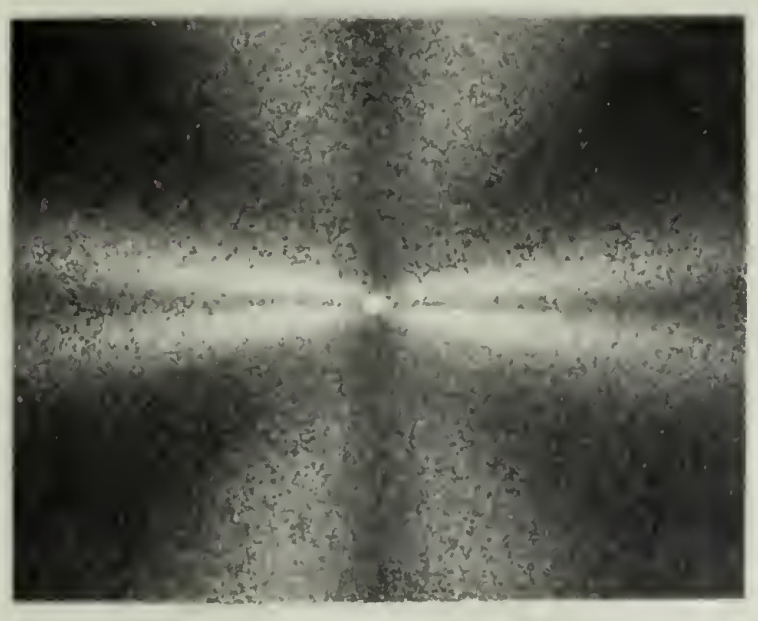

H_V

V_V

$\alpha = 1.90$

FIG. 11

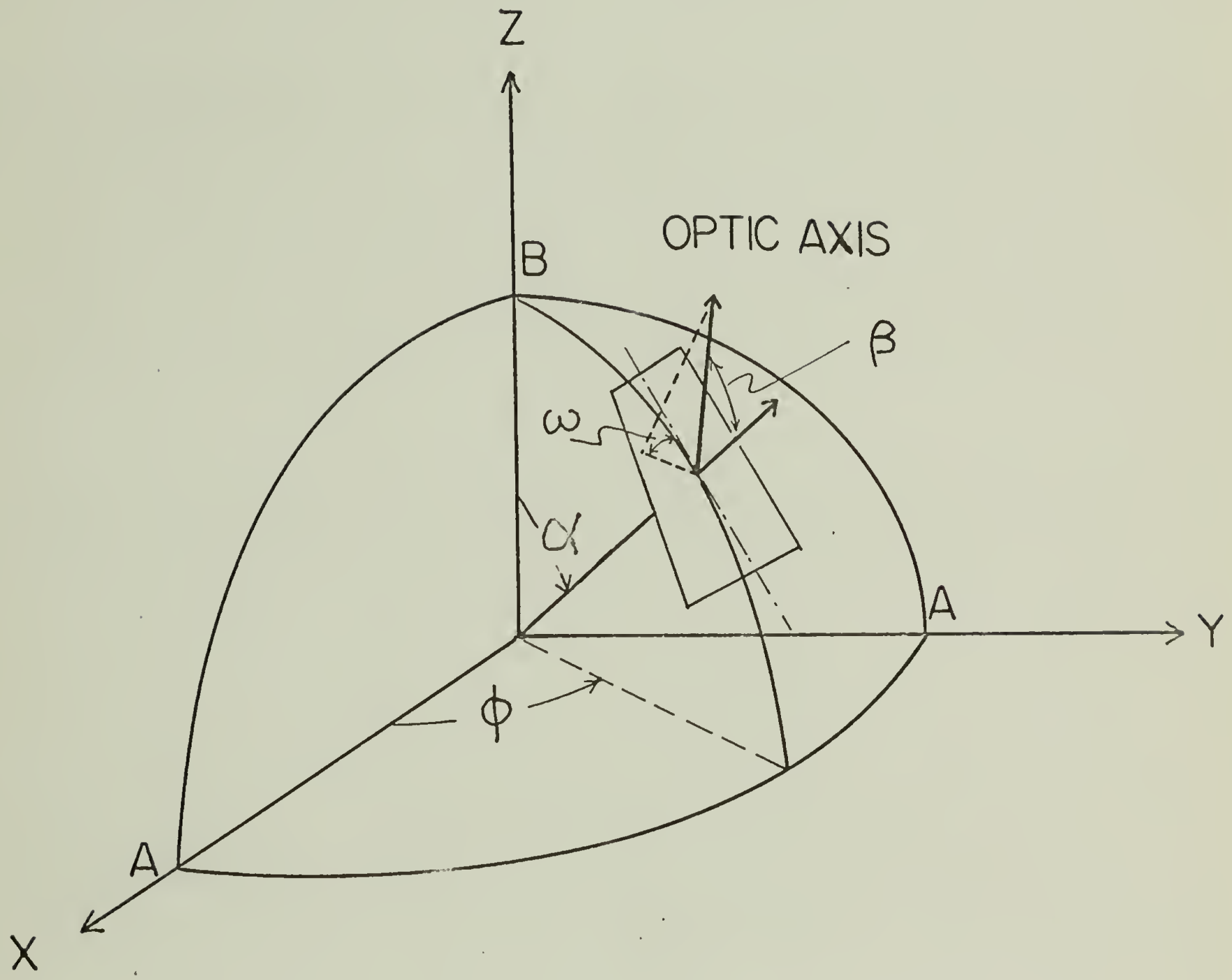

FIG. 42

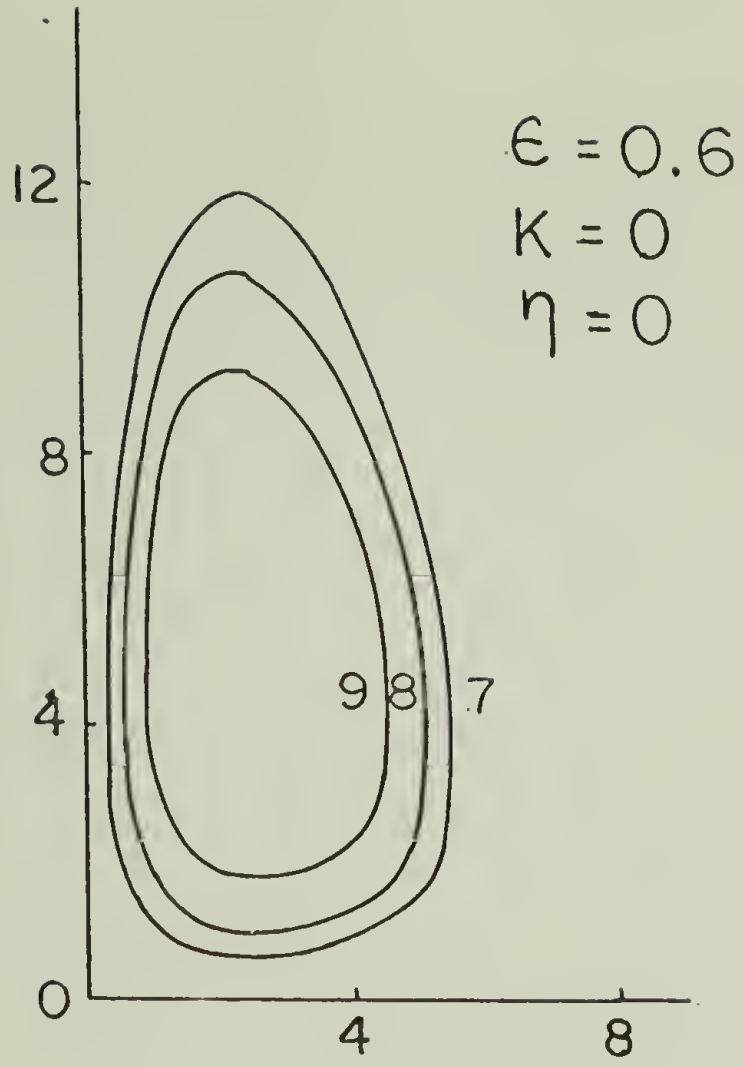
ϵ = 0.6
K = 0
η = 0
12
8
4
0
4
8
9
8
7

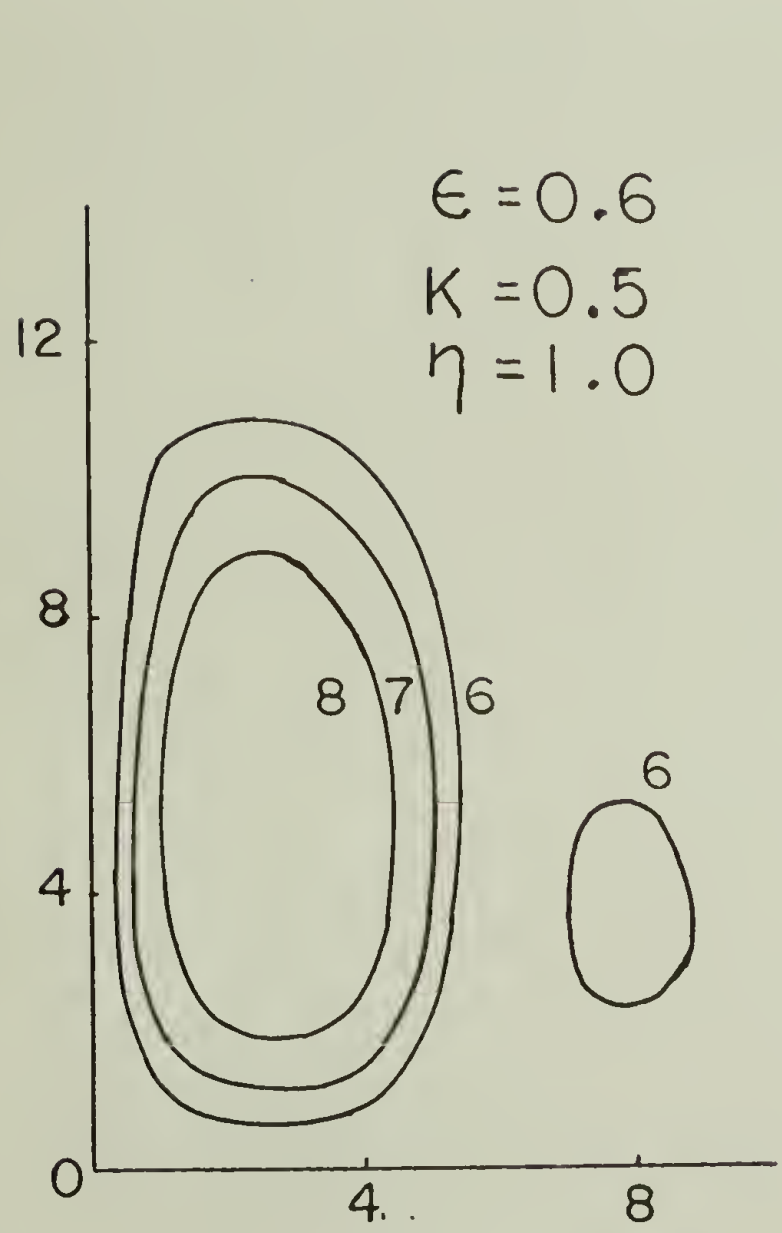
ϵ = 0.6
K = 0.5
η = 1.0
12
8
4
0
4
8
8
7
6
6

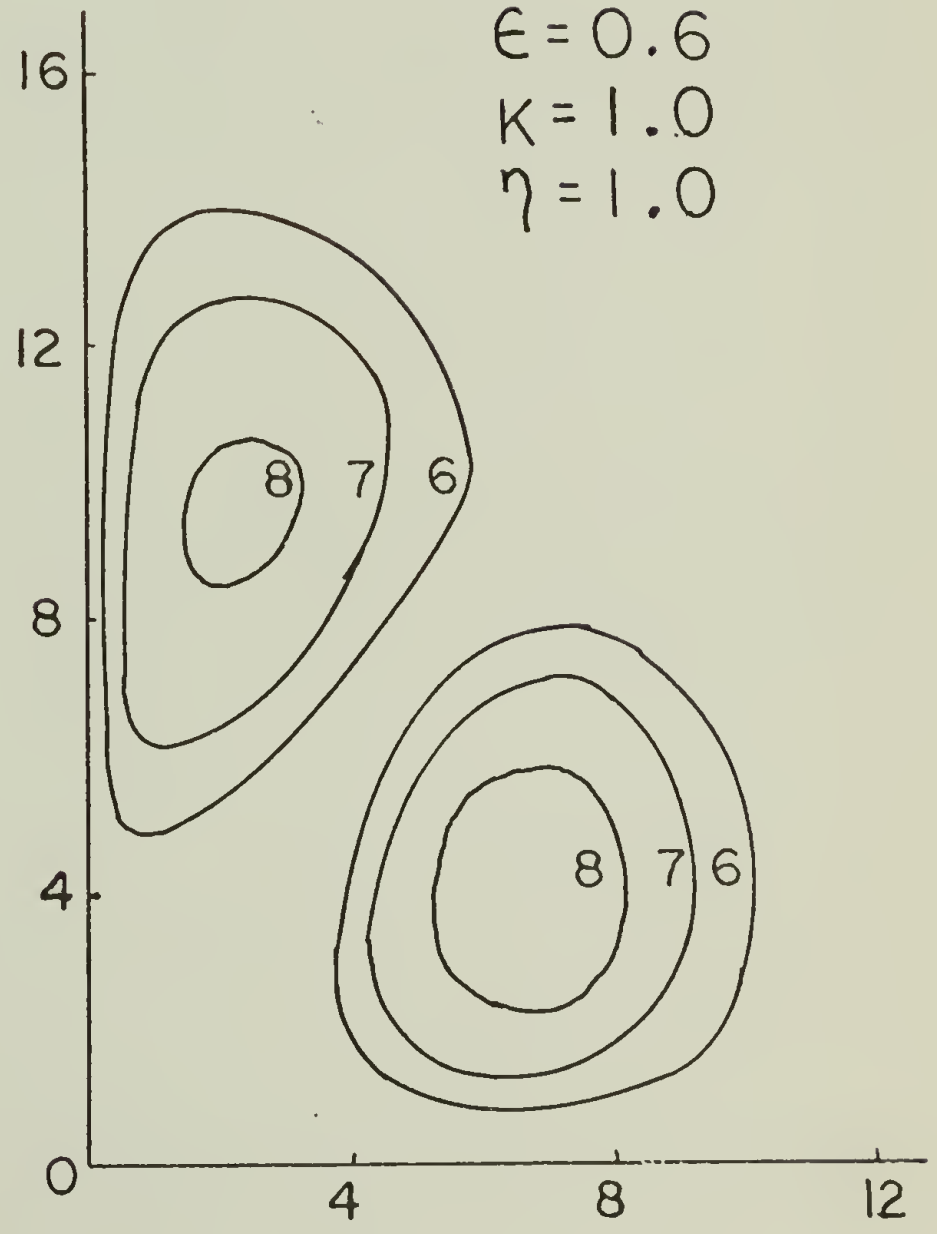
ϵ = 0.6
K = 1.0
η = 1.0
12
8
4
0
4
8
12
8
7
6
8
7
6

FIG. 43

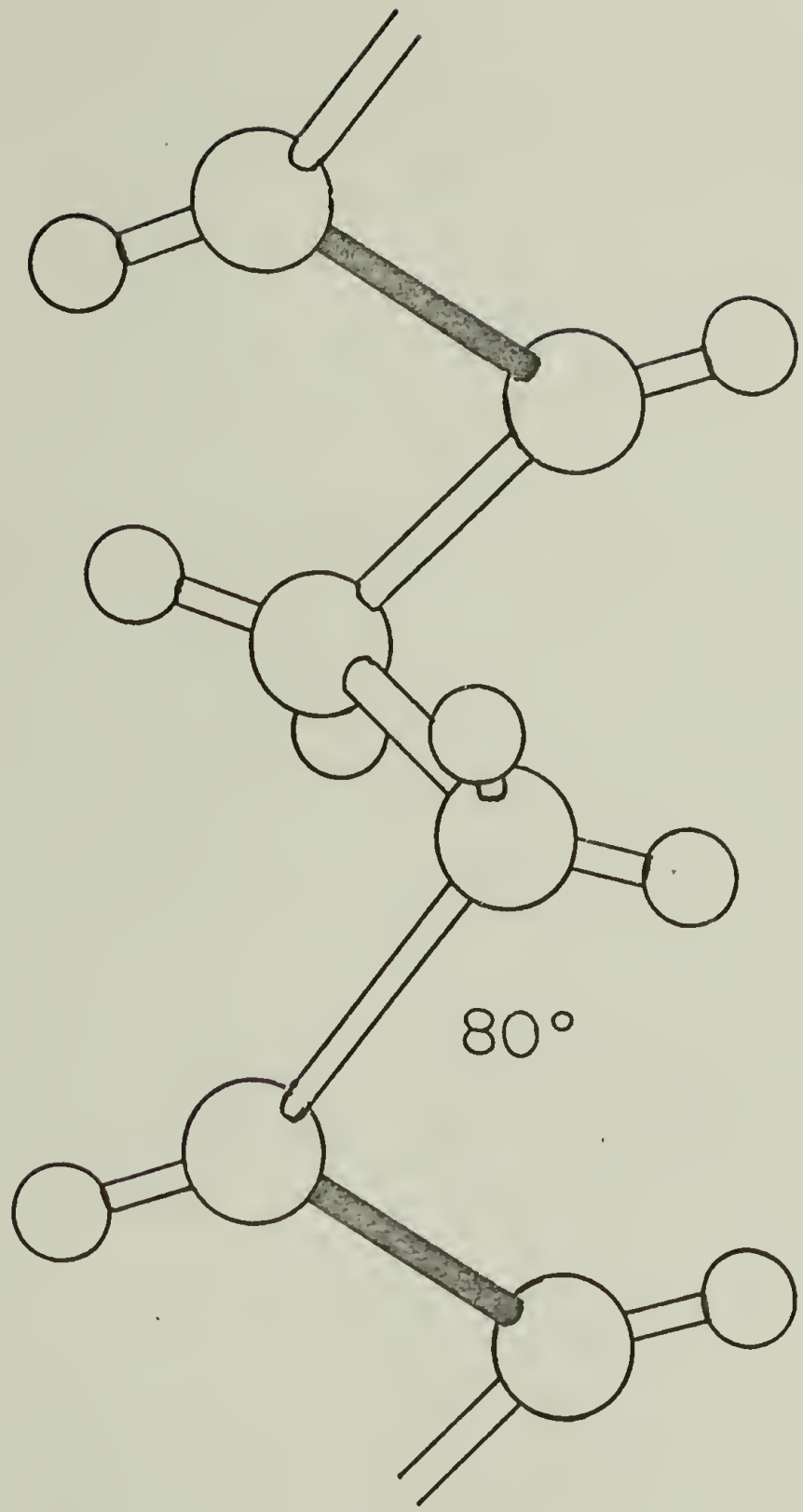

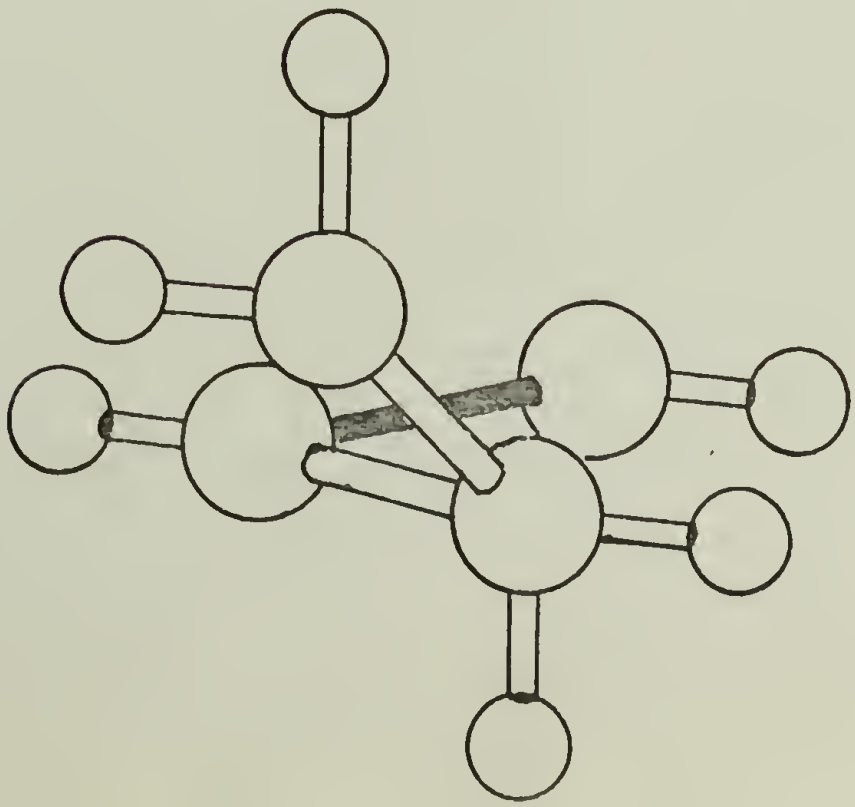

FIG. 44